Mu-opioid receptor gene variant *OPRM1* 118A>G:
A genetic modulator of opioid effects

Dissertation
zur Erlangung des Doktorgrades
der Naturwissenschaften

vorgelegt beim Fachbereich Chemische und Pharmazeutische Wissenschaften
der Johann Wolfgang Goethe-Universität
in Frankfurt am Main

von
Bruno Georg Oertel
aus Neuburg an der Donau

Frankfurt am Main (2008)
(D 30)

Vom Fachbereich Chemische und Pharmazeutische Wissenschaften der Johann Wolfgang Goethe-Universität als Dissertation angenommen.

Dekan: Prof. Dr. Harald Schwalbe

Gutachter: Prof. Dr. Dieter Steinhilber
                  Prof. Dr. Dr. Gerd Geißlinger

Datum der Disputation: 13.05.2008

Table of Contents

1 Introduction

The μ-opioid receptor is the primary target structure of most clinically used opioid analgesics. Activation of the receptor is accountable for the major part of the wanted and unwanted effects of opioid analgesics. The common genetic μ-opioid receptor variant N40D (allelic frequency 8.2-17%), coded by the single nucleotide polymorphism 118A>G of the μ-opioid receptor gene *OPRM1* (*OPRM1* 118A>G SNP), has been repeatedly associated with a decrease of the wanted and unwanted effects of opioid analgesics in carriers of this variant. The aim of the here presented thesis was to identify the mechanism by which the *OPRM1* 118A>G SNP diminishes the opioid effects and to explore its consequences for the pain treatment. This knowledge is important for the clinical pain therapy with opioid analgesics because it guarantees its effectiveness and safety when used in carriers of the *OPRM1* 118A>G SNP.

1.1 Pain

The individual experience of pain is generated by a complex network of cortical and subcortical brain regions and comprises sensory, qualitative and emotional components [1]. Thus, the International Association for the Study of Pain (IASP) defines pain as 'an unpleasant sensory and emotional experience that is associated with actual or potential tissue damage, or described in terms of such damage'. In contrast, nociception describes the body system that carries the information about a noxious stimulus to the spinal cord and brain. Nociception eventually leads to pain perception, but frequently occurs below the level of consciousness without the sensation of pain. The other way around, pain is usually caused by a noxious stimulus but may also be experienced in the absence of such stimuli.

1.1.1 Nociception

Depending on the point of origin, pain is differentiated in somatic and visceral pain. Somatic pain originates from the head, torso or extremities and visceral pain originates from the inner organs. A special kind of pain is the neuropathic pain, which is the result of nerve damage. Nociception starts with activation of peripheral nociceptors by a noxious stimulus. Nociceptors are free nerve endings of myelinated Aδ- or unmyelinated C- fibres and their axons terminate in lamina IV-VI or lamina I-II, respectively, of the spinal cord dorsal horn. Somatosensory signals are mainly transmitted by myelinated Aδ, whereas the viscerosensory signals are transmitted by unmyelinated C- fibres [2].

In the spinal cord dorsal horn, the nociceptive signal is transmitted via synaptic transmission to a second neuron, which ascends either to the thalamus via the spinothalamic tract (STT), to the medulla and brainstem via the spinoreticular (SRT) and spinomesencephalic (SMT) tracts, or to the hypothalamus via the spinohypothalamic tract (SHT). Since there are so many functional and anatomical subdivisions of the thalamus, the spinothalamic pathway can be further differentiated. Lamina I STT axons project to the ventral posterior lateral nucleus (VPL), the posterior part of the ventral medial nucleus (VMpo), the ventral posterior inferior nucleus (VPI) and the ventral caudal division of the medial dorsal nucleus (MDvc). Lamina V STT axons terminate in the ventral posterior nucleus (VP), the ventral posterior inferior nucleus (VPI), ventral lateral nucleus and intralaminar nuclei. In the brainstem regions, the nociceptive signal is transferred to a third neuron, which projects to the cortical and subcortical areas that are essential for pain perception. That is, midline thalamic nuclei (VMpo and MDvc) neurons project to limbic cortical areas such as the anterior cingulate cortex (ACC) and the insular cortex (IC) while more posterior lateral nuclei (VPL and VPI) of the thalamus project to the primary and secondary somatosensory cortices (S_I and S_{II}, respectively). SRT axons terminate in the nucleus raphe magnus and nucleus gigantocellularis of the formatio reticularis by which the variant receptors affect in the medulla oblongata. From there, neurons project into the medial thalamus, hypothalamus (HT) and the amygdala (AMYG) [3]. SMT axons terminate mainly in the midbrain periaqueductal gray (PAG), nucleus cuneiformis (Cnf) and nucleus pretectalis anterior. Neurons of these areas then further project to medial prefrontal and insular cortices and hypothalamus [4].

1.1.2 Pain perception

The cortical and subcortical areas activated by the several ascending pain transmission pathways during painful stimulation include the somatosensory cortices (S_I and S_{II}), primary motor cortex (M1), supplementary motor area (SMA), insular cortex (IC), anterior, middle and posterior cingular cortex (ACC, MCC and PCC), prefrontal cortex (PF), basal ganglia (BG; consisting of putamen, caudate nucleus, nucleus accumbens and globus pallidus), posterior parietal cortex (PPC), amygdala (AMYG), hypothalamus (HT) and thalamus (VMpo, MDvc, VPL; **Figure 1**; [5, 6]). Activation of these regions by nociceptive stimuli results in the conscious perception of pain. Thus, these areas are also referred to as the "pain matrix". It is assumed that each area plays a different role in the process of pain perception. For example, the somatosensory cortices S_I and S_{II} are deemed to be responsible for discrimination of the location and intensity of

painful stimuli, thus the sensory component of pain [7], whereas the amygdala as part of the limbic system is primarily thought to have a role in the affective dimension of pain, creating feelings of unpleasantness and emotions [8]. Prefrontal and parietal cortical areas are believed to be related to cognitive variables, such as memory or stimulus evaluation [7]. Motor areas such as the primary and supplementary motor cortices and caudate nucleus (basal ganlia) seem to be related to pain evoked movements or suppression of movement [9]. The insular cortex and the anterior cingulate cortex seem to be multi-integrative structures that play a role for both sensory and affective dimension of pain, but also for motor, cognitive and autonomic functions [10].

All areas are more or less interconnected by association fibers, creating a complex network of communicating regions within the brain. For example, there is a ventrally directed cortico-limbic pathway proceeding from S_I and S_{II} to the posterior parietal cortical areas and to the IC and from IC to amygdala, perirhinal cortex and hippocampus [11]. This pathway converges on limbic and subcortical structures that are also directly targeted by ascending spinal pathways and is suggested to integrate somatosensory input with other sensory input such as vision or audition and with learning and memory [11].

The individual pain perception depends on the activation pattern of the interconnected brain regions and changes in the activation pattern results in an alteration of pain perception. Disruption of the cortical and subcortical regions that form the pain matrix, and the pathways between them, can result in serious conditions. For example, patients after ischaemic injury (i.e. stroke) affecting the posterior insula and S_{II} suffer from a decrease of pain and temperature sensation [12]. Furthermore, opioid receptor expression in the pain network plays a very important role for pain perception. For example, in patients suffering from the poststroke pain syndrome after an ischaemic brainstem injury, a massive reduction of opioid receptor binding sites in the posterior thalamus and posterior insula and S_{II}, respectively, has been demonstrated [13].

Figure 1: Cortical and sub-cortical brain regions involved in pain perception, their inter-connectivity and ascending pain transmission pathways. Brain regions involved in pain perception include the primary and secondary somatosensory cortices (S1 and S2, red and orange), anterior cingulate (ACC, green), insula (blue), thalamus (yellow), prefrontal cortex (PF, purple), primary and supplementary motor cortices (M1, blue and SMA), posterior parietal cortex (PPC), posterior cingulate (PCC), basal ganglia (BG, pink), hypothalamus (HT), amygdale (Amyg), parabrachial nuclei (PB) and periaqueductal grey (PAG). The schematic was originally published in 2000 [5] and modified in 2005 [6].
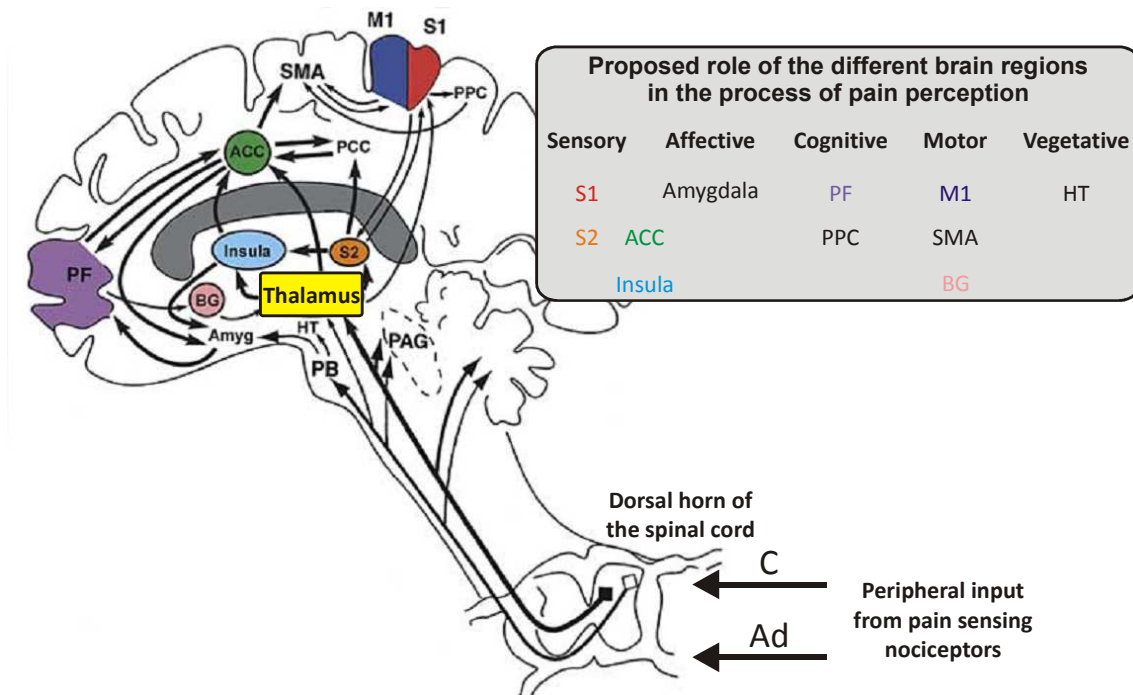
1.2 Mu-opioid receptors

One of the most important neurotransmitters involved in pain and nociception are the endogenous opioid peptides including endorphins, enkephalines, dynorphines, and the recently discovered endomorphins and nociceptin (not to be mixed up with the above mentioned ´nociception`). Endorphins, enkephalines, dynorphines and nociception are derived from different precursor proteins, the proopioimelanocortin (POMC), proenkephalin (PENK) and prodynorphin (PDYN) and pronociceptin. Their targets are four separate receptors, the μ- (mu), δ- (delta) and κ- (kappa) receptors, and the opioid receptor-like protein (ORL1) [14, 15].

It has been shown that μ-opioid receptor-knockout mice do not respond to morphine with analgesia, respiratory depression, constipation, physical dependence reward behaviours, or

immunosuppression [16]. Morphine – and also other opioid analgesics – bind not only µ-opioid receptors but also δ- or κ-receptors [17]. However, no behavioral responses related to δ- or κ-opioid receptor activation was observed in the µ-opioid receptor-knockout mice during morphine treatment, although these receptors were still present in these mice [16]. Thus, µ-opioid receptors are essential for the action of morphine and other clinically used opioid analgesics and the major part of their analgesic and unwanted side-effects.

1.2.1 Structure, anatomical localization and function of the µ-opioid receptor

The µ-opioid receptor belongs to the superfamily of G-protein-coupled receptors (GPCRs) and the subfamily of rhodopsin receptors. The structure of the receptor includes seven transmembrane domains, an extracellular N-terminus with multiple glycosylation sites, third intracellular loop with multiple amphiphatic α-helices, and fourth intracellular loop formed by the putative palmitoylation sites at the carboxyl tails. They are prototypical "G_i/G_o-coupled" receptors because receptor signaling can be blocked by pertussis toxin (PTX), a bacterial toxin produced by *Bordetella pertussis* that inactivates the α-subunit of G_i/G_o proteins ($G_{\alpha i/o}$ subunits) [18].

The anatomical localization of the µ-opioid receptors is consistent with known pathways related to nociceptive signaling. They are expressed on peripheral nociceptors after inflammation, on spinal cord dorsal horn neurons and on neurons of the various brain regions involved in pain processing. In the spinal cord, µ-opioid receptors are expressed on primary afferent nociceptors that terminate in lamina I and II of the dorsal horn and on glutamatergic interneurons in lamina II [19]. Cortical and subcortical areas expressing µ-opioid receptors include primary and secondary somatosensory cortices S_I and S_{II}, the insula, the anterior cingulate cortex and midcingulate cortex, the striatum, nucleus accumbens, septal nuclei, islands of Calleja, hippocampal regions, amygdaloid nuclei, several thalamic nuclei, habenular nuclei, interpeduncular nuclei, several raphe nuclei (e.g. nucleus raphe magnus), colliculi, parabrachial nuclei, locus coeruleus, nucleus ambiguous, nuclei of the sensory trigeminal complex and nucleus of the solitary tract [20, 21]. In contrast, the occipital lobe of the brain is known to be absent of µ-opioid receptors [22].

Activation of µ-opioid receptors results in an inhibition of adenylyl cyclases (AC) and calcium (Ca^{2+}) channels (**Figure 2**). It further results in a stimulation of potassium (K^+) channels, phospholipase C and MAP-Kinase. Activation of µ-opioid receptors on pre-synaptic neurons results

in a decrease of the calcium ion (Ca^{2+}) influx, which leads to a reduction of neurotransmitter release, e.g. the release of Substance P, into the synaptic gap. On the post-synaptic side, activation of µ-opioid receptors enhances the potassium ion (K^+) efflux resulting in a hyperpolarisation of postsynaptic neurons. Thus, activation of pre- and post-synaptic µ-opioid receptors on spinal cord dorsal horn neurons leads to a decrease of synaptic nociceptive transmission. In the brainstem, activation of µ-opioid receptors results in the excitation of the descending pain inhibitory system by a disinhibition of GABAergic neurons that inhibit pain-inhibitory neurons. In contrast to the immediate effects on pain transmission, alterations of cAMP levels are associated with cellular changes that lead to the development of tolerance and physical dependence [23]. Taken together, the activation of µ-opioid receptors leads to a decrease of the release of excitatory neurotransmitters from pre-synaptic neurons into the synaptic cleft and to a hyperpolarisation of post-synaptic neurons, finally resulting in a reduced excitability of nociceptive pathways and brain regions involved in pain perception.

Figure 2: Intracellular effects after activation of µ-opioid receptors. Binding of µ-opioid receptor agonists (e.g. morphine) results G-protein mediated in the following intracellular effects: i, inhibition of the adenylylcyclase, ii, inhibition of voltage dependent calcium channels, iii, activation of inward rectifying potassium channels, iv, activation of phospholipase C and v, activation of MAP-Kinase.
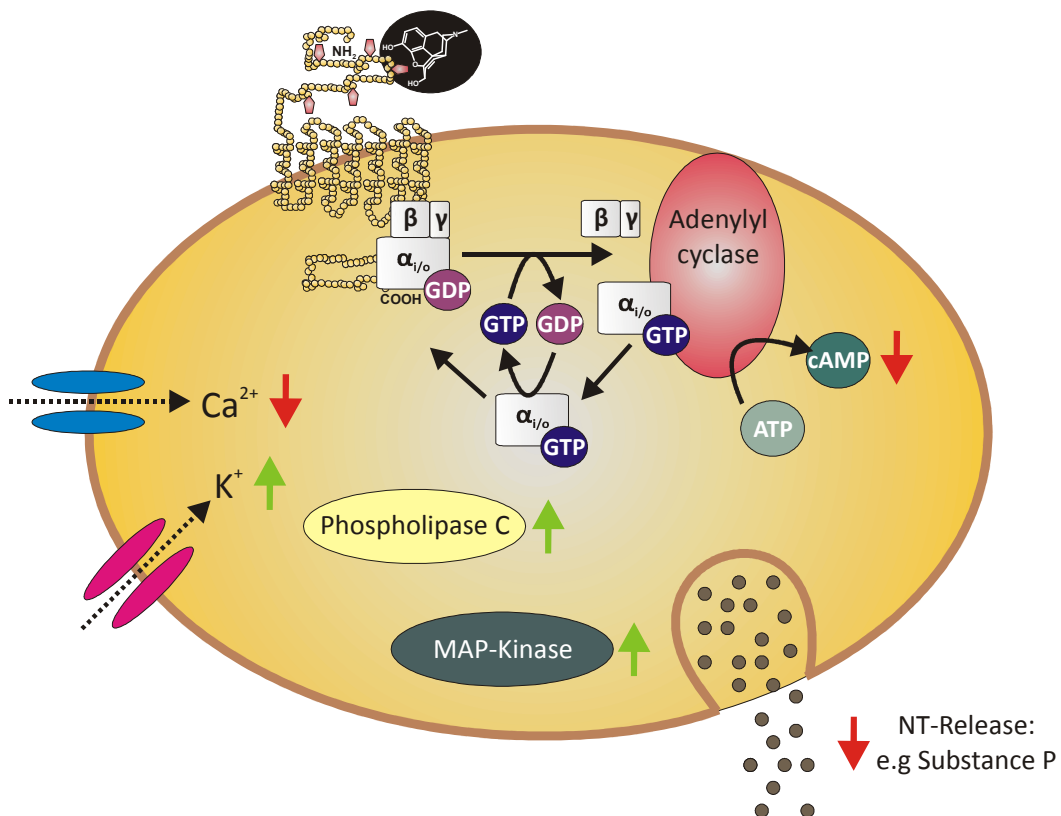
1.2.2 Pharmacological effects of opioid analgesics

The effectiveness of opioid analgesics in pain treatment is based on their interaction with μ-opioid receptors interrupting nociceptive signaling on nearly every level of pain transmission and pain perception. However, since the receptors are expressed in the whole body and not only in pain processing brain regions, activation of the receptor triggers not only analgesia but also numerous unwanted effects such as sedation, nausea and vomiting, constipation and respiratory depression, confusion, hallucinations, nightmares, urinary retention, miosis, multifocal myoclonus, dizziness, dysphoria and hyperalgesia [24]. For example, constipation is triggered by μ-opioid receptor activation in the gastrointestinal tract, and anatomical and *in vitro* studies suggest that μ-opioid receptors on pre-Bötzinger complex neurons are responsible for opioid induced respiratory depression [25].

Respiratory depression is the most life-threatening unwanted effect that occurs during opioid treatment and that patients die due to an opioid treatment is nearly always because of respiratory rest. Even under controlled clinical conditions opioid administration can result in fatal respiratory depression [26-30]. Thus, opioid treated subjects must be under tight medical supervision including measurements of their blood oxygenation level and, under critical conditions, the respiratory depression must be reversed by administration of the specific opioid antagonist naloxone.

1.2.3 Mu-opioid receptor coding gene *OPRM1*

The magnitude of opioid effects is subject to a large inter-individual variability. They depend on factors like age, organ dysfunctions, extent of disease, concurrent administration of certain drugs, prior opioid exposure and the route of drug administration [24]. In addition, advances in genetic research revealed that there is also a genetic component involved.

Besides genetic variations affecting the pharmacokinetics of opioid analgesics, genetic variations affecting their primary target structure, the μ-opioid receptor, are primary candidates for investigations regarding the inter-individual variability of opioid effects. The *OPRM1* gene codes for μ-opioid receptors [31, 32]. It is located on chromosome 6q24-q25 (**Figure 3**). Several mutations in the promoter, exons (coding regions) and introns (non-coding regions) of the *OPRM1* gene have been identified [33, 34]. The mutations cause amino acid exchanges in the receptor protein or alternative splicing, thus, possibly affecting receptor function or receptor expression. Four single nucleotide polymorphisms of the *OPRM1* gene have been shown to

alter agonist binding or impair receptor signaling: The *OPRM1* 118A>G single-nucleotide poly-
morphism (SNP) in exon 1, which affects the extracellular binding domain of the µ-opioid re-
ceptor, as well as SNP 779G>A, SNP 794G>A and SNP 802 T>C in exon 3, which affect the third
intracellular loop of the µ-opioid receptor [35].

The 118A>G single-nucleotide polymorphism (SNP) in exon 1 of the *OPRM1* gene emerges as
one of the most interesting mutations [36]. It causes an amino acid exchange at position 40 of
the µ-opioid receptor protein from asparagines (Asn; N) to aspartate (Asp; D) (N40D), deleting
a putative N-glycosylation site in the extracellular receptor region. Due to its allelic frequency
of 17.2 % (according to the dbSNP database at http://www.ncbi.nlm.nih.gov/SNP/; SNP ref-
erence ID rs1799971), a change in receptor functionality would imply immediate clinical relev-
ance for the administration of opioids in a larger part of the population. In contrast, SNP
779G>A, SNP 794G>A and SNP 802 T>C are not of immediate clinical importance because of
their low reported allelic frequency (<<1%).

**Figure 3: Location of the most common SNPs of the *OPRM1* gene and their respective location in the
µ-opioid receptor protein.** SNPs with reported functional consequences (red) are the *OPRM1* 118A>G
(N40D) and 779G>A (R260H), 794G>A (R265H) and 802T>C (S268P; [35]).
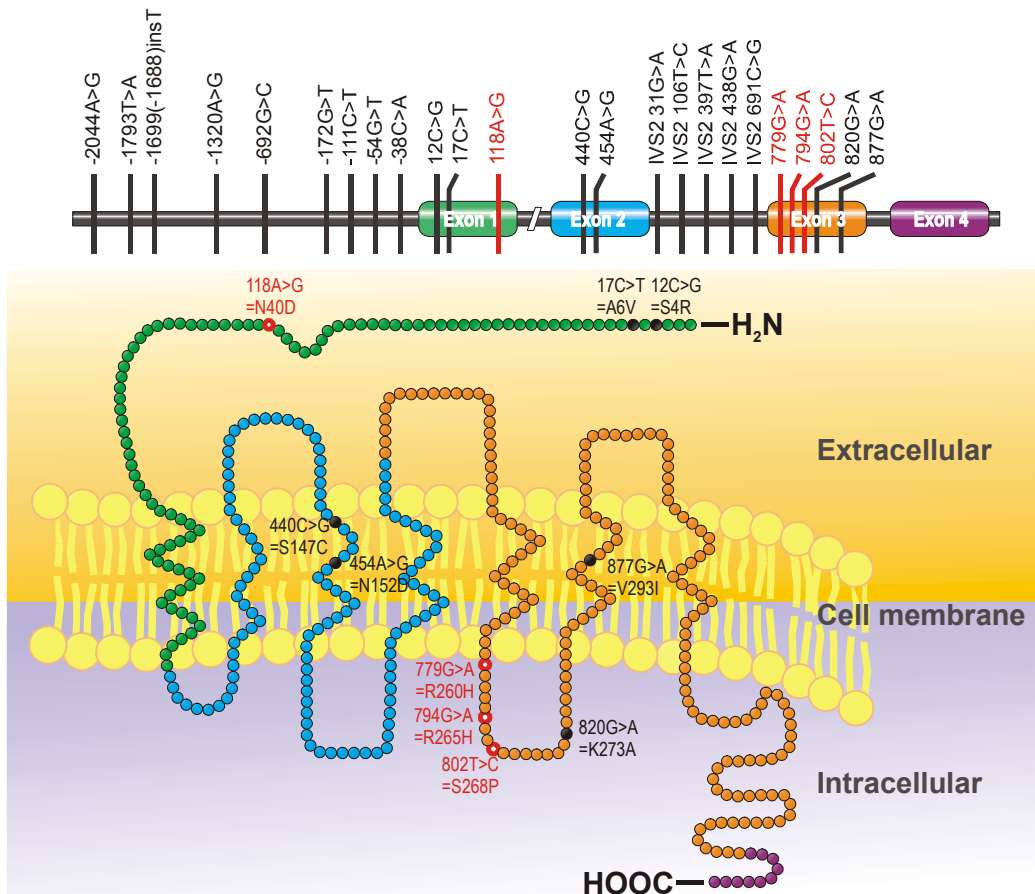
1.2.4 Mu-opioid receptor gene variant *OPRM1* 118A>G

The earliest report regarding SNP *OPRM1* 118A>G as a μ-opioid receptor gene variant with functional consequences stated that N40D variant μ-opioid receptors expressed in Syrian hamster adenovirus-12-induced tumor cells (AV-12) had, in contrast to other opioids like morphine and M6G, a 3-fold higher binding affinity to its endogenous ligand β-endorphine compared to wildtype receptors [37]. Furthermore, β-endorphine was more potent in activation of the G-protein activated inwardly rectifying potassium (K^+) channel (GIRK) in Xenopus oocytes expressing the variant receptors. Contrary to this publication, two succeeding studies demonstrated that μ-opioid receptor binding affinity to opioid agonists including β-endorphine and, in addition, μ-opioid receptor signaling, measured by [^{35}S]-GTPγS binding and cAMP accumulation, was unaffected in μ-opioid receptor mutant N40D expressing Cercopithecus aethiops cells (COS) [38] and human 293 embryonic kidney cells (HEK 293) [39]. Most recently, a 2-fold increase of the potency of DAMGO and morphine to activate N-type Ca^{2+} channels in rat superior ganglion neurons transfected with *OPRM1* 118G cDNA has been shown [40].

In addition, μ-opioid receptor density decreasing effects of *OPRM1* variant 118G had been suggested, based on [^{3}H]-DAMGO saturation binding experiments in HEK 293-cells transfected with μ-opioid receptor mutant N40D. However, *OPRM1* variant 118G has no effects on μ-opioid receptor endocytosis and desensitization [39]. In agreement with this result, a recent publication demonstrated reduced mRNA expression of the 118G allele in human autopsy brain tissues of pons and cortical lobes of eight heterozygous carriers. In addition, the authors demonstrated a 1.5-fold lower mRNA level and 10-fold lower μ-opioid receptor expression in Chinese hamster ovary cells (CHO) transfected with *OPRM1* 118G cDNA. Since the mRNA stability was unaffected by the polymorphism, the authors suggested that this is due to a defect of transcription or mRNA maturation [41].

In vivo, *OPRM1* variant 118G has repeatedly been associated with decreased opioid analgesia. Patients treated because of postoperative pain with alfentanil or morphine needed 1.3-fold and 2-fold higher concentrations, respectively, to achieve adequate analgesia [42-44]. Furthermore, a 3-fold reduction of the analgesic potency of M6G in healthy carriers of *OPRM1* variant 118G treated with experimental pain has been reported [45, 46].

Similar to the analgesic effects of opioids, the miotic effects of morphine [47], morphine-6-glucuronide [47, 48] and levomethadone [49] were decreased in carriers of the variant *OPRM1* 118G allele. Furthermore, carriers of *OPRM1* variant 118G vomited less frequently after high

M6G doses [47] and good tolerance of high plasma M6G concentrations by a homozygous carrier of the 118G allele has been reported [50]. To this sharply contrasts a report of similar respiratory depression despite lower analgesia produced by M6G in four heterozygous carriers of the 118G allele as compared to 12 non-carriers [46], without including homozygous carriers.

In addition, *OPRM1* 118A>G has been associated with vulnerability to substance abuse [51-53] and an increase of the cortisol response to mu-opioid receptor blockade with naloxone in homozygous carriers of mu-opioid receptor variant N40D [54, 55].

1.3 Aim of the study

Taken together, despite the clear functional consequences of *OPRM1* variant 118G for opioid analgesia and opioid side-effects, the molecular mechanism by which the variant causes the decrease in clinical opioid effects is currently unclear. Investigations using µ-opioid receptor transfected cell lines produced conflicting results and although a reduction of µ-opioid receptor binding sites in carriers of *OPRM1* variant 118G has been reported, the importance of the investigated brain regions for nociceptive transmission and pain perception is unknown. In addition, the consequences of the 118G allele for the drug safety and the therapeutic range of opioid analgesics are currently unclear but of immediate importance for clinical pain therapy with opioid analgesics. If the variant affects only opioid analgesia but leaves respiratory depression unchanged, the advice of increased dosing to achieve adequate analgesia in 118G carriers would be dangerous. On the other hand, if both analgesia and respiratory depression were affected, increasing the opioid dose would be safe.

The aim of the study was to identify the mechanism by which the *OPRM1* 118A>G SNP diminishes opioid effects and to explore its consequences for opioid effects in carriers of this variant.

To achieve this, following step-wise approach was taken: In the first step, *OPRM1* 118A>G SNP affected brain regions of healthy homozygous 118G variant carriers were identified by observing variations of the response to opioid analgesics after painful stimulation using functional magnetic resonance imaging (fMRI). Afterwards, samples of brain regions displaying variations of the response to opioid analgesics were collected *post mortem* and the molecular mechanism underlying the variations was investigated. Finally, the consequences of the *OPRM1* 118A>G SNP for the analgesic and respiratory depressive effects of opioids were quantified in healthy carriers and non-carriers of the *OPRM1* 118A>G SNP and it was analyzed whether the therapeutic range of opioid analgesics is altered in carriers of this variant.

2 Material and Methods

2.1 Enrolment of healthy subjects

The participants of the clinical studies were mostly medical students recruited via flyers distributed at the campus of the University of Frankfurt. During recruitment, subjects were given detailed information about the testing procedures and written informed consent was obtained. The subjects´ current health was ascertained by medical examination and routine laboratory analyses. Exclusion criteria were drug addiction, any chronic disease, the use of any medications except for anticonceptionals within the last week before the actual experiments, pregnancy and lactation. A total number of 740 unrelated volunteers of Caucasian ethnicity, who had consented into genotyping, were screened for the *OPRM1* 118A>G single nucleotide polymorphism.

2.2 Collection of human brain tissue

Human brain tissue was sampled during autopsy at the Institute of Forensic Medicine and the Senckenberg Institute for Pathology of the Johann Wolfgang Goethe-University of Frankfurt am Main, Germany. Tissue was collected from a total number of 95 subjects. The included subjects neither received an opioid treatment nor had a known history of drug addiction. The collected tissue included the secondary somatosensory cortex S_{II} and the ventral posterior part of the lateral thalamus. Tissue samples were stored at − 80°C pending further analysis.

2.3 Genetic screening for carriers of SNP *OPRM1* 118A>G

For genotyping of the healthy subjects and *post mortem* brain samples, genomic deoxyribonucleic acid (DNA) was extracted from either heparinized blood samples (10 ml) using the EZ1 DNA Blood 200 µl Kit or from brain tissue (10 mg) using the EZ1 DNA Tissue Kit on a BioRobot EZ1 Workstation (Qiagen, Hilden, Germany). Subsequently, an *OPRM1* DNA segment of 393 nucleotides including position 118 was amplified by using the following primers: biotinylated forward primer 5´-CTC CGC CTG ACG CTC C-3´ with reverse primer: 5´-GTA GAG GGC CAT GAT CGT GAT-3´. The polymerase chain reaction (PCR) was performed by use of 5 µl genomic DNA (20-30 µg/ml) mixed with 0.5 µl Hotmaster Taq (Thermus aquaticus; Eppendorf, Hamburg, Germany) DNA polymerase, 1 µl of 10 mM deoxynucleotide triphosphate mix (Roche, Penzberg, Germany), 0.1 µl of each PCR primer (100 µM), 5 µl concentrated (10*) PCR reaction buf-

fer without magnesium chloride and 38.3 µl HPLC-purified water (J.T. Baker, Deventer, The Netherlands). The thermal cycler protocol was set at 40 cycles and used an initial denaturation step at 95°C for 5 minutes, with amplification at 95°C for 30 seconds, followed by annealing at primer-specific temperatures (55.5°C) for 60 seconds, 30 seconds of elongation at 72°C, and cooling down to 4°C.

Genetic polymorphisms were detected by use of validated Pyrosequencing [56] assays on a PSQ 96MA device (Biotage, Uppsala, Sweden; Figure **4**). Samples with known sequences at the respective SNP positions (previously obtained by classic sequencing) were included in each analysis as quality control. A small volume of 25 µl of the PCR-template was transferred into a single well of a microtest plate U96 (Ratiolab GmbH, Dreieich, Germany) containing a mixture of 3 µl streptavidin-coated sepharose beads (Amersham Pharmacia Biotech, Uppsala, Sweden), 37 µl Binding-buffer (Biotage, Uppsala, Sweden) and 15 µl purified H2O. Subsequently, the mixture was incubated for 10 min at room temperature while shaking. The template was further treated according to the pyrosequencing protocol with Ethanol 70%, 0.2M NaOH and 10mM Tris Acetate buffer before it was transferred into a PSQ 96 Plate Low (Pyrosequencing AB, Uppsala, Sweden), containing 0.35 µM of sequencing primer and 40 µl of Annealing-Buffer (Biotage, Uppsala, Sweden). The mixture of template and sequencing primer was incubated for 60 seconds at 80°C and then transferred to the PSQ 96MA device. Genotyping for OPRM1 mutation 118A>G was performed with sequencing primer 5´-TGG GTC GGA CAG GT-3´.

From the 740 healthy subjects, 588 were non-carriers, 136 were heterozygous and 16 were homozygous carriers of the variant *OPRM1* 118G allele. The allelic frequency of the variant 118G allele in this random sample was 11.4%. The 95 samples of *post mortem* human brain tissue included 68 non-carriers, 24 heterozygous and three homozygous carriers of the variant *OPRM1* 118G allele. The allelic frequency of the variant 118G allele in this random sample was 15.8%. Both samples corresponded to the Hardy-Weinberg equilibrium [57] (Chi^2-test: p=0.89) indicating a random sample of subjects with respect to 118A>G.

Figure 4: Pyrosequencing. Left side: Principle of Pyrosequencing according to manufacturer Biotage (http://www.pyrosequencing.com/DynPage.aspx?id=7454). A sequencing primer is hybridized to a single stranded, PCR amplified DNA template, and incubated with the enzymes, DNA polymerase, ATP sulfurylase, luciferase and apyrase, and the substrates, adenosine 5´ phosphosulfate (APS) and luciferin. The first of four deoxynucleotide triphosphates (dNTP) is added to the reaction. DNA polymerase catalyzes the incorporation of the deoxynucleotide triphosphate into the DNA strand, if it is complementary to the base in the template strand. Each incorporation event is accompanied by release of pyrophosphate (PPi) in a quantity equimolar to the amount of incorporated nucleotide. ATP sulfurylase quantitatively converts PPi to ATP in the presence of adenosine 5´ phosphosulfate. This ATP drives the luciferase-mediated conversion of luciferin to oxyluciferin that generates visible light in amounts that are proportional to the amount of ATP. The light produced in the luciferase-catalyzed reaction is detected by a charge coupled device (CCD) camera and seen as a peak in a pyrogram™. Each light signal is proportional to the number of nucleotides incorporated. Apyrase, a nucleotide degrading enzyme, continuously degrades unincorporated dNTPs and excess ATP. When degradation is complete, another dNTP is added. Addition of dNTPs is performed one at a time. As the process continues, the complementary DNA strand is built up and the nucleotide sequence is determined from the signal peak in the pyrogram. Right side: Appropriate pyrograms™ of non-carriers, hetero- and homozygous carriers of *OPRM1* variant 118G.
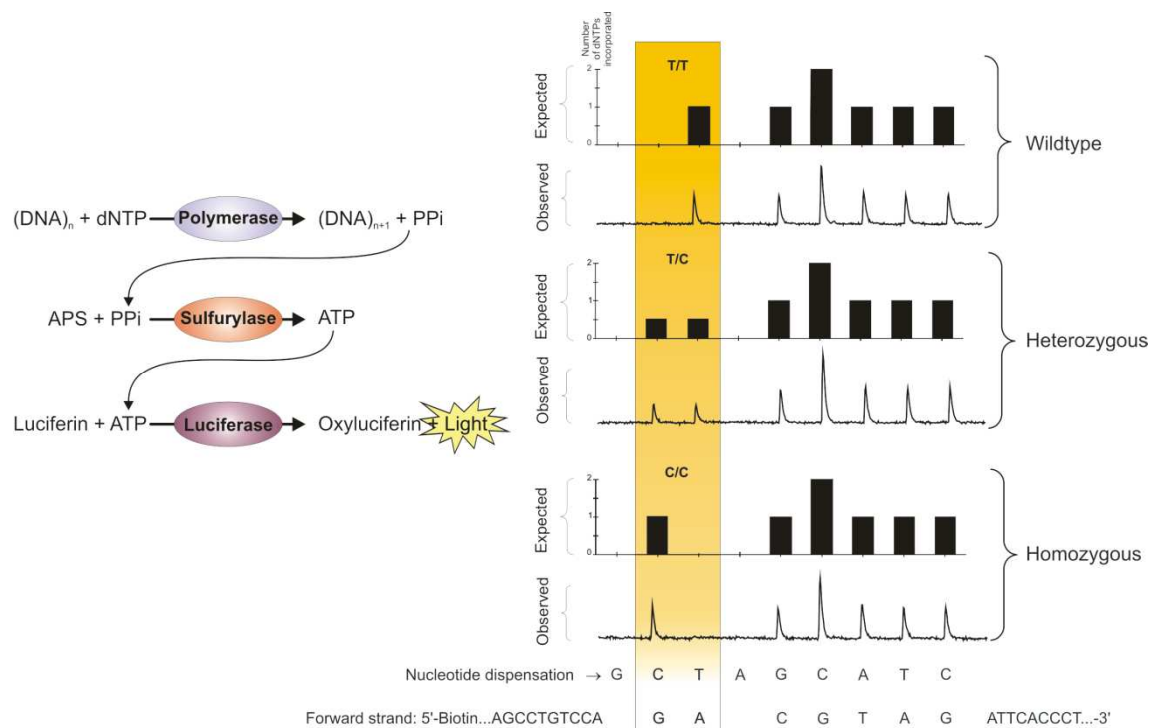
2.4 Study designs

All study protocols were in accordance with the Helsinki Declaration of Biomedical Research Involving Human Subjects and were approved by the Medical Faculty Ethics Review Board of the Johann Wolfgang Goethe-University of Frankfurt.

All trials were performed without a placebo condition because (i) previous experiments in the laboratory did not suggest a temporal bias of the pharmacodynamic target parameters of the studies, (ii) we wanted to compare differences among genotypes, so that a possible placebo effect should have affected both genotypes in a similar manner and not compromised their comparability, and (iii) opioid administration is usually noticed by both the subjects and the observers when compared with saline administration, thus compromising the blinding, and an established active placebo is not available.

2.4.1 Investigation of pain-related brain activation during alfentanil administration in non-carriers and homozygous carriers of *OPRM1* 118A>G SNP

In this study, *OPRM1* 118A>G SNP affected brain regions of healthy homozygous 118G variant carriers were identified by observing variations of the response to opioid analgesics after painful stimulation using functional magnetic resonance imaging (fMRI).

This study was a single-occasion open-label design. Experiments included one pain model, the gaseous CO_2 pain model (2.5.3.2). All subjects received a computer-controlled intravenous infusion of alfentanil (2.5.1) to establish four predefined different levels of plasma concentrations, which were 0 ng/ml at baseline (level 0) and, according to liquid chromatographic tandem mass spectrometric (LC-MS/MS) determination, 19.6±2.7 (level 1), 47.2±7.6 (level 2) and 76.6±11.3 ng/ml (level 3). We allowed 5 minutes equilibration time for each concentration level before the brain activation by the pain stimuli was quantified by means of functional magnetic resonance imaging (fMRI; 2.5.3.2.3). At each alfentanil concentration level, 24 specific nociceptive stimuli, consisting of short (300 ms) pulses of gaseous carbon dioxide (CO_2; 66% v/v) were delivered to the nasal mucosa of the right nostril. To avoid adaptation and habituation to the pain stimuli, an interstimulus interval of 26 sec was used [58]. Concomitantly, we recorded the changes in the blood-oxygenation level dependent (BOLD) response to these specific nociceptive stimuli by means of fMRI, employing an event-related design (2.5.3.2.3). Subsequent to recordings at concentration level 3, the alfentanil infusion was stopped and

after a break of 20 minutes, during which the participant remained in the scanner, an additional measurement was performed to explore reversal of opioid effects (level 4; 47.8 ± 9.0 ng/ml). Following completion of the experiment, ratings of the mean pain intensity at each opioid concentration level were obtained by a visual analogue scale (length 100 mm, ranging from "no pain" to "pain experienced at maximum"). This post-hoc intensity estimation avoided confounding the pain-related brain activation by the activation associated with the rating task [59]. The actual experiments were performed between 9 a.m. and 2 p.m. The subjects´ breathing rate, heart rate and blood oxygenation were constantly monitored to exclude opioid induced changes of the haemodynamic response function (HRF). Since blood oxygenation was never below 98%, an influence of opioids on the HRF can be excluded. At a separate day prior to the study occasion, subjects underwent a training session in the MRI scanner that corresponded to a complete measurement at level 0.

A total number of 16 non-addicted healthy homozygous carriers of the *OPRM1* variant 118A (eight men, eight women, mean age 27.8±4.8 years, mean body weight 69.1±12.6 kg) and nine homozygous carriers of the *OPRM1* variant 118G (four men, five women, mean age 27.5±4.1 years, mean body weight 71.3±18.7 kg) were included into the study. All participants were unaware of their individual genotype. Subjects were right-handed except for one. The groups (118AA, 118GG) did not differ significantly with respect to gender distribution, age, body weight, and measured alfentanil concentrations at levels 0 to 3 (Wilcoxon tests: p>0.13).

2.4.2 Investigation of μ-opioid receptor expression and function in pain processing brain regions of non-carriers and carriers of *OPRM1* 118A>G SNP

The molecular mechanism underlying the *in vivo* observations that the SNP *OPRM1* 118A>G alters opioid effects in pain processing brain regions was investigated in human brain samples collected *post mortem*. Based on the fMRI findings, the collected tissues included a brain region shown to be affected by the SNP *OPRM1* 118A>G, namely the S_{II}-region, a cortical region that is associated with processing the sensory information of pain [7]. On the other hand, a brain region was collected that was unaffected by the SNP *OPRM1* 118A>G, but which is known to be important for the pain processing and to express μ-opioid receptors, namely the ventral posterior part of the lateral thalamus, a sub-cortical region that is known to route afferent nociceptive signals to the somatosensory cortices S_I and S_{II} [5].

OPRM1 mRNA expression analysis was performed by means of real-time PCR analysis (see chapter 2.6.1). Furthermore, saturation binding-experiments (see chapter 2.6.4) were performed with the µ-opioid receptor specific ligand [^{3}H]-DAMGO (^{3}H-[D-Ala^2,N-MePhe^4,Gly-ol^5]-enkephalin) to investigate µ-opioid receptor density and µ-opioid receptor affinity in both brain regions. In addition, [^{3}H]-DAMGO displacement binding experiments were performed with samples of the S_{II}-region to determine the affinity of the endogenous, predominantly µ-opioid receptor binding neurotransmitter β-endorphine and to determine the affinity of commonly used opioid analgesics (morphine, methadone and alfentanil) and their metabolites (M6G). Last but not least, the ability of the µ-opioid receptor to activate the intracellular G-protein after binding of DAMGO was studied by means of [^{35}S]-GTPγS binding assays (see chapter 2.6.5).

Brain tissue samples were analyzed from all three homozygous subjects and from 21 heterozygous carriers. For analysis of non-carriers, a random sample of n=22 was taken to match the heterozygous carriers (for subject related data see **Table 1**). However, because of limited tissue availability it was not possible to employ every subject in all experiments. The exact sample sizes are indicated at the respective results. *OPRM1* genotype groups did not differ with respect to sex, age at death, *post mortem* delay and tissue storage period (analyses of variance: not significant).

Table 1: Information about the genotype, sex, age at death, *post mortem* delay until sample extraction, storage time and cause of death of each subject included into the analysis.

Subject	OPRM1 118	Sex [m/f]	Age at death [yrs]	pm delay [h]	Storage time [months]	Cause of death
1	AA	m	67	12	29	Pulmonary embolism
2	AA	m	58	24	28	Myocardial infarction
3	GG	f	42	48	28	Respiratory failure
4	AG	f	66	10	28	Myocardial infarction
5	AA	m	73	48	28	Aspergillus pneumonia
6	AG	m	89	36	28	Pneumonia
7	AA	f	59	48	28	Myocardial infarction
8	AG	m	68	48	28	Myocardial infarction
9	AA	f	77	6	25	Cardiac failure
10	AA	m	64	72	25	Myocardial infarction
11	AA	m	65	48	25	Endocarditis
12	AA	f	80	24	24	Mamma carc. (no therapy)
13	AG	m	62	9	24	Myocardial infarction
14	AG	m	62	24	23	Renal failure
15	AG	m	73	7	23	Myocardial infarction
16	AA	f	56	7	23	Liver failure
17	AA	f	53	12	23	Respiratory failure
18	AA	m	74	24	23	Myocardial infarction
19	AA	m	63	12	23	Hemorrhagic shock
20	AG	f	91	12	23	Hemorrhagic shock
21	AA	m	87	24	22	Hemorrhagic shock
22	AG	m	81	24	22	Myocardial infarction
23	AG	f	51	72	20	Liver failure
24	AG	m	70	8	19	Myocardial infarction
25	AA	m	28	23	17	Hemorrhagic shock
26	AA	m	25	85	16	Sepsis
27	AG	f	39	85	16	Respiratory failure
28	AG	m	47	19	16	Intoxication
29	AA	f	42	20	15	Hemorrhagic shock
30	AA	f	20	19	15	Hemorrhagic shock
31	AG	m	65	24	14	Hemorrhagic shock
32	AA	f	49	4	15	Homicide
33	AA	f	19	26	14	Pulmonary embolism
34	AG	m	47	47	14	Myocardial infarction
35	AA	f	84	46	14	Hemorrhagic shock
36	AA	m	49	28	14	Cardiac failure
37	AG	m	50	67	14	Hemorrhagic shock
38	AG	f	92	0	14	Cardiac failure
39	AG	m	71	67	14	Hemorrhagic shock
40	AG	f	39	29	13	Cardiac failure
41	AG	f	34	15	11	Hemorrhagic shock
42	AG	f	41	11	11	Hemorrhagic shock
43	AG	f	38	48	11	Hemorrhagic shock
44	AA	f	71	39	9.9	Myocardial infarction
45	GG	f	23	17	9	Multiple organ failure
46	GG	f	68	22	9	Heart failure
	Mean ± SD	23m/23f	58.1 ± 19.5	30.4 ± 22.2	19.3 ± 6.2	

2.4.3 Investigation of the therapeutic range of alfentanil in non-carriers and carriers of *OPRM1* 118A>G SNP

This study investigated the consequences of the *OPRM1* 118A>G SNP for the analgesic and respiratory depressive effects of opioids. Furthermore, it was analyzed whether the therapeutic range of opioid analgesics is altered in carriers this variant.

The study was a single-occasion open-label design. Experiments included two pain models, namely the transcutaneous electrical pain stimulation (2.5.3.1) and the short (200 ms) pulses of gaseous CO_2 (65% v/v) applied to the nasal mucosa (2.5.3.2). In addition, experiments included two methods for the quantification of respiratory depression, namely the hypercapnic challenge test according to Read (2.5.4.1) and monitoring of the spontaneous breathing (2.5.4.2). Experiments started with assessment of baseline values of respiratory depression and analgesia (Level 1). Measurements were always exhibited in the same order, as following: transcutaneous electrical stimulation, CO_2 re-breathing, CO_2 pain stimulation (20 CO_2 stimuli, inter-stimulus interval 20 sec) and assessment of the respiratory frequency. After assessment of baseline values, an intravenous line was inserted into each forearm for drug administration and for blood sampling. The participants received in an open-label fashion an intravenous infusion of alfentanil hydrochloride (2.5.1). Three different alfentanil target concentrations at effect site (Level 2-4) were employed by means of a computerized infusion. The study began with a target alfentanil concentration at effect site of 33.33 ng/ml for 65 minutes. After an equilibration period of 15 min, which was found by PK/PD simulations to be sufficient for complete equilibration between plasma and effect site, all experiments were performed again within the remaining 50 min (Level 2) before switching to the next higher concentration. This procedure was repeated twice with higher target alfentanil concentrations at effect site of 66.67 ng/ml (Level 3) and 100 ng/ml (Level 4). In the beginning (15th min), in the middle (40th min) and at the end of each Level (65th min), a venous blood sample was collected to a Na-EDTA tube for analysis of alfentanil plasma concentrations. The blood samples were kept on ice until the end of the study day and were then immediately centrifuged at 3,000 rpm for 10 min. The plasma was frozen at -78°C pending further analysis. During the study day participants were rested in a comfortable position and the subjects were under constant medical supervision. Medical symptoms reported by the subjects and the occurrence of vomiting were recorded (2.5.5). Intake of alcoholic beverages was prohibited for 24 h and intake of food for 6 h prior to experiments. The subjects were under continuous medical supervision throughout

the study day. Heart rate, respiration frequency and blood oxygenation were monitored using a pulseoxymeter. The subjects remained at the laboratory for at least another 2 hours after the end of infusion. All subjects completed a training session prior to the actual study occasion.

The aim of the study was to assess the consequences of the *OPRM1* 118G allele for the therapeutic range of alfentanil, rather than to establish a gene dose effect. A group size of six was obtained by case number calculations based on previous data [60] and on a statistical power of 0.8. For safety, the group size was defined at 10. Since we did not find more than six homozygous carriers of the variant 118G allele who consented into participation in the study, we recruited four heterozygous carriers to match the recruited ten controls. The study population was then separated into three genetic groups (118AA, 118AG, 118GG). The 118AA group consisted of homozygous carriers of the 118AA allele (five women, five men, mean age = 28.8 years, mean BMI = 22.0), the 118AG group (three women, one man, mean age = 24.0 years, mean BMI = 21.3) consisted of heterozygous carriers and the 118GG group (two women, four men, mean age = 28.4 years, mean BMI = 26.1) consisted of homozygous carriers of the 118GG allele variant (Proportion of female/male between groups: Fishers exact test p=0.63; BMI: Kruskal-Wallis test (AA vs. AG vs. GG) p=0.39, Wilcoxon test (AA vs. AG/GG) p=0.31). All subjects were unaware of their *OPRM1* genotype.

2.5   Assessment of opioid effects in healthy humans

2.5.1   Administration of alfentanil by computerized infusion

In both clinical trials described in this thesis, the participants received in an open-label fashion an intravenous infusion of alfentanil hydrochloride (Rapifen®, JANSSEN-CILAG GmbH, Neuss, Germany). Alfentanil was chosen because of its fast equilibration between plasma and effect site, the central nervous system (CNS), which allows to consider the plasma concentrations as being similar to the brain concentrations after 5 min equilibration time ($t_{1/2,ke0(Alfentanil)}$ = 0.6-1.2 minutes; [61]). In addition, the fast equilibration between plasma and brain and the short time of alfentanil action allowed for keeping the duration of the experiments short and ensured quick recovery of the subjects from the opioid effects after the end of the alfentanil infusion. To maintain a constant alfentanil concentration at the effects site, alfentanil was administered by means of computerized infusion using STANPUMP program ([62] freely available from Steven L. Shafer, MD at http://anesthesia.stanford.edu/pkpd) with Scott's pharmacokinetic

parameters for alfentanil (weight adjusted; [61]) and the Harvard pump 22 (Instech Laboratories, Plymouth Meeting, PA, USA).

2.5.2   Analysis of alfentanil plasma concentrations

To assure that all subjects received similar treatment, drug plasma concentrations were determined by means of liquid chromatographic tandem mass spectrometric (LC-MS/MS). In addition, analysis of the drug plasma concentrations allowed for pharmacokinetic-pharmacodynamic modelling (PK-PD modelling, chapter 2.7.3). Therefore, venous blood samples (4 ml) were collected into Na-EDTA tube at predefined time points. After centrifugation at 4000 min^{-1} for 10 min, plasma was separated and deep frozen at -78°C pending further analysis. Alfentanil (Janssen-Cilag, Neuss, Germany) was extracted by protein precipitation using fentanyl (Janssen-Cilag, Neuss, Germany) as internal standard. Therefore, 20 μl human plasma was thoroughly mixed with 20 μl fentanyl-solution (12 ng/ml in acetonitrile), 50 μl acetonitrile and 200 μl methanol. Calibration standards were prepared in the same manner with blank human plasma (Blutspendedienst Hessen, Frankfurt am Main, Germany), but instead of 50 μl acetonitrile, 50 μl of standard solution in acetonitrile was used. The samples were centrifuged for 5 min at 10,000 g and 20 μl of the supernatant was diluted with 200 μl acetonitrile/formic acid (100:0.25, v/v). After another 5 min of centrifugation at 10,000 g, 100 μl of the solution was transferred to glass vials (Macherey-Nagel, Düren, Germany) prior to injection into the LC-MS/MS system. The LC-MS/MS system consisted of an API 4000 triple-mass spectrometer (Applied Biosystems, Darmstadt, Germany) equipped with a Turbo-V-source operating in positive ESI mode, an Agilent 1100 binary HPLC pump and degasser (Agilent, Böblingen, Germany) and a HTC Pal autosampler (Chromtech, Idstein). For the chromatographic separation an Alltima HP HILIC column and precolumn were used (50 x 2.1 mm I.D., 3 μm particle size from Alltech, Unterhaching, Germany). Mobile phase was acetonitrile/water/formic acid (90:10:0.25, v/v/v), flow rate was 700 μl/min and total run time 2.5 min. Injection volume of samples was 20 μl. Retention time of alfentanil and fentanyl was 1.16 min and 1.03 min, respectively. HPLC-solvents were of HPLC-quality (Merck KgaA, Darmstadt, Germany). Multiple reaction monitoring (MRM) was used for quantification. The mass transitions used were *m/z* 417 → *m/z* 268 for alfentanil and *m/z* 337 → *m/z* 188 for fentanyl. Quantitation was performed with Analyst Software V1.4 (Applied Biosystems, Darmstadt, Germany) using the internal standard method (isotope-dilution mass spectrometry): Ratios of alfentanil and fentanyl peak area were plotted against concentration. Lower limit of quantification of alfentanil was 0.1 ng/ml (14 fg on col-

umn). Accuracy of the method over the calibration range (0.1 to 500 ng/ml) was 100.01 ± 5.98 % (n = 8).

2.5.3 Assessment of pain

2.5.3.1 Transcutaneous electrical stimulation

2.5.3.1.1 Procedure

Short electrical stimuli (2 sec) of increasing intensity were applied to the subjects´ left forefinger. Therefore a constant current device (NEUROMETER CPT, Neurotron Inc., Baltimore, MD, USA) with a maximum output of 20 mA was used to administer painful electrical 5Hz sine wave pulses via two gold electrodes placed on the medial and lateral side of the distal phalangeal joint (middle finger of the left hand as default-testing site). The electrical stimulus has been shown to primarily activate C-fibers (Kiso et al. 2001; Lötsch and Angst 2003).

2.5.3.1.2 Psychophysical quantification of pain and analgesia

To assess each individuals pain tolerance threshold after electrical stimulation, i.e. the electrical current when the subjects pain experience changes from tolerable to intolerable, the stimulation started with an electrical current known not to be painful, whereas stimulus intensity varied randomly between 1.2 mA and 2.8 mA. The current was then further increased in an ascending staircase design until the subjects reported to feel pain (**Figure 5**). The magnitude of subsequent stimuli was determined by the subject's response to the two preceding stimuli. If a subject's response to two preceding stimuli was "no pain – no pain" or "pain – pain" the next stimulus was equal to the magnitude of the last delivered stimulus plus or minus 130% of the difference between the last and the second last stimulus, respectively. If a subject's response to two preceding stimuli was "no pain – pain" or "pain – no pain" the next stimulus was equal to the magnitude of the second last stimulus plus 75 or 25% of the difference between the last and the second last stimulus, respectively. The purpose of the outlined algorithm was to increase or decrease the magnitude of delivered stimuli quickly as long as a subject gave a uniform response, i.e., "no pain" or "pain". Whenever a subject changed the response from "no pain" to "pain" or from "pain" to "no pain", the outlined algorithm allowed the magnitude of stimuli evoking a change in response at a higher resolution. Subsequently, the pain threshold was obtained from 10 stimuli by logistic regression of "pain" or "no pain" (corresponding to "0" or "1") versus the intensity of the electrical current. The interstimulus interval was approximately 30-60 sec. After opioid administration an increase of the pain tolerance threshold is

expected, indicating analgesic opioid effects. This pain model has been repeatedly demonstrated to be suitable to quantify the analgesic effects of opioids such as hydromorphone [63], morphine [64], remifentanil [36], or alfentanil [65].

Figure 5: Electrical pain model. The subjects received a 5 Hz sine waves pulses with a length of two seconds in the range from 0-20 mA intermitted by short breaks of approximately 30-60sec. The amount of the electrical current was increased until the subject described the stimulus as painful. Subsequently, the current is decreased until the subject describes the stimulus as non painful. Whenever a subject changes the response from "no pain" to "pain" or from "pain" to "no pain", the outlined algorithm allows the magnitude of stimuli evoking a change in response at a higher resolution. Subsequently, the pain threshold was obtained from a maximum of 10 stimuli by logistic regression of "pain" or "no pain" (corresponding to "0" or "1") versus the intensity of the electrical current.
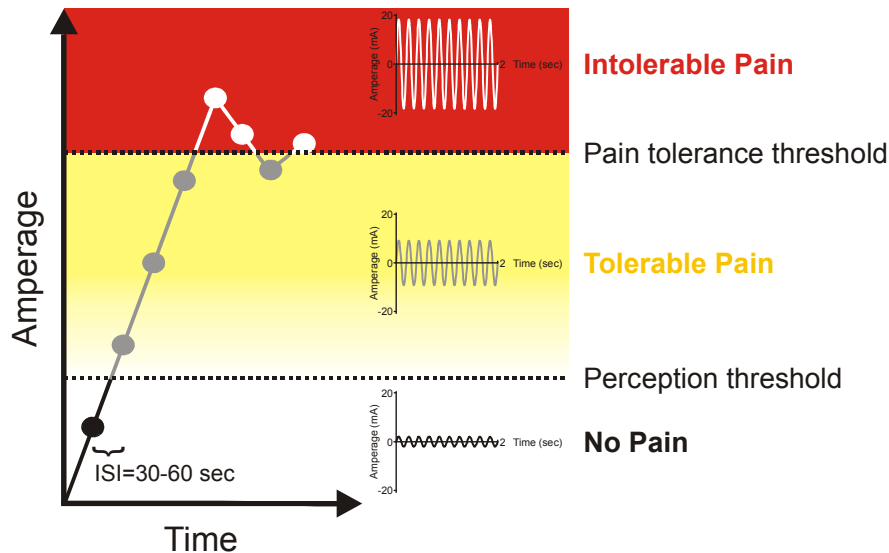
2.5.3.2 Painful gaseous carbon dioxide stimuli applied to the nasal mucosa

2.5.3.2.1 Procedure

In this pain model, short pulses of gaseous carbon dioxide (CO_2) were applied to the subjects´ nasal mucosa of the right nostril (**Figure 6**). A special device (Olfactometer OM/2, Burghart Instruments, Wedel, Germany) allows for precise control of the concentration and duration of the rectangular CO_2 stimuli [66]. The CO_2 pulses evokes pain with a stinging character and have been shown to excite trigeminal A_δ-fibers, with co-activation of trigeminal C-fibers [67] via a local pH decrease and stimulation of vanilloid receptors (TRPV1) [68] that are expressed in trigeminal sensory neurons projecting to the nasal mucosa. The nociceptive specificity of the chemical pain stimuli is supported by the localization of the cortical generators of the resulting

nociceptive event related potentials (ERPs) in the somatosensory area S_{II} [69], which is considered to be a primary projection area for nociceptive afferents [7]. To maintain the nociceptive specificity of the CO_2-stimuli, concomitant alteration of mechanical or thermal conditions at the mucosa is avoided by embedding the CO_2-pulses in a constantly flowing air stream (8 l/min) with controlled temperature and humidity (36.5°C, 80 % relative humidity). This carrier stream is led to the right nasal cavity via a thin Teflon tube with an outer diameter of 1.5 mm. This pain model has repeatedly been demonstrated to reliably and sensitively quantify the analgesic effects of opioids such as fentanyl [70], alfentanil [65] or morphine [36].

Figure 6: CO_2 pain model. Flow schema of the air stream between two CO_2 stimuli (left side) and during application of a stimulus.

No Stimulus CO_2 Stimulus
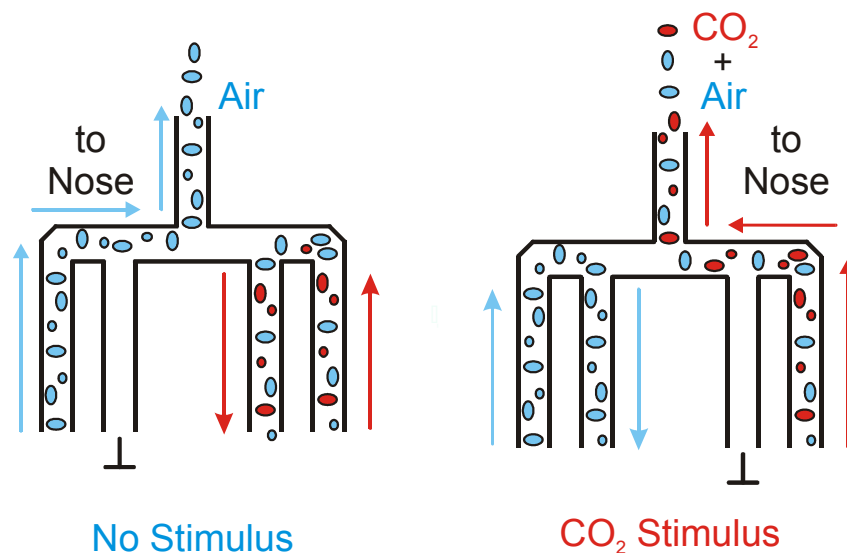
2.5.3.2.2 Psychophysical quantification of pain and analgesia

The painful CO_2 pulses were rated by means of a visual analogue scale (VAS) ranging from zero ("no pain") to 100 ("severe pain"). Prior to the experiment, subjects received 10 CO_2 pulses of five different concentrations (46, 53, 65, 68, 73% v/v). Since the highest technical possible CO_2 concentration is still perceived as only moderate painful by the most subjects, subjects were told that they should rate the lowest concentration (46% v/v) as zero ("no pain") and the highest concentrations (73% v/v) as 100 ("severe pain"). During the experiment, between two stimuli the subjects had to perform a tracking task on a video screen (**Figure 7**). Within 3-4 sec after the presentation of each CO_2 stimulus, a visual analogue scale was displayed on the video screen and subjects estimated the pain intensity relative to the presented concentrations prior to the experiment. The visual analogue scale appeared as a horizontal bar without numbers.

The length of this bar was manipulated by the subjects by means of a joystick. After opioid administration, an decrease of the ratings is expected indicating analgesic opioid effects

Figure 7: Tracking task and visual analogue scale. The tracking task was presented in the interval between two CO_2 stimuli. The green square was constantly moving in random directions on the screen and the subjects were instructed to keep the red square within the green square by joystick movements. Three to four seconds after a CO_2 stimulus, the video screen displayed a green visual analogue scale with a white bar. By moving the white bar the subjects indicated the magnitude of their pain experience during the last presented stimulus. After the rating, the video screen continued to display the tracking task.
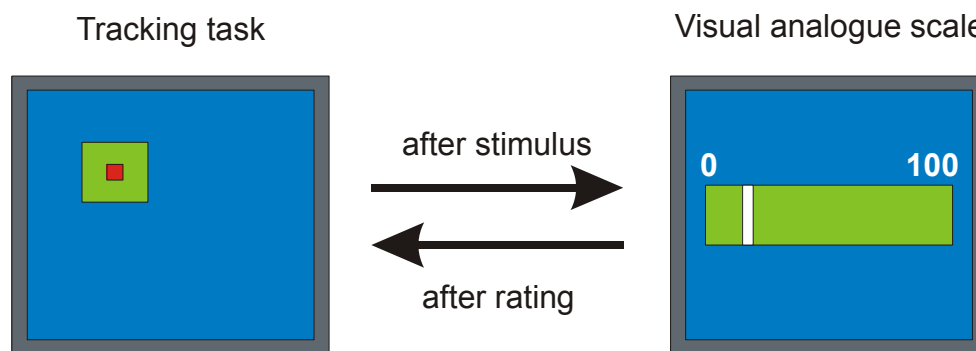
2.5.3.2.3 Quantification of pain and analgesia by means of functional magnetic resonance imaging (fMRI)

In addition to the psychophysical methods, functional magnetic resonance imaging (fMRI) was used to study the cerebral pain network during painful stimulation (**Figure 8**). By means of fMRI it is possible to record event related activation of brain regions, e.g. brain activation due to the nociceptive stimulation by CO_2. The ability of fMRI to measure brain activity is based on the increase of the blood flow to local vasculature after an increase of oxygen consumption that accompanies neural activity in the brain. This increase of blood flow occurs with a delay of approximately one to five seconds after neuronal activation and rises to a peak over four to five seconds before falling back to baseline levels. This results in a corresponding local reduction of deoxyhemoglobin as the increase in blood flow occurs without an increase of similar magnitude in oxygen extraction. Since deoxyhemoglobin is paramagnetic, it alters the T2* weighted magnetic resonance imaging signal [71, 72]. Thus, deoxyhemoglobin is referred to as an endogenous contrast enhancing agent. The mechanism is an indirect measure for neuronal activity and is called the blood-oxygenation level dependent effect (BOLD-effect). The magnetic field is generated by a MRI scanner. The MRI scanners have a typical magnetic field strength

of 0.3 to 3.0 tesla (T), which is approximately 6,000 to 60,000 times greater than the earth magnetic field.

Figure 8: Funtional magnetic resonance imaging. Upper left picture presents the average increase of blood flow or MRT signal with time (blue line, grey dots present the single events), respectively, of a brain region with event related neuronal activity after a specific stimulus (red). The other pictures present a sagittal (upper right), horizontal (lower left) and frontal (lower right) slice of subjects with painful CO_2 stimulus related increase of neuronal activity in the insular cortex and cingular cortex, respectively, indicated by the yellow areas in the slices.
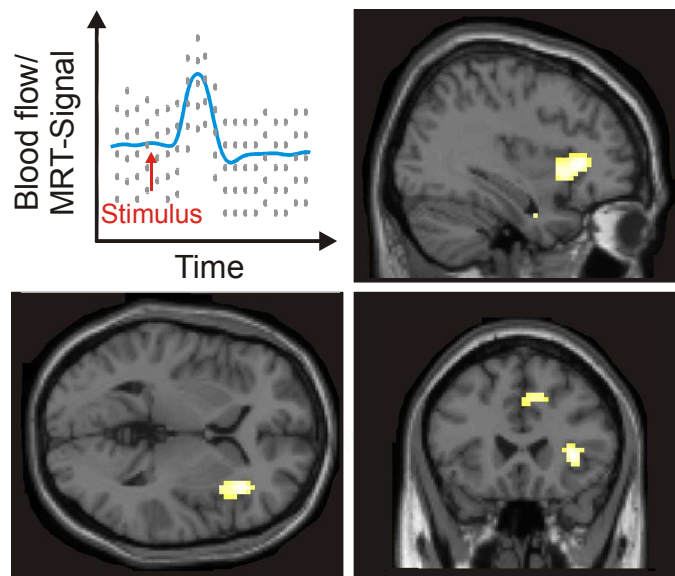
Brain activation of subjects was recorded while they received painful CO_2 stimuli. Functional activity of the brain determined from the magnetic resonance signal has been repeatedly used to determine brain areas involved in the processing of pain [9]. In addition, it has been shown to reliably assess the effects of morphine [73] and remifentanil [74] on pain related brain activation. After opioid treatment, a decrease of the pain related activation in the pain processing areas is expected. A 3.0 T magnetic resonance head scanner (Siemens Magnetom Allegra, Siemens AG, Erlangen, Germany) equipped with a 4-channel head coil was used to investigate pain related brain activation. The blood-oxygenation level dependent (BOLD) response to painful CO_2 stimuli was recorded by employing an event-related design, which means that acquisition and stimulus application were synchronized (**Figure 9**). Imaging parameters of the employed gradient echo EPI sequence were: parallel imaging method: GRAPPA (reduction factor R = 2), TE/TR 30 ms/1530 ms, FA 90°, 29 slices, distance factor 40%, matrix size 64x64, voxel size 3x3x3 mm. Additionally, a magnetic field mapping was performed with the identical slice posi-

tions and geometric parameters, and then used for an offline correction of distortions of the echo-planar images resulting from inhomogeneities of the B0 field [75, 76].

Figure 9: Paradigm of CO_2 stimulus-correlated functional magnetic resonance imaging (fMRI). Before alfentanil administration and at each alfentanil concentration level, 24 specific nociceptive stimuli, consisting of short (300 msec) pulses of gaseous carbon dioxide (CO_2; 66% v/v) were delivered to the nasal mucosa of the right nostril. To avoid adaptation and habituation to the pain stimuli, an interstimulus interval of 26 sec was used [58]. In each session 392 volumes were acquired which took about 10 min.

24 CO_2 stimuli
Interstimulus intervall: 26 sec
Length of stimulus: 300 msec
66% v/v CO_2

▶ 10 min

392 fMRI recordings
Repetition time: 1.53 sec
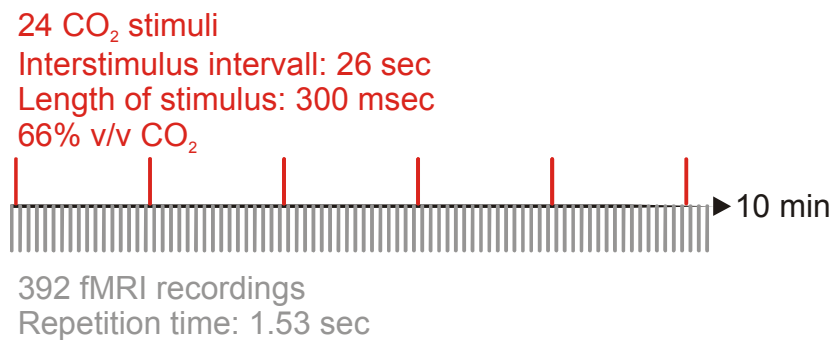
2.5.4 Assessment of respiratory depression

2.5.4.1 Provoking hyperventilation by means of CO_2 re-breathing

Respiratory depression was assessed by means of CO_2 re-breathing. The CO_2 re-breathing was executed according to Read´s method [77] with slight modifications. The subjects were instructed to re-breathe into a plastic bag connected to a special device (Oxycon Pro, Jaeger, Hoechberg, Germany) that continuously records the minute expiratory volume (V_{Emin}), end-tidal CO_2 levels (pCO_2) and ventilatory rate. The re-breathing leads to an increase of the CO_2 concentration in the plastic bag and as a consequence in the lungs and the body fluids. The progressive rise of the CO_2 concentration in the body fluids due to the continuing metabolism results in an activation of chemoreceptors in the respiratory center. Thus, breathing is further stimulated, finally resulting in hyperventilation, which is indicated by an increase of the minute expiratory volume (V_{Emin}). To prevent the development of any hypoxic stimulus to the ventilation [77], the plastic bag was enriched with oxygen (O_2). The high initial O_2 concentration in the re-breathing bag provides enough O_2 for metabolism. The slope of the linear relationship between the $V_{E[min]}$ and pCO_2 ($\frac{\Delta y}{\Delta x}$; **Figure 10**) is defined as the primary target parameter for the quantification of the respiratory depressive effect. In addition, another reliable parameter is

the expiratory volume per minute at a CO_2 concentration of 55 mmHg ($V_{E(55mmHg\ pCO2)}$), which can be calculated from the slope and intercept of the obtained linear relationship between expiratory volume and CO_2 concentration [78]. While changes in the x- and y- intercepts can be misleading and therefore should not be used as parameter, a decrease in the slope and $V_{E(55mmHg\ pCO2)}$ can be considered as a reliable indication for respiratory depression during opioid treatment. This method has repeatedly demonstrated to reliably asses the respiratory depressive effects of morphine [60, 79].

Figure 10: Assessment of the respiratory depression by means of CO_2 re-breathing. Fictitious data acquired during a typical CO_2-rebreathing test. The minute expiratory volume V_E rises with increasing CO_2 concentration (dots). Data is analyzed by fitting a linear equation to the data. Respiratory depression is indicated by a decrease of the slope of the linear relationship or a decrease of the minute expiratory volume at a CO_2 concentration of 55 mmHg ($V_{E(55mmHg\ pCO2)}$).
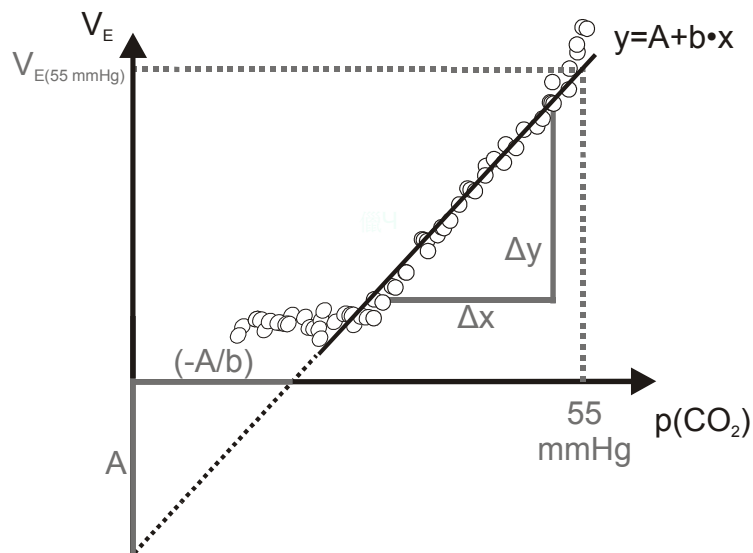
2.5.4.2 Monitoring of spontaneous respiration

Additionally, opioid induced respiratory depression was measured by analyzing changes of the frequency of spontaneous breathing. Therefore, a respiratory belt transducer (MLT1132 Piezo Respiratory Belt transducer, ADInstruments GmbH, Spechbach, Germany; **Figure 11**) was fastened around the subject's upper abdomen and connected to an integrated data recording unit featuring a built-in amplifier (Powerlab 4/25T, ADInstruments GmbH, Spechbach, Germany). The subjects were instructed to remain silent, while recording their respiratory frequency for a period of 10 min, during which slow music was played and the laboratory was otherwise

kept completely silent. The first three and the last minute were rejected from analysis. Respiratory depression is indicated by a decrease in the respiratory frequency (Breaths/minute).

Figure 11: Monitoring of spontaneous respiration. Fictitious data acquired during the experiment. Each peak represents a single breath. Results were presented as number of breaths per minutes.
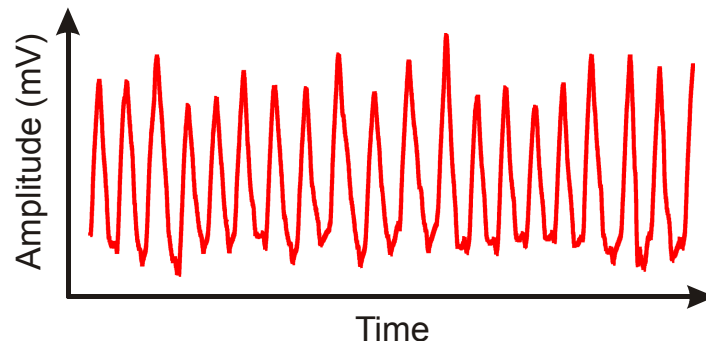
2.5.5 Assessment of opioid related medical symptoms

Medical symptoms reported by the subjects and the occurrence of vomiting were recorded by the investigator. Opioid related side-effects such as tiredness, sickness, drowsiness, euphoria, vertigo, and itching were rated by the subject using visual analogue-scales (VAS, length 100mm ranging from 0="no such symptom" to 100="symptom experienced at maximum").

2.6 Assessment of µ-opioid receptor expression and function in *post mortem* human brain tissue

2.6.1 *OPRM1* mRNA expression analysis

OPRM1 mRNA expression was assessed by means of real-time PCR (rt-PCR). Therefore, messenger-RNA (mRNA) was isolated from tissue by means of the EZ1 RNA Universal Tissue Kit (Qiagen, Hilden, Germany). After reverse transcription of RNA (30 ng/µl) using random hexamers and the High capacity cDNA Archive Kit (Applied Biosystems, Darmstadt, Germany), rt-PCR was performed with 50 ng RNA-equivalent in triplicates using the Taqman Universal PCR Master Mix without Amperase® UNG and the validated TaqMan® gene expression assay for the *OPRM1* gene (Hs00168570_m1, Applied Biosystems, Germany). This generated an amplicon of 67 base pairs (bp) corresponding to the NM_000914.2 transcript (http://www.ncbi.nlm.nih.gov/entrez/viewer.fcgi?val=NM_000914.2). The *ACTB* (β-Actin) RNA was employed as endogenous housekeeping gene (Hs99999903_m1, Applied Biosystems,

Germany) generating a 171 bp long amplicon from the NM_001101.2 transcript (http://www.ncbi.nlm.nih.gov/entrez/viewer.fcgi?val=NM_001101.2). Quantification of mRNA was conducted on a Taqman 7900HT platform (Applied Biosystems, Darmstadt, Germany) by IMGM Laboratories GmbH (Gene Expression Center Martinsried, Martinsried, Germany). From raw fluorescence data, a threshold cycle value, Ct, corresponding to the cycle number at which the fluorescence signals of the reporter dye passed a fixed threshold (ten standard deviations from the baseline) on the amplification plot was obtained for each sample (Sequence Detection Software, SDS version 2.0; Applied Biosystems). This ensured that the Ct value was proportional to the number of RNA copies present at the start of the PCR. Negative controls showed no amplification in the range of Ct < 40 indicating the absence of cross-contamination and unspecific amplification of primer or sensor dimers. *OPRM1* mRNA expression was determined using the comparative Ct method as described by

$$OPRM1-2\ mRNA_{\text{expression}_{\text{relative}}} = 2^{(-\Delta\Delta Ct)}$$
$$\Delta\Delta Ct = \left(Ct_{sample} - Ct_{reference}\right)_{Ct_x} - \left(Ct_{sample} - Ct_{reference}\right)_{Ct_{control}}$$

Equation 1,

where Ct_{sample} and $Ct_{reference}$ stand for the Ct values for the *OPRM1* and *ACTB* mRNA samples, respectively, being the respective means of three analysis repetitions from control and the sample of interest. To test whether *OPRM1* mRNA expression differed between genotypes and brain regions, a sample with the Ct value closest to the median of the Ct values of the secondary somatosensory cortex S_{II} of the wildtype group was chosen to serve as $Ct_{control}$.

2.6.2 Tissue preparation for binding assays

Tissue samples (1-1.5 g) were homogenized with a fast rotating Ultra-Turrax (Janke & Kunkel GmbH, Staufen i. Breisgau, Germany) in 10-15 volumes of homogenization buffer (10 mM Tris-HCl pH 7.4, 290 mM D(+)-Saccharose). The crude tissue lysate was immediately centrifuged at 1,000×g at 4°C for 15 min and the supernatant recentrifuged at 45,000×g, 4°C for 45 min. The pelleted proteins were resuspended in ice-cold isolation medium (50 mM Tris-HCl pH 7.4) and used for experiments or stored at -80°C.

2.6.3 Protein concentration analysis

Protein concentrations were measured by the method of Bradford [80]. 10 µl of the membrane suspensions were diluted in water to a final volume of 100 µl. 10 µl of the resulting dilution were transferred into a 96 well plate. Subsequently, 190 µl of Bradford reagent were add-

ed to each well. Within 5 to 15 minutes the absorption at 595 nm was measured. The amount of protein in each sample was calculated by means of a concomitantly measured calibration curve of in water diluted bovine serum albumine (BSA) in the concentration range of 0 to 7 ng/ml. The protein concentrations of the membrane suspensions of the brain samples were usually between 1.4 and 7.8 ng/ml.

2.6.4   [³H]-DAMGO binding assays

2.6.4.1 Saturation binding

The µ-opioid receptor affinity (K_D) and µ-opioid receptor density (B_{Max}) of the secondary somatosensory S_{II} and lateral thalamus were assessed by measuring the saturation binding of the µ-opioid receptor specific radioligand [³H]-DAMGO (Perkin Elmer Life Sciences Inc., Boston, MA, USA). To determine the total binding of [³H]-DAMGO to the membrane proteins, equal volumes of membrane proteins (25 µl) were diluted in a final volume of 250 µl assay buffer (50 mM Tris-HCl pH 7.4) and incubated with at least 10 different concentrations of [³H]-DAMGO in the range of 0.07 nM – 14.42 nM. In addition, to determine the non-specific binding of [³H]-DAMGO to the membrane proteins, equal volumes of membrane proteins were incubated with 0.07 nM and 14.42 nM [³H]-DAMGO, respectively, in the presence of 10 µM naloxone (Naloxon-Curamed, Curamed, Karlsruhe, Germany). K_D([³H]-DAMGO) and B_{Max}([³H]-DAMGO) were calculated by non-linear regression of the specific binding according to the equation:

$$B([^3H]-DAMGO) = \frac{B_{Max}([^3H]-DAMGO) \times F([^3H]-DAMGO)}{(K_D([^3H]-DAMGO) + F([^3H]-DAMGO))}$$

Equation 2,

where B([³H]-DAMGO) is the concentration of µ-opioid receptor bound [³H]-DAMGO (specific binding), F([³H]-DAMGO) the concentration of the free [³H]-DAMGO, B_{Max}([³H]-DAMGO) the maximum number of [³H]-DAMGO binding sites (µ-opioid receptor density) and K_D([³H]-DAMGO) the equilibrium dissociation constant of [³H]-DAMGO. Specific [³H]-DAMGO binding to the membranes was calculated by subtraction of non-specific binding from total binding.

2.6.4.2 Displacement binding

In addition, the ability of the µ-opioid receptor agonists morphine, morphine-6-glucuronide (M6G), alfentanil, methadone and human β-endorphin to displace [³H]-DAMGO from the µ-opioid receptor in the secondary somatosensory area S_{II} was measured. Therefore, membrane proteins were incubated with increasing concentrations (0 nM–10 µM) of the unlabelled agon-

ists in the presence of 2.5 nM [³H]-DAMGO to determine the agonist concentration needed to displace half of the μ-opioid receptor bound [³H]-DAMGO, IC_{50}(Agonist).

Displacement binding data was normalized, whereas the zero percent value was obtained from incubation of 2.5 nM [³H]-DAMGO in the presence of 10 μM unlabeled agonist and 100 percent value was obtained from incubation with 2.5 nM [³H]-DAMGO in the absence of unlabeled agonist. The IC_{50}(Agonist) was determined using non-linear-regression according to the equation:

$$B\,([^3H]-DAMGO) = \frac{100}{1+10^{(\log IC_{50}(Agonist)-\log L\,(Agonist)}}$$

Equation 3,

where L(Agonist) is the competitor concentration, and B([³H]-DAMGO) is the associated binding rate of [³H]-DAMGO. Considering that the concentration and K_D of the radioligand affects the true position of the displacement binding curve, it is necessary to correct the IC_{50}(Agonist) values to obtain the radioligand independent inhibition constant K_I (Agonist) for the competitor. Thus, the obtained IC_{50}(Agonist) are corrected by the method of Cheng and Prusoff [81] according to the equation:

$$K_I(Agonist) = \frac{IC_{50}(Agonist)}{\dfrac{L_V([^3H]-DAMGO)}{K_D([^3H]-DAMGO)}+1}$$

Equation 4,

whereas L_V([³H]-DAMGO) is the concentration of [³H]-DAMGO (2.5 nM) and K_D([³H]-DAMGO) is the [³H]-DAMGO related equilibrium dissociation constant measured in the saturation binding experiment.

The experiments were carried out at a constant temperature of 25°C while shaking at 1,000 rpm (Thermomixer compact, Eppendorf, Hamburg, Germany). After an incubation period of 120 minutes, the membrane bound [³H]-DAMGO was separated from unbound [³H]-DAMGO by rapid filtration through Whatman GF/B filters (Whatman plc, Brentford, Middlesex, UK), followed by six washes with 1 ml of ice-cold assay buffer. The filters were transferred into vials (Zinsser Polyvials®, Zinsser Analytic GmbH, Frankfurt, Germany), filled with 5 ml of scintillation liquid (Quicksafe® A, Zinsser Analytic GmbH, Frankfurt, Germany) and the decays per minute (dpm) of the filter bound [³H]-DAMGO were counted by a Liquid Scintillation Analyzer (Packard Tri-Carb® 2100TR, Canberra-Packard Central Europe GmbH, Schwadorf, Austria).

2.6.5 [^{35}S]-GTPγS binding assays

The ability of DAMGO (Sigma-Aldrich, St. Louis, MO, USA) to activate intracellular μ-opioid receptor signaling was measured by means of the [^{35}S]-GTPγS binding assay. Therefore, membrane proteins (40 μg) of the secondary somatosensory cortex S_{II} and thalamus were diluted in a final volume of 250 μl assay buffer. The assay buffer contained 50 mM Tris pH 7.4, 100 mM NaCl, 0.2 mM EGTA, 3 mM MgCl$_2$, 1 mM DTT, 50 μM GDP, 0.5 nM [^{35}S]-GTPγS (Amersham Biosciences, Uppsala, Sweden) and increasing concentrations (0 nM–100 μM) of DAMGO. Following an incubation period of 120 min at a temperature of 25°C while shaking at 1,000 rpm, the reaction was terminated by rapid filtration through Whatman GF/B filters, followed by six washes with 1 ml of ice-cold washing buffer (50 mM Tris pH 7.4, 100 mM NaCl, 0.2 mM EGTA, 3 mM MgCl$_2$). Subsequently, filters were placed in scintillation vials containing 5 ml liquid scintillation cocktail and decays per minute (dpm) of the filter bound [^{35}S]-GTPγS were measured.

The basal binding of [^{35}S]-GTPγS without stimulation of DAMGO, B_0(DAMGO), the maximum binding of [^{35}S]-GTPγS after stimulation of DAMGO, B_{Max}(DAMGO), and the concentration of DAMGO needed to stimulate half maximal [^{35}S]-GTPγS binding, EC_{50}(DAMGO), were determined according to the equation:

$$B([^{35}S]-GTP\gamma S) = B_0([^{35}S]-GTP\gamma S) + \frac{B_{Max}([^{35}S]-GTP\gamma S) - B_0([^{35}S]-GTP\gamma S)}{1+10^{(\log EC_{50}(DAMGO)-\log L(DAMGO))}} \qquad \text{Equation 5,}$$

where L(DAMGO) denotes the DAMGO concentration and B([^{35}S]-GTPγS) the associated binding rate of [^{35}S]-GTPγS. Subsequently, DAMGO related net [^{35}S]-GTPγS binding per μ-opioid receptor, B_{Net}(DAMGO), was calculated according to the equation:

$$B_{Net}(DAMGO) = B_{Max}(DAMGO) - B_0(DAMGO) \qquad \text{Equation 6.}$$

For each brain region, the net effect of agonist binding per μ-opioid receptor was calculated as the quotient of the net DAMGO stimulated [^{35}S]-GTPγS binding data and the μ-opioid receptor density,

$$\frac{B_{Net}(DAMGO)}{B_{Max}([^{3}H]-DAMGO)} \qquad \text{Equation 7.}$$

This analysed whether the G-protein activation correlated with the respective μ-opioid receptor densitiy in the analysed brain region and allowed for comparison of the efficacy of μ-opioid receptor coupling to G-proteins between brain regions and genotype groups [82-84].

2.7 Data analysis

2.7.1 Investigation of pain-related brain activation during alfentanil administration in non-carriers and homozygous carriers of *OPRM1* 118A>G SNP

Spatial pre-processing and statistical analyses were performed using the statistical parametric mapping software SPM2 (Wellcome Department of Imaging Neuroscience, London, UK) [85, 86]. Data were corrected for acquisition time (slice timing), realigned to the first volume for motion correction [87], spatially normalized [88] to a standard EPI template [89], and smoothed using a 9 mm full width at half maximum isotropic Gaussian kernel. Data analysis employed voxel-wise estimation of regression coefficients according to the general linear model as implemented in SPM2 [87], where painful stimuli were modeled by the built in canonical hemodynamic response function. Low frequency fluctuations were removed with a high pass filter with a cutoff at 128 s. The single subject analyses resulted in a contrast image for each subject and each alfentanil brain concentration level. Subsequently, these contrast images were incorporated into a second level analysis of variance to assess the influence of the alfentanil brain concentrations on the brain responses to painful stimuli. In a first step, statistically significant pain-related brain activation at each alfentanil concentration level was tested with appropriate contrasts in non-carriers of SNP *ORPM1* 118A>G, setting the level of interest as 1 and the remaining levels to 0, e.g. main effects of level 0 tested by contrast (1 0 0 0 0), main effects of level 1 tested by contrast (0 1 0 0 0) and so forth. Subsequently, for analysis of the relation between alfentanil brain concentration and pain-related brain activation in wild-type subjects, the following contrasts were used: (1) A linear function (1.5 0.5 -0.5 -1.5 0), detecting brain regions with linear concentration-dependent alfentanil effects and (2) a step function (3 -1 -1 -1 0), detecting brain regions with non-concentration-dependent alfentanil effects. To illustrate brain regions displaying predominantly concentration-dependent or concentration-independent alfentanil effects, each contrast was exclusively masked by the other one at $p < 0.001$, uncorrected. In addition, contrast (1) was inclusively masked with contrast (2) allowing for detection of brain regions where the pain-related activation showed intermediate behavior. The resulting statistical parametrical maps of *t*- statistics were interpreted with regard to the probabilistic behavior of Gaussian random fields [90]. Results are only reported if they were at least significant at an FDR (False Discovery Rate) corrected level of $p<0.05$. In the second step, areas with significant alfentanil effects on pain related activation in non-carriers

of SNP *ORPM1* 118A>G were defined as regions of interest for the analysis of the pharmaco-genetic effects of SNP *ORPM1* 118A>G. Thus, activations in the regions of interest were corrected for multiple comparisons within a sphere of 15 mm radius (small volume correction). The influence of the SNP *ORPM1* 118A>G on the identified concentration-dependent alfentanil effects was analyzed using contrasts: 1.5 0.5 -0.5 -1.5 0 -1.5 -0.5 0.5 1.5 0, indicating levels 0 – 4 for non-carriers and levels 0 – 4 for carriers of SNP *ORPM1* 118A>G. Similarly, concentration independent effects were analyzed using the 3 -1 -1 -1 0 -3 1 1 1 0, again indicating levels 0 – 4 for non-carriers and levels 0 – 4 for carriers of SNP *ORPM1* 118A>G. Level 4 was excluded from alfentanil concentration effects analysis because it was only included in the experiment as additional measurement to demonstrate the reversibility of opioid effects. Therefore, level 4 is set to 0 in the alfentanil concentration effects analysis. Results were only reported if they were at least significant at an FDR (False Discovery Rate) corrected level of $p<0.05$. Localizations of significant results are reported as MNI (Montreal Neurological Institute) coordinates (mm).

2.7.2 Investigation of μ-opioid receptor expression and function in pain processing brain regions of non-carriers and carriers of *OPRM1* 118A>G SNP

Equations parameters (Eq 1 – 7) were fitted to the respective data separately for each subject (GraphPad Prism® 5, GraphPad Software, San Diego, CA, USA). Effects of *OPRM1* 118A>G SNP on $2^{-\Delta\Delta Ct}$, $B_{Max}([^3H]\text{-DAMGO})$, $K_D([^3H]\text{-DAMGO})$, $B_0(DAMGO)$, $B_{Max}(DAMGO)$, $B_{Net}(DAMGO)$, $EC_{50}(DAMGO)$ and on the quotient of DAMGO stimulated net $[^{35}S]\text{-GTP}\gamma S$ binding to μ-opioid receptor density ($B_{Net}(DAMGO)/B_{Max}([^3H]\text{-DAMGO})$) were analysed by means of multivariate analysis of variance for repeated measures (rm-ANOVA), with "region" (i.e., S_{II} or thalamus; degrees of freedom, df=1) as within-subject factor and "118A>G" (i.e., 118AA, 118AG, 118GG; df=2) as between-subject factor (SPSS 12.0.2, SPSS Inc., Chicago, IL, USA). The effects of the *OPRM1* 118A>G SNP on K_I (Agonist), were analysed by means of univariate analysis of variance with between-subject factors "agonist" (i.e., morphine, M6G, endorphin, methadone and alfentanil; df=4) and "118A>G" (i.e., 118AA, 118AG, 118GG; df=2). The α-level was set at 0.05. Post-hoc comparisons for statistical main effects were done by *t*-tests, with α-correction (Bonferroni) when indicated.

2.7.3 Investigation of the therapeutic range of alfentanil in non-carriers and carriers of *OPRM1* 118A>G SNP

To judge the consequences of the variant *OPRM1* 118G allele for the therapeutic range of alfentanil, the data were transformed into percent changes from baseline in order to compare the different measurements of analgesia and respiratory depression. As a precondition, the baselines were not permitted to differ between genotypes, which was true in our case (Kruskal-Wallis tests: p>0.1 for the baseline values of all pharmacodynamic measures). The subsequent analysis focused on the comparison of the relationship of these effects to the alfentanil plasma concentrations between different pharmacodynamic end points and of the consequences of the variant 118G allele for these relationships.

Simulations of the alfentanil concentrations at effect site based on published pharmacokinetic-pharmacodynamic parameters of alfentanil with a transfer-half-life between plasma and effect site of 1.1 min [61] had shown, that equilibration between effect site and plasma concentrations had been safely reached after 15 min. This was the latency after each change of alfentanil target concentrations before pharmacodynamic measurements started. In fact, simulations with STANPUMP had shown that less than two minutes were enough to reach the target concentration at effect site. Therefore, the effect versus concentration relationship could be confidently calculated using the alfentanil plasma concentrations. For analysis, effects of experiments between the two successive blood samples closest to the actual measurements were related to the average concentration calculated from these samples. For example, the average concentration of blood sample 1 (15th min) and 2 (40th min) was allocated to effects of transcutaneous electrical stimulation and CO_2 re-breathing in Level 2, which took place between the two blood samplings.

The relationship between the effects of alfentanil and its concentrations was described by a power model of

$$Effect \quad [\%] = a \cdot C^{\gamma}_{alfentanil} \qquad \text{Equation 8,}$$

whereas *a* denotes the slope and γ the shape factor of the concentration response relationship. A power model was preferred to a sigmoidal effect versus concentration relationship (i.e., an E_{max} model) because the complete theoretical sigmoidal shape was not observed during the study. In contrast, the pharmacodynamic measures did not come close to the maximum theoretical effect due to ethical considerations. That is, tolerance to electrical pain could have in-

creased far above the cut-off of 20 mA with very high alfentanil doses. Similarly, respiratory depression was only moderate because the healthy volunteers could not have been brought into danger. The theoretical maximum being apnoea, i.e., respiratory frequency of zero, was not possible to be achieved. Exceptions from this rule are the estimates of the pain intensity of the CO_2 stimuli, which could have reached zero. However, a sigmoid model provided no better fit than the power model, judged by goodness-of-fit assessment as explained later in this section and was therefore not used.

The pharmacokinetic-pharmacodynamic modeling was performed with NONMEM V (version 1.1, Globomax, Hanover, MD, USA). All concentration and effect data (separately for each particular pharmacodynamic effect) from all individuals were analyzed in one single step, however, without pooling the data but maintaining individual assignment for each data point to allow for assessment of the parameter values and their interindividual variability in one single step as being the standard procedure of population pharmacokinetic-pharmacodynamic modeling [91]. The modeling process repeatedly employed goodness-of-fit procedures, which were (i) the NONMEM objective function being minus two times the log likelihood (-2LL) and the χ^2 approximation with the number of degrees of freedom equal to the difference in the number of terms between two models (α-level 0.05), (ii) the median absolute weighted residuals, calculated as (*measured – predicted) / predicted*, and the mean of the individual mean absolute weighted residuals, and (iii) visual inspection of the fits versus observed data. Log-normally distributed interindividual variance of the slope parameter *a* was used: $P_i = \theta_{i,TV} \cdot e^{\eta_i}$, where P_i is the value of the parameter of the individual, $\theta_{i,TV}$ is the typical value *(TV)* of this parameter in the population, and η is a variable accounting for the interindividual variability, with mean zero and variance ω^2. Normally-distributed interindividual variance of the shape parameter γ was used: $P_i = \theta_{i,TV} + \eta$. Interindividual variability was assigned to parameters of the final model in case that this improved the fit. The residual error ε was modeled using an additive error model. Proportional or combined proportional and additive error models resulted in worse fits or impossibility to obtain a fit and were therefore rejected. Calculations were performed using "first order conditional estimation" and "η-ε interaction". Ninety-five percent confidence intervals of parameter values were calculated from 200 runs of each of the four models for each effect measure (see below) with data sets that were obtained by Bootstrap resampling from the original data set [92], using Wings for NONMEM (N. Holford, Auckland, NZ

[93]; http://wfn.sourceforge.net/index.html). The 95% confidence intervals of the parameter values were obtained as the 2.5[th] and 97.5[th] percentiles of the results of the 200 model runs.

The influence of the *OPRM1* 118G SNP on the model parameters was assessed as follows: First, it was checked whether a particular parameter varied interindividually. If this was found to be the case, which was true for the slope parameter *a* (Equation 1), it was assessed whether the variability was partly explained by the presence of the 118G allele. This was done by multiplying the model parameter found to exhibit interindividual variability with 1 in case of wild-type, with a factor θ_1 in case of the presence of the 118G allele (i.e., genotype 118AG and 118GG). The alternatives were multiplying the model parameter with 1 in case of wild-type and heterozygous carriers of the 118G allele (i.e., genotype 118GG), or multiplying the model parameter with 1 in case of wild-type, with a factor θ_1 in case of heterozygous presence of the mutation, and with a factor θ_2 in case of homozygous presence of the mutation. The final model was identified on the basis of goodness-of-fit assessment as described above. Thus, identification of a pharmacogenetic influence of the *OPRM1* 118A>G SNP was based on the likelihood ratio test. This test compares the NONMEM objective functions being minus two-times the log likelihood (-2LL) between two models, i.e. the reduced and the full model. The reduced model in the present context contains only one parameter *a* for the slope of the linear effect vs. concentration relationship for all genotypes (Equation 1). The full model contains in addition the factors θ_1 and θ_2. The likelihood ratio test focuses on the difference between the values of -2LL using the χ^2 approximation with the number of degrees of freedom equal to the difference in the number of terms between two models. We tested whether introduction of one or two additional parameters (θ_1 and θ_2.) into the model provided a statistically significant improvement of the fit of the data. For one parameter, statistical significance was reached at an α-level of 0.05 when the introduction of one parameter into the model resulted in a decrease in -2LL by ≥3.84, and at an α-level of p=0.01 when -2LL decreased by ≥6.63. For two parameters the respective reductions in -2LL were ≥5.99 and ≥9.21 for α-levels of 0.05 and 0.01, respectively. This is a standard procedure in population modeling with NONMEM [91]. In addition to the *OPRM1* 118A>G SNP, influences of the subjects' sex were analyzed analogously.

Based on the identified models, the alfentanil concentrations required for 50% analgesia or 50% change in parameters of respiratory depression were calculated for the identified groups with respect to the 118A>G polymorphism.

Comparisons of the body mass index, alfentanil doses, frequency of vomits or magnitude of other medical symptoms, and of the gender distribution among *OPRM1* genotypes were performed using Kruskal-Wallis tests, Wilcoxon signed rank tests or the Fisher's exact test, where appropriate. These additional statistics were performed using the SPSS statistical software (version 12.0.2, SPSS Inc., Chicago, IL, USA).

3 Results

3.1 Pain-related brain activation in non-carriers and homozygous carriers of *OPRM1* 118A>G SNP during alfentanil administration

3.1.1 Pain-related brain activation in non-carriers of SNP *ORPM1* 118A>G

Pain-related activation was detected in non-carriers of the SNP *ORPM1* 118A>G bilaterally in the insular cortex (x, y, z (mm), -30, 18, 9 and 36, 24, 6 at the left and right hemisphere, respectively), the primary somatosensory area S_I (x, y, z, -63, -18, 21 and 63, -18, 24, respectively), the secondary somatosensory area S_{II} (x, y, z, -57, 0, 12 and 60, -15, 21, respectively), the parahippocampal gyrus, amygdala and superior temporal gyrus (temporal pole) (x, y, z, -21, 3, -15 and, 36, 6, -15, respectively), the anterior cingulate cortex (x, y, z, -6, 6, 42 and 6, 15, 39, respectively), and the supplementary motor area (x, y, z, -6, 6, 45 and 6, 3, 63, respectively).

3.1.2 Effects of increasing alfentanil concentrations on pain-related brain activation in non-carriers of SNP *ORPM1* 118A>G

Stepwise increasing alfentanil concentrations led to a decrease in both, magnitude and extent (t-values and cluster size, respectively; **Figure 12** and **Table 2**), of pain-associated brain activation, up to an absence of activation at the highest alfentanil concentration level. This decrease in pain related brain activation was accompanied by a decrease in subjective pain perception (**Figure 12**; analysis of variance for repeated measures: p<0.001 for the within-subjects effect of "alfentanil concentration level"; α-corrected post-hoc t-tests indicating significant differences of concentration level 3 from concentration level 0 at p<0.01). With decreasing alfentanil concentrations at level 4, pain-associated activation reappeared in all brain regions, indicating that the decrease of activation during level 1 to 3 was opioid related.

Figure 12: Pain-associated brain activation at different concentrations of alfentanil in non-carriers of SNP *OPRM1* 118A>G. The glass brains show decreasing pain-associated brain activation (p<0.05 FWE corrected) with increasing alfentanil concentrations. The mean alfentanil plasma concentrations are given as thick solid lines below the glass brains, and the individual concentrations are indicated as dots connected with thin dotted lines. Decreasing pain-related brain activation with increasing alfentanil concentrations was associated with a reduction of the individual pain ratings, given at the bottom as bars. At the additional level 4 at 20 min after the alfentanil infusion was stopped, we observed partial restitution of pain related brain activation, associated with restitution of the painfulness of the stimuli.
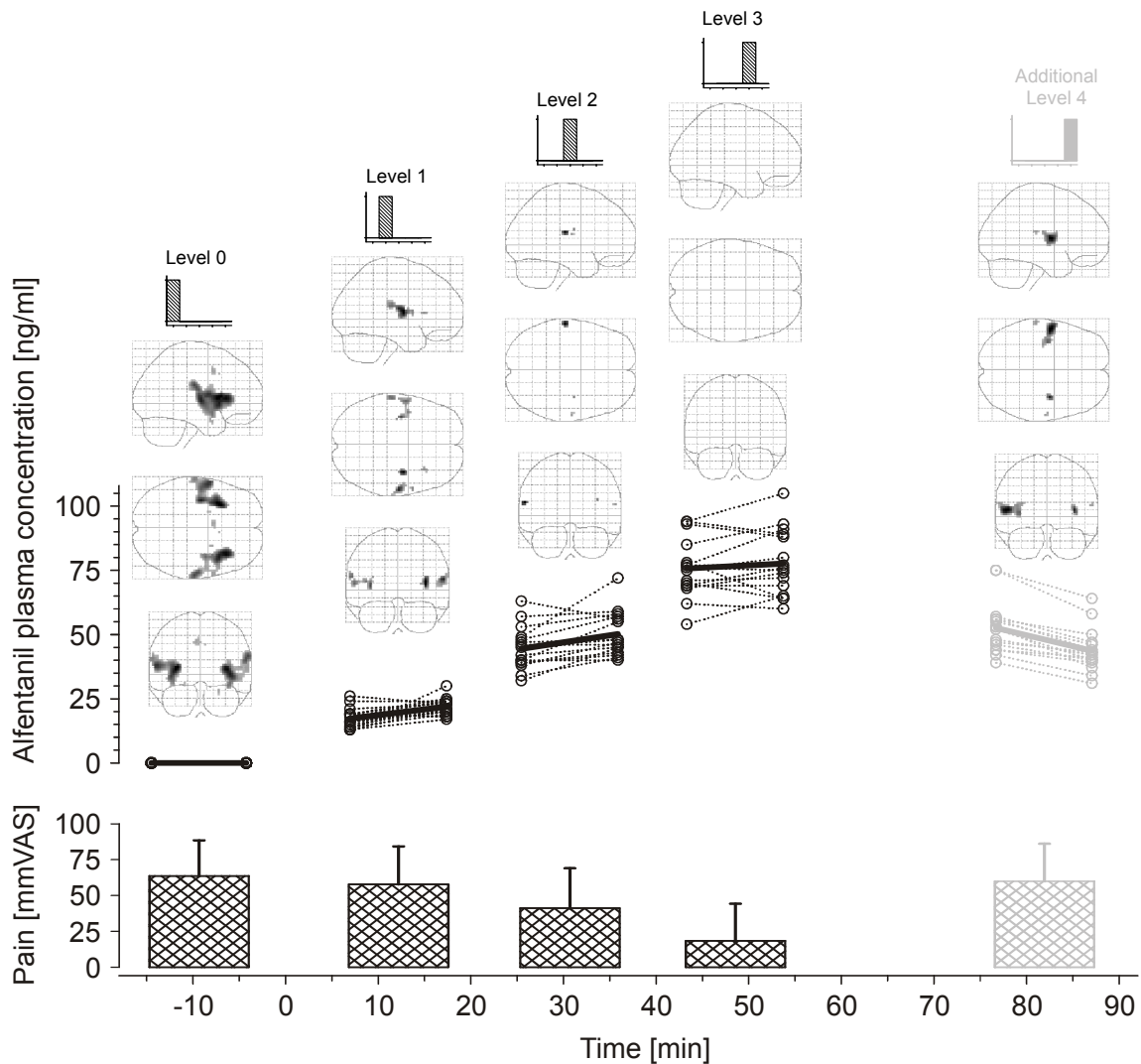
Table 2: Brain regions with pain-associated activation at different alfentanil concentrations in non-carriers of SNP *OPRM1* 118A>G. Pain-related brain activation observed at baseline (Level 0; 0 ng/ml Alfentanil) decreased with increasing alfentanil concentrations (Level 1 and 2; 47.2 and 76.6 ng/ml, respectively) until it vanished completely at the highest concentration of alfentanil (Level 3; 76.6 ng/ml). It reappeared after the end of infusion with decreasing alfentanil concentrations (Level 4; 47.8 ng/ml). Presented results are statistically significant at p<0.05, FDR corrected at voxel level (MNI: Montreal Neurological Institute; * p<0.05 FWE corrected at voxel level).

Anatomic location		MNI coordinates			Main effects, voxel-level (T)				
		x	y	z	Level 0	Level 1	Level 2	Level 3	Level 4
Insula	L	-30	18	9	8.06*	3.89	—	—	3.52
		-36	12	-3	6.54*	4.55	—	—	—
		-36	-9	3	7.45*	5.36*	3.98	—	5.57*
		-33	-15	15	5.06*	4.78	3.62	—	5.08*
		-33	-15	18	4.54	5.13*	3.94	—	5.25*
	R	36	24	6	7.81*	4.55	—	—	4.07
		33	21	9	7.34*	5.20*	—	—	4.11
		39	15	-3	7.30*	3.52	—	—	—
		36	-9	9	4.69	5.72*	3.43	—	5.60*
		36	-9	21	4.56	4.22	5.12	—	3.86
S$_I$ (Postcentral Gyrus, Supramarginal Gyrus)	L	-63	-18	21	5.84*	5.05*	4.66*	—	4.09
		-60	-21	18	5.42*	5.39*	5.62*	—	4.76
		-63	-24	18	4.84	5.37*	5.09*	—	5.21*
	R	54	-12	27	3.92	—	—	—	—
		63	-18	24	6.77*	4.78	3.27	—	3.91
		60	-15	27	5.64*	4.08	—	—	3.32
S$_{II}$ (Rolandic Operculum)	L	-57	0	12	7.10*	5.34*	4.33	—	5.82*
		-57	0	6	6.22*	—	3.62	—	5.83*
		-57	-3	9	6.91*	5.41*	3.9	—	6.36*
	R	60	-15	21	6.63*		3.26	—	4.21
		60	-12	15	6.11*	5.86*	5.02*	—	5.14*
		57	-12	15	6.07*	5.73*	4.94*	—	4.86
Parahippocampal Gyrus, Amygdala, Superior Temporal Gyrus	L	-24	3	-24	4.25	—	—	—	—
		-18	3	-21	3.56	—	—	—	—
		-21	3	-15	5.01*	—	—	—	—
		-36	0	-18	4.69	—	3.49	—	4.56
		-42	-6	-21	3.81	3.50	—	—	4.65
	R	24	6	-24	5.25*	—	—	—	3.73
		36	6	-15	6.05*	4.23	—	—	3.54
		60	6	-3	4.07	3.62	4.30	—	3.54
Anterior Cingulate	L	-6	6	42	5.26*	—	—	—	—
		-9	9	42	5.08*	—	—	—	3.48
	R	6	15	39	4.97*	3.86	—	—	—
		6	12	39	4.83	3.81	—	—	3.38
		6	21	42	3.28	—	—	—	—
Supplementary Motor Area / Median Cingulate	L	-6	6	45	5.25*	—	—	—	—
	R/L	0	0	63	4.31	—	—	—	—
	R	6	3	63	3.57	—	—	—	—
Posterior Cingulate	L	-6	-30	24	—	—	—	—	4.66
	R	6	-33	27	3.51	—	—	—	3.93

Pain-associated brain activation displayed two distinct main patterns with respect to alfentanil effects. Alfentanil produced predominantly linear concentration-dependent effects (statistical SPM contrast 1.5 0.5 -0.5 -1.5 for levels 0 – 3, respectively; **Figure 13** and **Table 3**) on pain-related brain activation at the right primary somatosensory area S_I and at the left somatosensory area S_{II}. A similar behavior was observed in the posterior parts of the left and right insula. In contrast, concentration-independent alfentanil effects (statistical SPM contrast 3 -1 -1 -1 for levels 0 – 3, respectively) on pain-related brain activation were observed in the right parahippocampal gyrus and amygdala, and in the most anterior part of the left insula. An exception from this duality of clearly concentration-dependent or independent effects was seen in large parts of the left and right median insula, in the anterior cingulate cortex and in the amygdala, where an intermediate behavior dominated the alfentanil effects on brain activation.

Figure 13: Brain regions displaying a predominantly linear, intermediate or predominantly step-like negative correlation of pain-related activation with increasing alfentanil concentrations in non-carriers of SNP *OPRM1* 118A>G (from top to bottom). The activation decreased predominantly linearly in regions related to the processing of sensory information, i.e. the primary somatosensory area S_I, the secondary somatosensory area S_{II}, and the posterior part of the insular cortex (contrast 1.5 0.5 -0.5 -1.5 0 exclusively masked by 3 -1 -1 -1 0 at p<0.001 uncorrected; yellow colored areas). Intermediate concentration-dependent behavior was seen in more anterior parts of the insular cortex, which increasingly processes affective instead of the sensory dimensions of pain, and in the anterior cingulate cortex, a multi-integrative structure of stimulus perception involved in affective and attentional processing of pain (3 -1 -1 -1 0 exclusively masked by 1.5 0.5 -0.5 -1.5 0 at p<0.001 uncorrected; red colored areas). In contrast, activation in parts of the amygdala, processing affective components of pain, decreased in a step-like concentration-independent manner (cyan colored areas; contrast 1.5 0.5 -0.5 -1.5 0 inclusively masked by 3 -1 -1 -1 0 at p<0.001 uncorrected). The right column visualizes the contrast estimates at the location with the highest T-value within these regions.

Table 3: Brain regions displaying a predominantly linear, intermediate or predominantly step-like negative correlation of pain-related activation with increasing alfentanil concentrations in non-carriers of SNP *OPRM1* 118A>G. Presented results are statistically significant at p<0.05, FDR corrected at voxel level (MNI: Montreal Neurological Institute; * p<0.05 FWE corrected at voxel level).
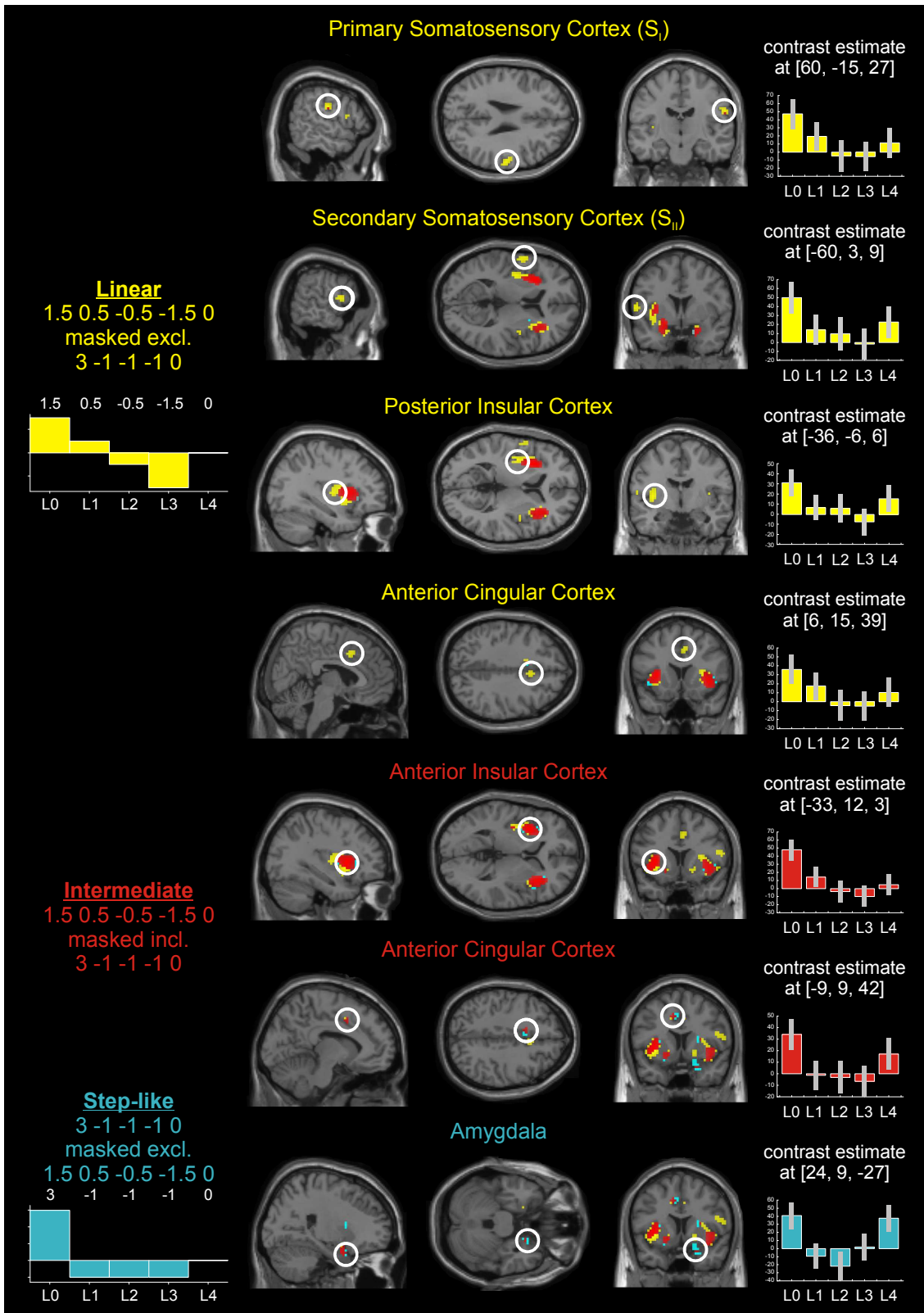
| Anatomic location		predominantly linear 2 1 -1 -2 exkl. 3 -1 -1 -1					combined 2 1 -1 -2 inkl. 3 -1 -1 -1					predominantly step 3 -1 -1 -1 exkl. 2 1 -1 -2				
		MNI coord. x	y	z	cluster size	voxel-level T	MNI coord. x	y	z	cluster size	voxel-level T	MNI coord. x	y	z	cluster size	voxel-level T
Insula	L	-33	9	-3	126	4.67*	-33	12	3	148	5.76**	-42	15	-3	14	4.06*
		-36	-9	9		4.17*	-36	-9	6	4	4.51*	-36	21	0		3.38
		-36	6	9		4.03*										
		-30	24	0	1	3.21										
	R	30	18	9	39	4.28*	39	15	-3	199	5.33**	48	15	-3	2	3.32
		36	9	3		3.43	33	24	6		5.29**	45	6	-6	1	3.23
		42	21	-6	17	3.80*										
		39	-3	9	10	3.57*										
		36	6	-12	8	3.68*										
S$_I$ (Postcentral Gyrus)	R	60	-15	27	28	4.07*					—					—
S$_{II}$ (Rolandic Operculum)	L	-57	3	9	22	3.76*					—					—
Parahippocampal Gyrus, Amygdala	L	-18	3	-24	10	3.65*	-21	3	-24		3.49*					
	R						24	3	-21	22	4.20*	18	6	-21	14	3.63
												24	9	-27	4	3.79*
Anterior Cingulate	L						-9	9	42	6	3.54*	-6	9	45	8	3.5
	R	6	15	39	18	3.68*					—					—
Putamen	L															
	R	18	9	-6	14	3.64*	-21	6	-9	58	4.21*					
Inferior frontal Gyrus, Opercular Part	R	51	9	18	20	3.54					—					

3.1.3 Consequences of SNP *OPRM1* 118A>G for alfentanil effects on pain-related brain activation

The consequences of SNP *OPRM1* 118A>G for the alfentanil effects on pain-associated brain activation were predominantly observed at brain regions where the pain-associated activation decreased linearly or intermediately with increasing alfentanil concentrations, but not in regions with a step-like concentration-independent response (**Figure 14** and **Table 4**). These regions included the primary somatosensory cortex S_I, the insular cortex and the anterior cingulate cortex.

Table 4: Brain regions displaying differences in the negative correlation of pain related activation between carriers and non-carriers of SNP *OPRM1* 118A>G. Areas with significant alfentanil effects on pain related activation in non-carriers of μ-opioid receptor variant N40D were defined as regions of interest for the analysis of the pharmacogenetic effects of μ-opioid receptor variant N40D. Activations in the regions of interest were corrected for multiple comparisons within a sphere of 15 mm radius (small volume correction). Statistical significant differences between carriers and non-carriers of μ-opioid receptor variant N40D were observed only in brain regions with a predominantly linear or intermediate decrease of pain-related brain activation and not in areas with a predominantly step-like decrease. Presented results are statistically significant at p<0.05, FDR corrected at voxel level (MNI: Montreal Neurological Institute; * p<0.05 FWE corrected at voxel level).

Anatomic location		Predominantly linear 1.5 0.5 -0.5 -1.5 0 -1.5 -0.5 0.5 1.5			
		MNI coordinates			voxel-level (T)
		x	y	z	
Insula	R	36	27	3	3.95*
		39	15	-3	3.85*
S_I (Postcentral Gyrus)	R	54	-36	57	3.38*
		54	-12	27	3.56*
Anterior Cingulate	R	6	18	42	3.38*
Posterior Cingulate	R	6	-36	24	3.71*
Supplementary Motor area /Median Cingulate	R	6	3	63	3.51*

Figure 14: Brain regions displaying differences in the negative correlation of pain related activation between carriers and non-carriers of SNP *OPRM1* 118A>G. The influence of SNP *OPRM1* 118A>G on the concentration dependent decrease of pain-related brain activation was only existent in regions of the right brain hemisphere with a predominantly linear or at most intermediate decrease of brain activation (contrast 1.5 0.5 -0.5 -1.5 0 -1.5 -0.5 0.5 1.5 0 at p<0.001 uncorrected). The right column visualizes the contrast estimates at the location with the highest T-value within these regions of non-carriers of SNP *OPRM1* 118A>G (solid white columns) and of carriers of SNP *OPRM1* 118A>G (solid red columns). Step-like contrasts did not display any significant genotype difference (**Table 4**) and are therefore omitted.
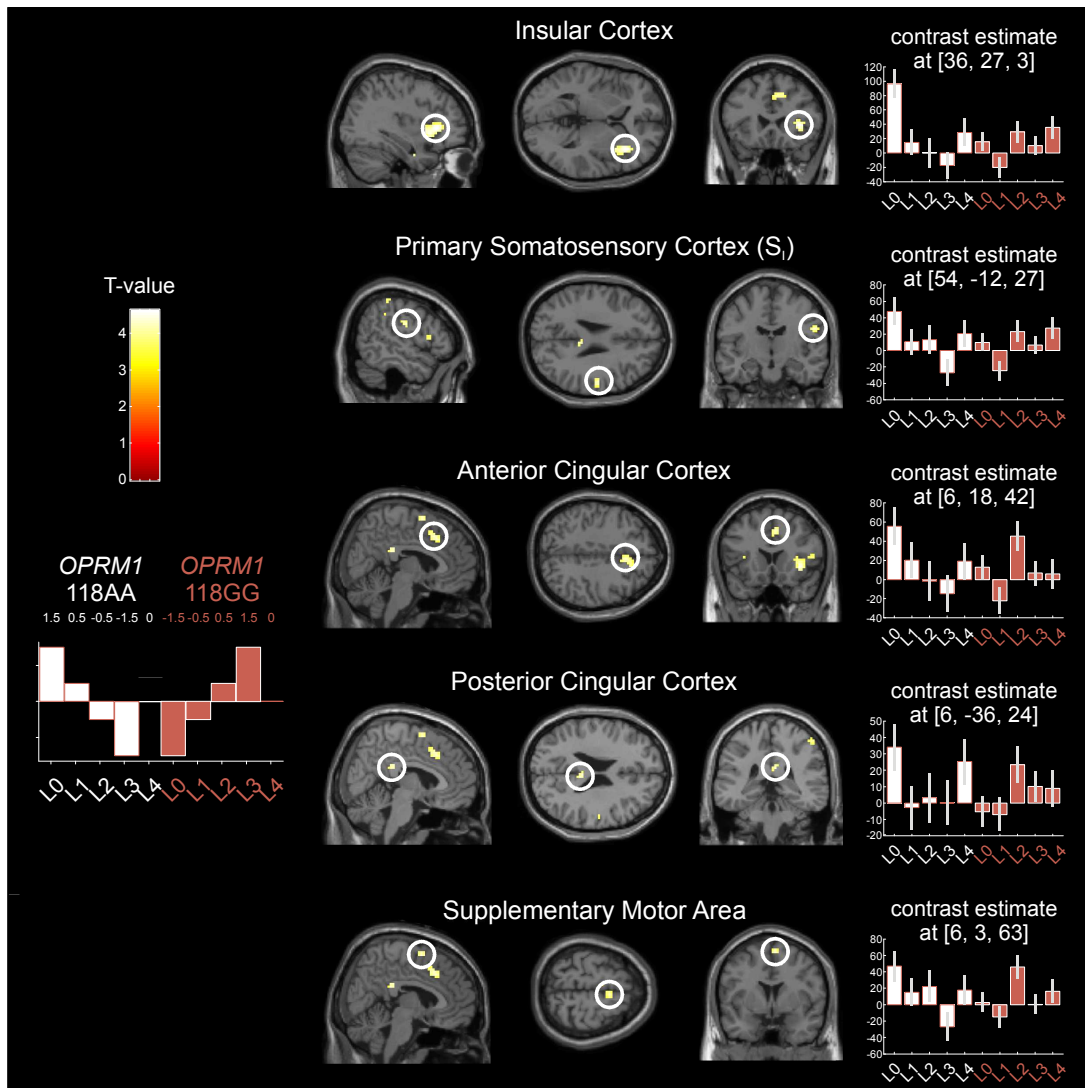
3.2 Mu-opioid receptor expression and function in pain processing brain regions of non-carriers and carriers of *OPRM1* 118A>G SNP

3.2.1 *OPRM1* mRNA expression

Analysis of the *OPRM1* mRNA expression in relation to *ACTB* mRNA expression included samples of 12 non-carriers (118AA), 9 heterozygous carriers (118AG) and 3 homozygous carriers (118GG) of the *OPRM1* 118A>G SNP. *OPRM1* mRNA expression was significantly lower in the S_{II}-region than in the lateral thalamus (Factor 0.29 to 0.82; rm-ANOVA factor "region": $F_{(1,21)}=5.80$, p=0.025; **Figure 15** and **Table 5**). The 118A>G SNP had no significant influence on *OPRM1* mRNA expression in both brain regions.

Figure 15: *OPRM1* mRNA expression. The expression was significantly lower in the S_{II}-region than in the lateral thalamus. mRNA expression was unaffected by the 118A>G polymorphism (median/solid lines, mean/dashed lines, 5th and 95th percentiles/bars).
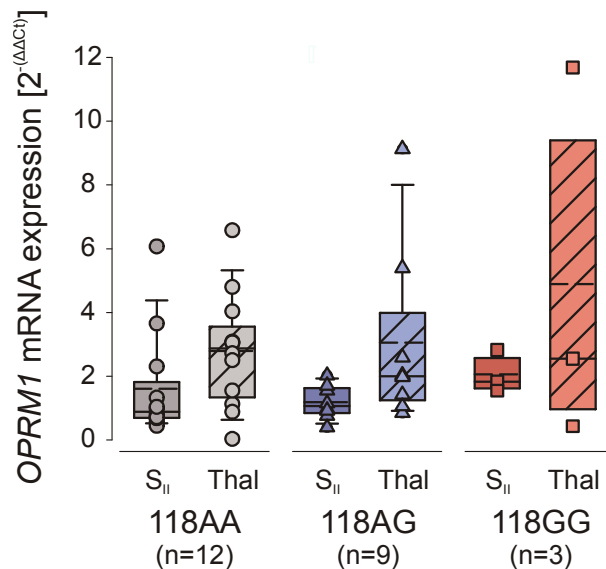
Table 5: Summary of the descriptive data of the 46 *post mortem* human brain samples (Mean ± SEM).

| Test	Value	N	*OPRM1* 118	Region S_{II}	Thalamus	Unit
OPRM1 mRNA expression	$2^{-\Delta\Delta Ct}$	12	AA	1.60 ± 0.48	2.78 ± 0.52	-
		9	AG	1.22 ± 0.17	2.75 ± 0.93	
		3	GG	2.06 ± 0.39	4.89 ± 1.68	
[^{3}H]-DAMGO Saturation binding	B_{Max}([^{3}H]-DAMGO)	18	AA	100.1 ± 8.90	156.5 ± 13.6	fmol/mg of protein
		16	AG	112.2 ± 13.1	152.2 ± 16.9	
		3	GG	136.5 ± 38.7	166.7 ± 69.3	
	K_D([^{3}H]-DAMGO)	18	AA	2.1 ± 0.2	1.6 ± 0.3	nM
		16	AG	2.7 ± 0.4	1.8 ± 0.3	
		3	GG	2.8 ± 0.8	1.6 ± 0.2	
[^{3}H]-DAMGO Displacement binding	K_I(Endorphine)	14	AA	6.26 ± 2.00	-	nM
		7	AG	3.73 ± 1.06	-	
		3	GG	4.19 ± 1.58	-	
	K_I(Methadone)	14	AA	4.33 ± 0.61	-	nM
		7	AG	4.15 ± 0.88	-	
		3	GG	4.49 ± 0.82	-	
	K_I(Morphine)	14	AA	8.02 ± 0.81	-	nM
		7	AG	5.83 ± 0.91	-	
		3	GG	7.37 ± 0.90	-	
	K_I(M6G)	14	AA	17.72 ± 2.62	-	nM
		7	AG	13.43 ± 1.20	-	
		3	GG	15.06 ± 1.24	-	
	K_I(Alfentanil)	14	AA	25.19 ± 2.73	-	nM
		7	AG	16.86 ± 2.46	-	
		3	GG	21.55 ± 6.01	-	
[^{35}S]-GTPγS binding	B_0(DAMGO)	15	AA	1040.4 ± 95.0	963.4 ± 100.7	fmol/mg of protein
		7	AG	819.9 ± 142.2	737.9 ± 187.7	
		3	GG	724.8 ± 248.8	793.1 ± 180.1	
	B_{Max}(DAMGO)	15	AA	1323.6 ± 112.9	1184.9 ± 108.9	fmol/mg of protein
		7	AG	981.1 ± 165.0	1009.2 ± 222.3	
		3	GG	956.6 ± 271.7	1164.3 ± 326.6	
	B_{Net}(DAMGO)	15	AA	283.2 ± 42.7	221.4 ± 29.10	fmol/mg of protein
		7	AG	161.1 ± 28.0	271.3 ± 71.70	
		3	GG	231.9 ± 26.5	371.2 ± 156.5	
	EC_{50}(DAMGO)	15	AA	1269.2 ± 371.3	262.2 ± 62.9	nM
		7	AG	637.5 ± 284.2	257.4 ± 29.2	
		3	GG	1065.7 ± 750.7	130.1 ± 57.1	

3.2.2 [³H]-DAMGO binding assays

3.2.2.1 Saturation binding

Analysis of the μ-opioid receptor protein expression (B_{Max}) and the [³H]-DAMGO equilibrium dissociation constant (K_D) included samples of 18 carriers of 118AA, 16 carriers of 118AG and 3 carriers of 118GG. Similarly to the *OPRM1* mRNA expression, μ-opioid receptor protein expression was significantly lower in the S_{II}-region than in the lateral thalamus (Factor 0.51 to 1.16; rm-ANOVA factor "region": $F_{(1,34)}=9.19$, $p=0.005$; **Figure 16** and **Table 5**). The [³H]-DAMGO equilibrium dissociation constant was significantly higher in the S_{II}-region than in the thalamus (Factor 1.07 to 2.14; rm-ANOVA factor "region": $F_{(1,34)}=8.88$, $p=0.005$) indicating a lower affinity of [³H]-DAMGO to μ-opioid receptors of the S_{II}-region. However, the *OPRM1* 118A>G SNP had no significant effect on μ-opioid receptor expression and [³H]-DAMGO equilibrium dissociation constant in both brain regions.

Figure 16: Saturation binding. In line with *OPRM1* mRNA expression, μ-opioid receptor expression was significantly lower in the S_{II}-region than in the lateral thalamus. In addition, [³H]-DAMGO had a lower affinity to μ-opioid receptors of the S_{II}-region, indicated by a statistically significantly higher equilibrium dissociation constant (K_D) of [³H]-DAMGO. Receptor expression and affinity did not differ between carriers and non-carriers of *OPRM1* variant 118G (Nonlinear fit/solid and dashed lines, S.E.M/bars).
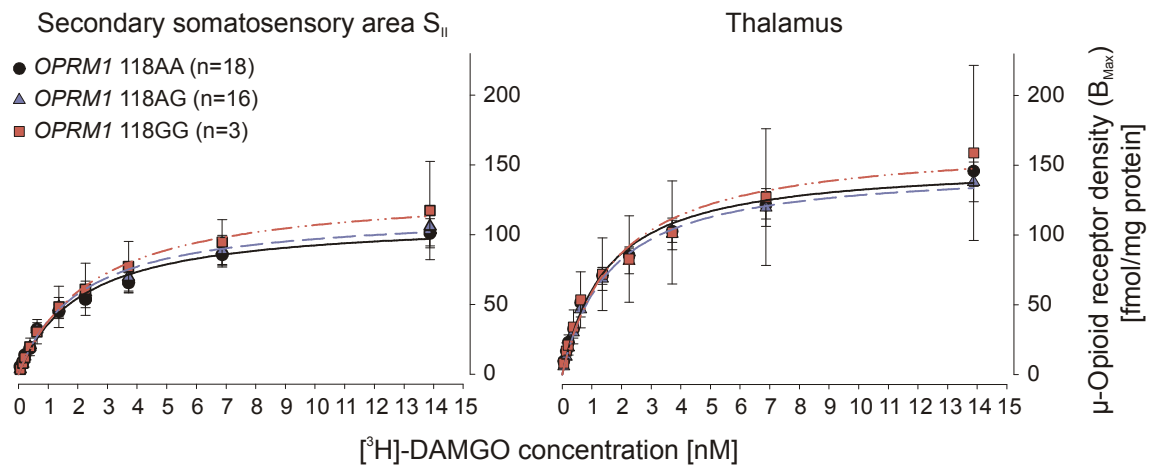
3.2.2.2 Displacement binding

The following order of µ-opioid receptor affinities of the tested agonists was derived from the [^{3}H]-DAMGO independent inhibition constants (K_I) determined in the S_{II}-region of 14 carriers of 118AA: β-endorphin ~ methadone > morphine > M6G > alfentanil (ANOVA factor "agonist": $F_{(4,105)}=23.76$, $p<0.001$; **Figure 17** and **Table 5**). However, despite the ability to detect significant differences in the K_I-values between the different agonists, the *OPRM1* genotype lacked significant effects on the [^{3}H]-DAMGO independent inhibition constants, although the expected magnitude of a potential genotype effect on the agonist-receptor-affinity would have been similar to the differences among the opioid receptor ligands.

Figure 17: Displacement binding. *Panel A* presents displacement binding data of the unlabeled µ-opioid receptor agonists in the S_{II}-region of 118AA carriers (n=14). *Panel B1-5* presents displacement binding data of each agonist in carriers of *OPRM1* 118AA compared to that of 118AG and 118GG. The *OPRM1* 118A>G had SNP had no significant effects on the affinity of the agonists in the S_{II}-region (Nonlinear fit/solid, dashed and dotted lines, S.E.M/bars).
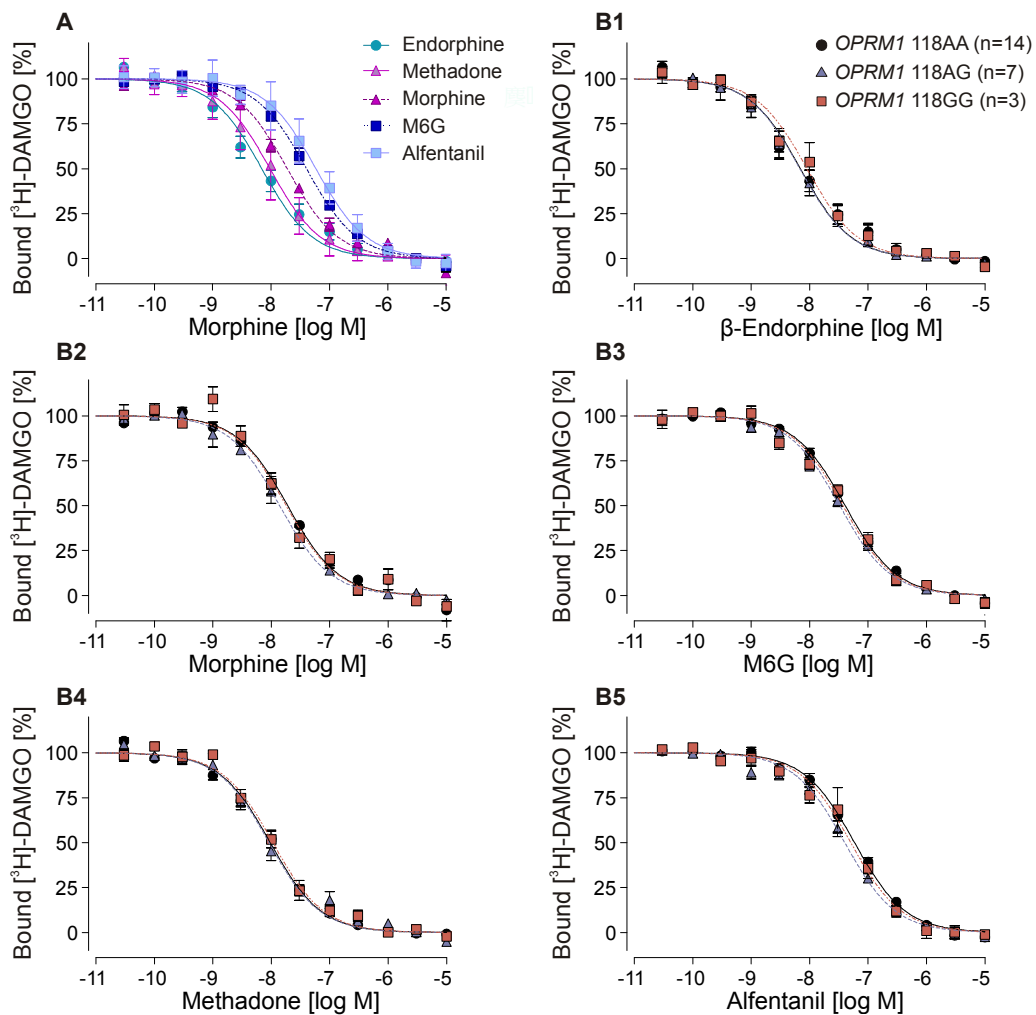
3.2.3 [^{35}S]-GTPγS binding assays

Analysis of the μ-opioid receptor signaling included brain samples of 15 carriers of 118AA, 7 carriers of 118AG and 3 carriers of 118GG. Basal (B_0) and maximum (B_{Max}) [^{35}S]-GTPγS binding did not differ between both brain regions (**Figure 18** and **Table 5**). In line with the lower affinity of [^{3}H]-DAMGO in the S_{II}-region, the DAMGO concentration needed to half-maximally stimulate the [^{35}S]-GTPγS binding (EC_{50}) in the S_{II}-region was significantly higher than needed in the thalamus (Factor 1.88 to 12.34; rm-ANOVA factor "region": $F_{(1,22)}=10.26$, $p=0.004$) indicating a lower potency of DAMGO to trigger μ-opioid receptor related intracellular G-protein signaling in the S_{II}-region. The genotype had no significant effects on any of the parameters.

Figure 18: [^{35}S]-GTPγS binding. Basal and maximum [^{35}S]-GTPγS binding were similar in both brain regions. In line with the lower affinity of [^{3}H]-DAMGO to μ-opioid receptors of S_{II}, the potency of DAMGO to trigger μ-opioid receptor signaling was lower in S_{II} than in the thalamus indicated by the significantly higher DAMGO concentration needed to stimulate half maximum [^{35}S]-GTPγS binding (EC_{50}). The genotype had no significant effects on basal and maximum binding and EC_{50} (Nonlinear fit to mean of data /solid and dashed lines, S.E.M/bars).
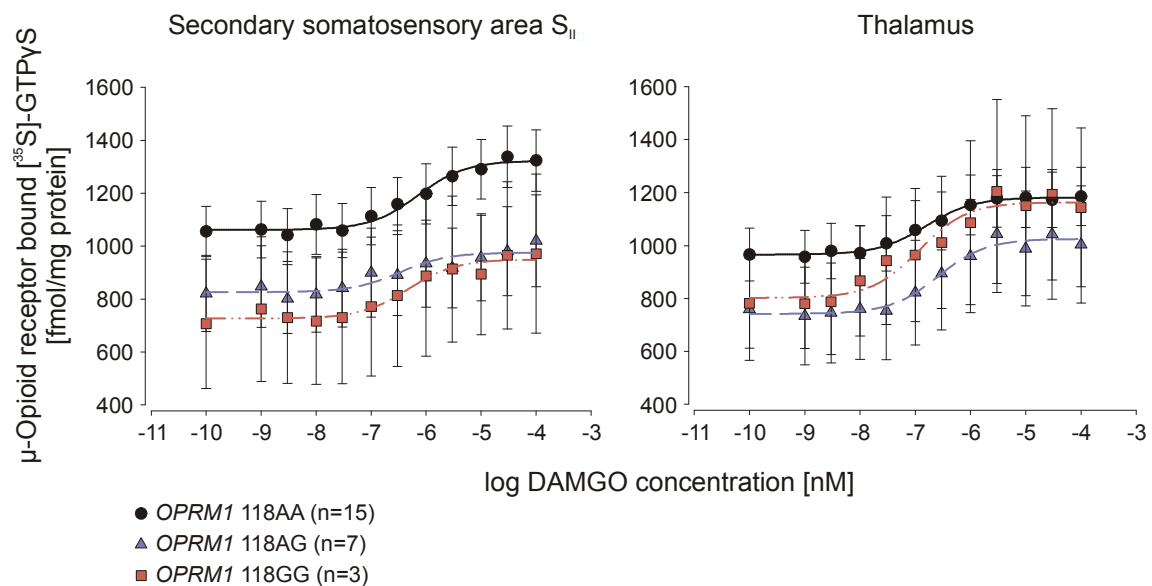
Despite the differences in receptor expression, the net increase of [^{35}S]-GTPγS binding after DAMGO stimulation, B_{Net}(DAMGO), was apparently similar in both brain regions (**Figure 19** and **Table 5**) as indicated by the absence of a statistical main effect of rm-ANOVA factor "region". However, a genotype-dependent difference in B_{Net}(DAMGO) was identified between the S_{II}-region and the lateral thalamus (rm-ANOVA interaction "region" by "118A>G"; $p=0.017$). Post-

hoc t-tests showed that non-carriers of the variant 118G allele had a 1.06 to 1.52 times higher net increase of $[^{35}S]$-GTPγS binding after DAMGO stimulation in the S_{II}-region than in the lateral thalamus (t-test: t(14)=2.244, p=0.041). In contrast, no difference between brain regions was observed for heterozygous (Factor 0.39 to 0.95; t-test: t(6)=1.91, p=0.10, n=7) and homozygous (factor 0.39 to 1.20; t-test: t(2)=0.91, p=0.46, n=3) carriers of the variant 118G allele.

Figure 19: Efficacy of DAMGO to stimulate $[^{35}S]$-GTPγS binding. Non-carriers of the variant 118G allele had a 1.06 to 1.52 times higher efficacy of DAMGO to stimulate G-protein signaling, measured as the net increase of $[^{35}S]$-GTPγS binding after DAMGO stimulation, in S_{II} than in the thalamus. In contrast, differences between brain regions were absent in heterozygous and homozygous carriers of the variant 118G allele (median/solid line, mean/dotted line, 5th and 95th percentiles/bars; n.s. not significant, * p<.05).
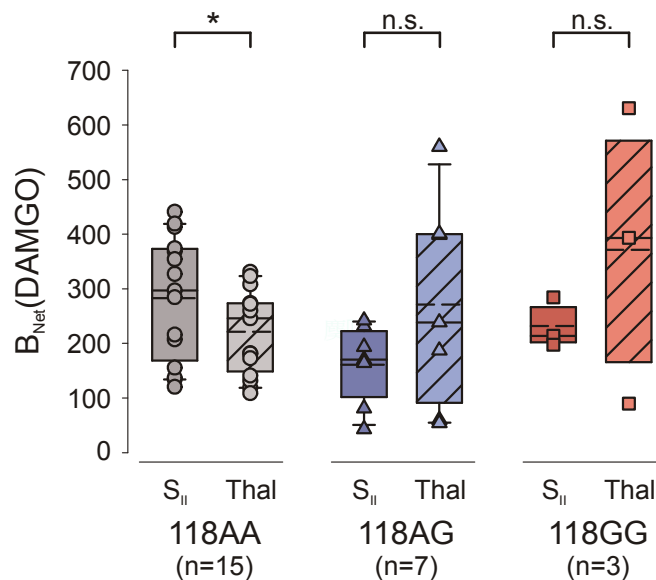
3.2.4 Mu-opioid receptor expression related receptor signaling

Mu-opioid receptor-G-protein-coupling efficacy, as measured by the DAMGO related net increase of $[^{35}S]$-GTPγS binding per μ-opioid receptor, $B_{Net}(DAMGO)/B_{Max}([^{3}H]$-DAMGO), was significantly higher in the S_{II}-region than in the thalamus (rm-ANOVA factor "region": F(1,22)=4.42, p=0.047; **Figure 20** and **Table 6**). The difference of μ-opioid receptor-G-protein-coupling efficacy between both brain regions was genotype-dependent (rm-ANOVA interaction "region" by "118A>G": p=0.008). The differences were only significant in non-carriers of the variant 118G allele, in whom the efficacy of DAMGO was approximately about 1.55 to 2.27 times higher in the S_{II}-region than in the thalamus (t-test: t(14)=5.36, p<0.001). In contrast, the brain region difference was absent in heterozygous (Factor 0.78 to 1.66; t-test: t(6)=0.98,

p=0.36, n=7) and homozygous (Factor 0.66 to 1.15; t-test: t(2)=0.41, p=0.72, n=3) carriers of the variant 118G allele.

Figure 20: Mu-opioid receptor expression related receptor signaling. While in non-carriers of *OPRM1* variant 118G the μ-opioid receptor-G-protein-coupling efficacy, measured as the DAMGO stimulated net increase of [^{35}S]-GTPγS binding per μ-opioid receptor, was significantly higher in the S_{II}-region than in the lateral thalamus, it did not differ significantly between both brain regions in carriers of *OPRM1* variant 118G (median/solid line, mean/dotted line, 5th and 95th percentiles/bars; n.s. not significant, ** p<.01, *** p<.001).

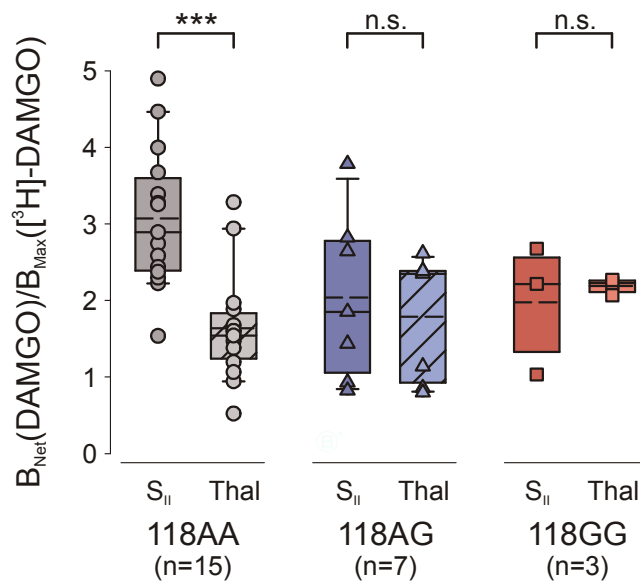
Table 6: Net increase of [^{35}S]-GTPγS binding per μ-opioid receptor after DAMGO stimulation.

Value	N	*OPRM1* 118	Region S_{II}	Thalamus	Unit
$B_{Net}(DAMGO)/$ $B_{Max}([^{3}H]\text{-}DAMGO)$	15	AA	3.07 ± 0.24	1.64 ± 0.18	[^{35}S]-GTPγS molecules/receptor
	7	AG	2.04 ± 0.41	1.79 ± 0.31	
	3	GG	1.97 ± 0.49	2.19 ± 0.06	

3.3 Therapeutic range of alfentanil in carriers and non-carriers of *OPRM1* 118A>G SNP

3.3.1 Plasma concentrations of alfentanil

Target and measured alfentanil concentrations are plotted in **Figure 21**. Mean alfentanil plasma concentrations at each level were not equal to target concentrations and subject to large interindividual variability. The target concentrations of 33.33 ng/ml were missed on average by -16 ± 4 percent, the target concentrations of 66.67 ng/ml were missed on average by 15 ± 5 percent and the target concentrations of 100 ng/ml were missed on average by 20 ± 5 percent. However, missing of the target concentration did not jeopardize the pharmacokinetic-pharmacodynamic analysis that related the effects to the actual individual alfentanil concentrations. The total amounts of administered alfentanil during the three levels of a total duration of approximately 195 min were 4.7 ± 0.3 mg for the 118AA group, 4.4 ± 0.5 mg for the 118AG group and 5.8 ± 0.6 mg for the 118GG group. These different doses owe to the fact that a weight-adjusted alfentanil infusion was administered. The doses did not differ statistically significantly between genotype groups (Kruskal-Wallis test: p=0.5).

Figure 21: Study design, timing, target and measured alfentanil plasma concentrations. Measured alfentanil plasma concentrations of all subjects categorized in study groups (118AA, 118AG, 118GG) and associated mean plasma concentration of the group (thin colored lines). The solid black line represents target alfentanil effect site concentrations. Colored bars represent time-frames of experiments. Time zero is the start of the alfentanil infusion.
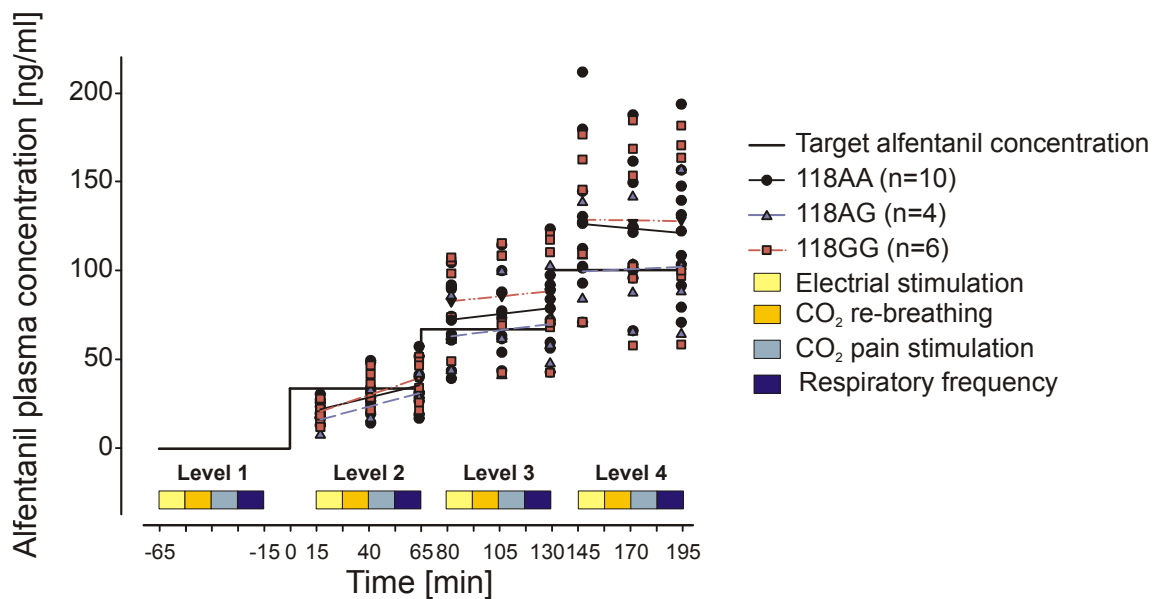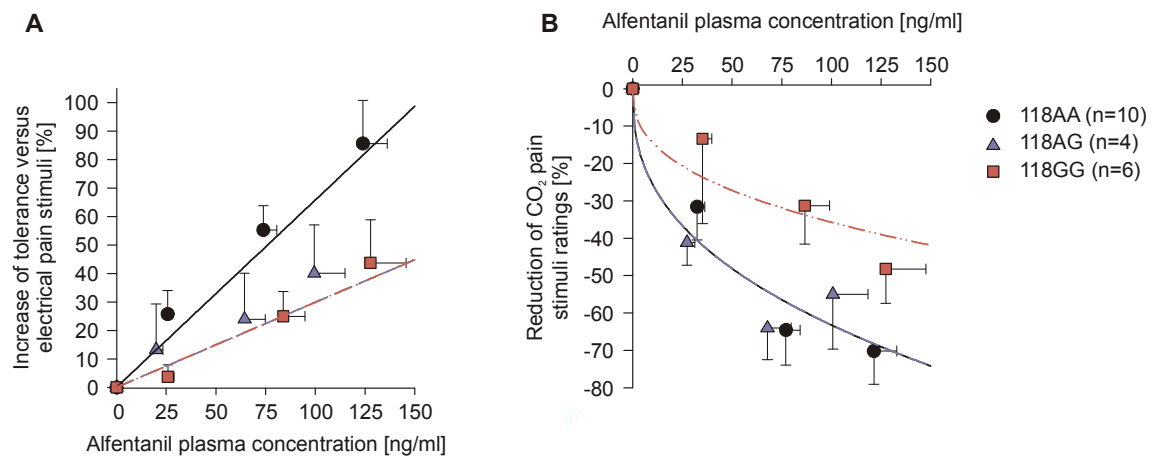
3.3.2 Analgesic effects of alfentanil

Analgesia was indicated by the increase of tolerance versus electrical pain stimuli and the decrease of the CO_2 pain stimuli rating with increasing alfentanil plasma concentrations (**Figure 22**). The 95% confidence interval of the slope parameter *a* (**Equation 1**) never included zero. While the CO_2 related pain ratings were best described by a power model (γ=0.394), data fits to the electrical pain stimuli test revealed a linear relationship between the alfentanil concentration and analgesia (γ=1). The concentration-effect relationships of the main pharmacodynamic measures are given in **Table 7**. By including a covariate θ_1 ("genotype") into the analysis of electrical pain stimuli test, fits to data improved statistically significantly for the combined groups 118AG and 118GG (p<0.05). Assigning two separate factors θ_1 and θ_2 to the slope of the concentration response relationship of groups 118AG and 118GG did not further improve the fits and heterozygous and homozygous carriers of the 118G variant allele were therefore not separated. As a result, heterozygous and homozygous carriers of the 118G allele variant needed a 2.2 times higher alfentanil concentration (167 ng/ml and 76 ng/ml for 118G carriers and non-carriers, respectively) to reach a 50% increase of analgesia above baseline in this pain model as compared to non-carriers.

Similarly, the fits to data of the pain intensity of CO_2-stimuli test improved statistically significantly by including the covariate θ_1 ("genotype"). But in contrast to the electrical pain model, fits improved only when assigning a factor θ to the slope of the concentration response relationship of the homozygous carriers of the 118G allele versus the combined groups 118AA and 118AG (p<0.05). From the fits resulted that the required alfentanil concentrations to increase analgesia 50% above baseline, were multiplied by the factor 4.3 for the 118GG group (235 ng/ml) as compared to the 118AA and 118AG group (55 ng/ml). Including a covariate "sex" into the analysis of the analgesic tests did not result in better fits to data.

Figure 22: Analgesia. (A) Electrical pain stimuli test: Population fit of the linear relationship between the alfentanil plasma concentrations and the increase of tolerance versus electrical pain stimuli. Fits to data improved by including a covariate θ_1 ("genotype") for combined groups 118AG and 118GG (p<0.05), indicating that both needed higher alfentanil plasma concentrations to reach same analgesia as 118AA group. (B) Pain intensity of CO_2-stimuli test: Population fit of the relationship between the alfentanil plasma concentrations and the change in pain intensity ratings of the CO_2-stimuli (duration 200 ms) delivered to the nasal mucosa. Including a covariate θ_1 for genotype improved the population fits to data for the 118GG group (p<0.05), indicating that only the 118GG group needed higher alfentanil plasma concentrations to reach the same analgesia as combined groups 118AA and 118AG in this test.

Table 7: Results of the population pharmacokinetic pharmacodynamic modeling relating the analgesic and respiratory depressive effects of alfentanil. Data is given as percent change from baseline, to its plasma concentrations by a power model (Equation 1). Complete model parameter values are given only for the final versions of the reduced and full models, i.e. of the models without and with implementation of the *OPRM1* 118A>G genotype. (#: Since no interindividual variability on the shape factor γ was observed as being a significant part of the models, the influence of the 118A>G SNP on the shape of the curve was not tested. %CV: percent coefficient of variation. CI: confidence interval. 2LL: minus two times the log-likelihood as goodness-of-fit measure. A change by 3.84 or 6.63 indicates a significance level of 0.05 or 0.01, respectively, for the improvement of fit by introduction of one additional model parameter (likelihood-ratio test, on which the statistics was based in the present study [91]).

| Pharmaco-dynamic measure	Reduced /full model	Effect versus concentration relationship				Role of the *OPRM1* 118A>G SNP			
		a		γ		Factor on a#	θ	-2LL	Difference in -2LL from reduced model
		Population central value (and 95% CI) [%ng/ml]	Inter-individual variability [%CV]	Population central value (and 95% CI) [%ng/ml]	Inter-individual variability [%CV]		Population central value (and 95% CI, only for final model)		
Tolerance to electrical pain stimuli	reduced	0.45	79.3	1	-	-	1	443.438	-
	full	0.658 (0.412-0.911)	70.3	1	-	θ₁ on 118AG and 118GG, 1 on 118AA	0.454 (0.167-0.809)	438.605	-4.833
						θ₁ on 118GG, 1 on 118AA and 118AG	Not given	440.713	-2.725
						θ₁ on 118AG, θ₂ on 118GG, 1 on 118AA	Not given	438.528	-4.91, but only -0.077 less from only one θ
Pain intensity of CO₂-stimuli	reduced	9.09	41.2	0.386	-	-	-	468.192	-
	full					θ₁ on 118AG and 118GG, 1 on 118AA	Not given	465.99	-2.202
		10.3 (4.7-19.2)	34.4	0.394	-	θ₁ on 118GG, 1 on 118AA and 118AG	0.565 (0.310-0.951)	462.968	-5.224
						θ₁ on 118AG, θ₂ on 118GG, 1 on 118AA	Not given		-5.233, but only -0.009 less from only one θ
Slope of the VE versus CO₂ concentration relationship	reduced	8.37	57.8	0.34	-	-	-	442.887	-
	full					θ₁ on 118AG and 118GG, 1 on 118AA	Not given	437.822	-5.065
		10.5 (4.7-20.1)	39.6	0.35	-	θ₁ on 118GG, 1 on 118AA and 118AG	0.416 (0.028-0.936)	433.482	-9.405, -4.34 less than previous
						θ₁ on 118AG, θ₂ on 118GG, 1 on 118AA	Not given	433.257	-9.63, but only -0.225 less from only one θ
Respiratory frequency	reduced	0.907	95.3	0.626	-	-	-	380.318	-
	full					θ₁ on 118AG and 118GG, 1 on 118AA	Not given	375.745	-4.573
		1.3 (0.27-3.48)	73.6	0.64	-	θ₁ on 118GG, 1 on 118AA and 118AG	0.222 (0.001-0.628)	371.455	-8.863, -4.29 less than previous
						θ₁ on 118AG, θ₂ on 118GG, 1 on 118AA	Not given	371.206	-9.112, but only -0.249 less from only one θ

3.3.3 Respiratory depressive effects of alfentanil

The slope of the relationship between the expiratory volume and CO_2 concentration in the inspired air and the respiratory frequency decreased with increasing alfentanil plasma concentrations (**Figure 23**). The 95% confidence interval of the slope factor *a* (**Equation 1**) did not include zero (**Table 7**). Data of both experiments were best described by a power model ($\gamma = 0.35$ and $\gamma = 0.64$, respectively).

Including a covariate θ_1 ("genotype") significantly improved the fits to data for the 118GG group compared to the 118AA and 118AG groups in the CO_2 re-breathing and the respiratory frequency test ($p < 0.01$). Assigning two separate factors θ_1 and θ_2 to the slope of the concentration response relationship of groups 118AG and 118GG or combining groups 118AG and GG worsened the fits. Therefore, a significant genotype effect could be established only for homozygous carriers of the 118G variant allele. The analysis yielded a 12.3 times increase (1059 ng/ml vs. 86 ng/ml for carriers of 118GG and 118AA/AG, respectively) and 10.5 times increase (3147 ng/ml vs. 300 ng/ml for carriers of 118GG and 118AA/AG, respectively) of the alfentanil concentration, respectively, to reach a 50% increase of the effect above baseline in the particular test. Including a covariate "sex" into the analysis of the applied tests did not result in better fits.

Figure 23: Respiratory depression. (A1-A4) Representative data of each a homozygous carrier of the 118A and 118G allele, respectively, with similar age, sex and BMI. The build-up of the expiratory volume due to increasing end-tidal CO_2 concentration is diminished with increasing alfentanil plasma concentrations. The respiratory depression developed differently in the different *OPRM1* genotypes with respect to cDNA position 118. Inserts: Raw data of respiratory frequency test: Associated raw data of the respiratory frequency test. (B1) Relative change of the slope of the linear relationship between the expiratory volume and end-tidal CO_2 concentration with increasing alfentanil plasma concentrations. (B2) Relative change of the respiratory frequency with increasing alfentanil plasma concentrations. The inclusion of the covariate θ_1 for genotype significantly improved the fit to data for the 118GG (p<0.01). Data are shown as relative decrease in percent ± SEM of baseline. Solid and dashed lines represent the population fits to the data.
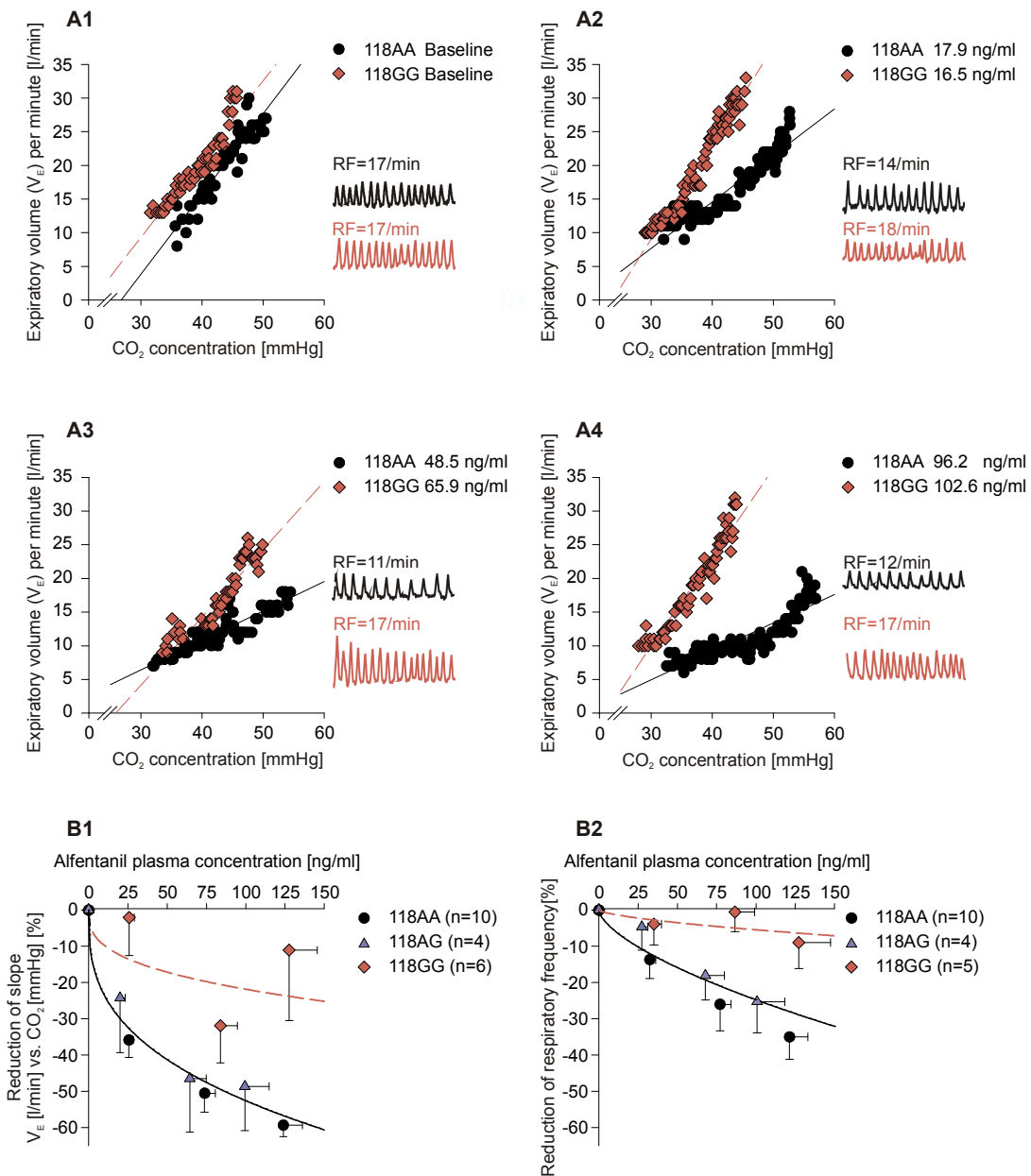
4 Discussion

Based on the findings that SNP *OPRM1* 118A>G diminishes opioid analgesia, we hypothesized that SNP *OPRM1* 118A>G will result in a modification of the concentration-dependent effect of opioids in brain areas involved in pain processing. To analyze the underlying mechanism, we identified pain processing brain regions in healthy non-carriers of SNP *OPRM1* 118A>G, which showed a reduction of pain related activation with increasing alfentanil concentrations, and analyzed the concentration-effect relationship of alfentanil in these areas. Subsequently, we analyzed in a second step, whether SNP *OPRM1* 118A>G alters the concentration-effect relationship of alfentanil in pain processing brain areas of homozygous *OPRM1* 118A>G carriers.

We observed brain activation in response to specific nociceptive trigeminal stimulation in regions repeatedly reported to be involved in the processing of pain [6, 9]. Analysis of opioid effects on the activation in these pain-relevant regions revealed a dual pattern of concentration-dependent and concentration-independent effects.

Concentration-dependent alfentanil effects were seen in the primary (S_I) and secondary (S_{II}) somatosensory cortex and posterior parts of the insula. These regions are known to be mainly associated with processing of the sensory intensity of pain [7, 69, 94-96]. Our results correspond to a linear relationship between pain-intensity and activation in the secondary somatosensory cortex S_{II} and the posterior insula [97], indicating that these regions reflect the opioid-induced decrease of the sensory dimension of pain.

In contrast, concentration-independent behavior was observed in the parahippocampal gyrus, the amygdala and anterior parts of the insula. These regions are known to be mainly involved in circuits processing the affective dimension of pain [59, 98-101]. In these regions, the pain-associated activation disappeared already at the lowest alfentanil concentration (level 1, 19.6±2.7 ng/ml), but subjects still perceived pain not significantly differently from baseline. Thus, the present observation provides a fMRI correlate for the previous observation that very low doses of morphine (0.04-0.06 mg/kg) significantly reduced the affective but not the sensory component of painful heat stimuli [102].

Thus, we observed that (i) pain-associated activation decreased linearly with increasing alfentanil concentrations in brain regions known to process the sensory intensity of pain [97], and that (ii) pain-associated activation disappeared at low opioid concentrations in regions known to process the affective components of pain. The demonstrated dual effect of opioids on pain-

associated brain activation may provide a neuroscientific basis for their use in pain treatment as advised by the WHO. On the one hand, low doses of opioids, which are not accompanied by opioid side effects, may indeed enhance non-opioid analgesia by reducing the affective dimensions of pain (WHO Step 2). On the other hand, our results indicate that opioid analgesia does not reach a plateau and that an increase in opioid dose as advised in WHO step 3 may indeed be expected to further reduce the intensity of pain.

The intermediate decrease of pain-associated brain activation, i.e. the neither clearly concentration-dependent nor clearly concentration independent, is in line with the hypothesis of dual opioid effects on sensory and affective dimensions of pain because it was observed in brain regions involved in the integrative processing of both sensory and affective nociceptive information such as the insular cortex [7, 9, 69, 96, 99], which due to this dual involvement has been proposed to be an integrative region for both dimensions [100]. It further applies to the anterior cingulate cortex, which similarly has been proposed as a multi-integrative structure of stimulus perception and affective and attentional processing of pain [6, 9, 103]. Due to this integrative processing in the presence of high opioid receptor densities [20, 104], both regions seem to be of high significance in central nervous opioid analgesia [105].

The hypothesized modification of the concentration-dependent opioid effects of alfentanil by SNP *OPRM1* 118A>G was mainly observed in brain regions that showed linear alfentanil-concentration dependent decreases in pain related brain activation and that are known to be part of the circuit processing sensory components pain. This is in line with the repeatedly observed decrease of opioid analgesia in experimental pain [65, 106] and decrease of opioid-induced miosis [47, 49, 107] in carriers of SNP *OPRM1* 118A>G. It suggests that the increased opioid requirements by pain patients who carry SNP *OPRM1* 118A>G [43, 44] are mainly due to the decreased reduction of the sensory intensity of pain. On the other hand, the results suggest that in the context of pain therapy, SNP *OPRM1* 118A>G is less likely to modulate affectivity as it has been suggested due to its association with substance addiction [53]. The more pronounced effects of SNP *OPRM1* 118A>G in regions associated with processing the sensory rather than the affective dimension of pain are also reflected in its functional associations, which are predominantly positive in the context of pain therapy while its functional associations in the context of addiction are more controversial (for review, see [36]).

Based on the fMRI findings that SNP *OPRM1* 118A>G affects primarily brain regions processing the sensory information of pain, the molecular mechanism of the SNP *OPRM1* 118A>G was

investigated in *post mortem* samples from the human S_{II} region. In addition, a sample from the ventral posterior part of the lateral thalamus, a region involved in the transmission of nociceptive information to the S_{II} region, was selected to serve as a control region that should be unaffected by the SNP *OPRM1* 118A>G.

On the molecular level, the brain-region specificity of the consequences of the *ORPM1* 118A>G polymorphism, which had been suggested by fMRI analysis of alfentanil analgesia [108] but had been neglected in the region-unspecific assessments of its consequences in human brain tissue [109] and for methodological reasons in all transfection experiments with cell lines not originating from human brain [37-39, 109, 110], was presently found to be the main effect of this genetic variant. The *ORPM1* 118A>G polymorphism appears to modulate the regional differences of DAMGO efficacy to stimulate G-protein binding. Due to the more efficient G-protein coupling, DAMGO was significantly more effective in G-Protein activation in S_{II} than in the thalamus of non-carriers of the 118G variant allele. This regional specificity was lost in carriers of the 118G variant, where G-Protein activation in S_{II} was equal to that in the thalamus. Thus, although the effects of *OPRM1* 118A>G seem to be regionally limited, the genetic variant appears to interfere with the connectivity of brain regions of the pain processing network. In contrast to former reports investigating *OPRM1* 118A>G SNP effects in transfected cell cultures, the results are gained from a random sample of human brain regions known to be important for pain transmission and processing. Thus, they are more likely to reflect the clinical context and provide for the first time a molecular correlate for the repeatedly and consistently reported decreased opioid effects in carriers of the μ-opioid receptor variant N40D.

In accordance to the fMRI results, the reduction of μ-opioid receptor signalling efficacy being observed much more in S_{II} than in the thalamus suggests that the 118A>G variant mainly modulates the subjective perception of nociceptive input rather than its transmission. Activation of S_{II}, posterior parts of the insula and the thalamus is known to correlate with the subjective perception of pain intensity [7, 97] and opioids such as remifentanil have been shown to diminish pain-related activation of S_{II} and the thalamus, which coincided with a decrease of the subjective pain intensity perception [111]. Thus, the present findings indicate that an important role in the reduced pain relief after opioid administration to carriers of the variant 118G as compared to non-carriers [43-46, 65] plays a decreased μ-opioid receptor signalling in S_{II} relative to that in the thalamus. It is likely that other brain regions are also differently affected, and based on the present results, future investigations may provide a more complete topography of the brain regions affected by the clinically functional *OPRM1* 118A>G variant.

Although receptor expression assessed twice by saturation binding and by mRNA quantification was significantly higher in the thalamus than in S_{II}, we could not reproduce a genotype difference in receptor expression levels [109]. This might again relate to the here proposed brain region specificity of the N40D consequences. The previously observed decreased expression might be limited to the pons and to the not further specified, possibly pooled cortical areas [109]. The brain region specificity of the N40D consequences makes receptor expression an unlikely general molecular basis of reduced analgesia in carriers of *OPRM1* variant 118G. In fact, this expression consequences have been observed so far in brain regions [6] not directly involved in pain perception [109], or in non-brain and non-human cell lines [38, 39, 110]. On the other hand, not related to the *OPRM1* 118A>G variant, regionally limited alterations of μ-opioid receptor expression have already been shown for other SNPs known to affect the opioid system such as the *COMT* 472G>A [112, 113]. This makes previous results of reduced brain μ-opioid receptor expression in other regions possible for the N40D variant [109] and thus does not dispute those results, but at the same time, it strengthens our conclusion that a μ-opioid receptor genetic variant can have brain-region specific effects, presently mainly found at a receptor signalling rather than expression level.

Further support for an effect of the N40D variant on the interaction between brain regions rather than on opioid effects within a single region is provided by the findings that although μ-opioid receptors of both brain regions differed in their affinity to DAMGO, they were unaffected by the *OPRM1* 118A>G SNP, and the μ-opioid receptor affinity of β-endorphin in the S_{II} region of non-carriers and carriers of *OPRM1* variant 118G was similar. The similar β-endorphin affinity disagrees with the reported three-times higher binding affinity of human β-endorphin to N40D variant μ-opioid receptor transfected AV-12 cells [37] but agrees with all other publications [38, 39, 110]. Also agreeing with most publications [38, 39, 110], the affinity of other opioids associated with decreased effectiveness in carriers of *OPRM1* variant 118G [43-47, 65, 107] was also unaffected by the *OPRM1* 118A>G SNP. Thus, a general decrease of the affinity of μ-opioid receptor agonists to N40D variant receptors is unlikely to be the cause of the reduced opioid effectiveness in carriers of *OPRM1* variant 118G.

Additional investigations will be necessary to finally uncover the brain region specific modulation of μ-opioid receptor signalling by the *OPRM1* 118A>G polymorphism as we cannot provide a clear mechanism of how the *OPRM1* 118A>G SNP diminishes μ-opioid receptor signalling. However, our results clearly demonstrate the advantages of brain region specific analysis of μ-opioid receptor binding and signalling characteristics in human brain tissue compared to

OPRM1 transfected cell cultures. The importance of brain-region dependent variable expression and function of opioid receptors [20, 21, 83, 114] for the functional consequences of the *OPRM1* 118A>G SNP might be the major reason for failed or contradictory investigations of its function in cell cultures sharply contrasting to the consistent clinical findings of decreased opioid effects in carriers of variant 118G [43-47, 65, 107]. To which extent region-specific expression of μ-opioid receptor splice variants and coupling to G_α and $G_{\beta\gamma}$ subunits, which is known to influence μ-opioid receptor signalling [115-118], contribute to the brain region dependent effects of the N40D variant, may be addressed in the future.

Last but not least, we addressed the problem of whether both, analgesic and respiratory depressive, effects are decreased in the presence of the *OPRM1* 118A>G SNP or whether this genetic variant decreases only the analgesic effects of opioids. This issue has major clinical implications. If the first is true, opioid doses may be safely increased to achieve adequate analgesia in carriers of the 118G variant allele. In contrast, if the second alternative is true, increasing the opioid doses to produce adequate analgesia would put the patients at risk for respiratory depression being the most dangerous opioid side effect. Results of previous investigations supported both alternatives. A protective effect of the 118G variant against opioid toxicity was hypothesized from the good tolerance of high plasma concentrations of morphine-6-glucuronide by a homozygous carrier of the 118G allele [36] and from the rarer occurrence of vomiting in carriers of the 118G allele after administration of high doses of morphine-6-glucuronide [47]. To this sharply contrasts a report of similar respiratory depression despite lower analgesia produced by morphine-6-glucuronide in four heterozygous carriers of the 118G allele as compared to 12 non-carriers of the variant [46], which suggests a narrowed therapeutic range of opioids in carriers of the 118G variant allele.

We demonstrate that the *OPRM1* 118A>G SNP results in a broadened therapeutic range of alfentanil in healthy homozygous carriers. Analysis of the effect versus concentration relationship showed that higher opioid concentrations are needed to achieve analgesia in 118GG carriers, a result which is in line with previous findings [43, 45-47, 107]. However, the required increase in opioid dosing appears to be safe because it does not increase the risk for respiratory depression. In contrast, based on the pharmacodynamic model (Equation 1) with the estimated parameters given in **Table 7**, when calculating the alfentanil concentrations needed to provide a 50% increase of the pain tolerance threshold to electrical pain or a 50% increase in the pain intensity of the CO_2 stimuli, 2 – 4 times higher alfentanil concentrations are sufficient to produce the same degree of analgesia in subjects with an *OPRM1* 118GG genotype as in

subjects not carrying this particular genotype. In contrast, 10 – 12 times higher alfentanil concentrations are needed to produce the same degree of respiratory depression in subjects with an *OPRM1* 118GG as in subjects not carrying this genotype. This is compatible with a broadened therapeutic range of opioids in healthy homozygous carriers of the *OPRM1* 118G variant allele. Thus, increasing the opioid dose in homozygous 118G carriers to achieve adequate analgesia is probably clinically safe. This consequence could not be observed by Romberg et al. [46] because that study did not include homozygous carriers of the 118G allele.

Heterozygous carriers of the 118G allele were recruited to substitute for the lacking of four homozygous carriers to match the ten healthy controls. Due to the smaller sample size, the results for the heterozygous subjects are of lower confidence level compared to those of the homozygous subjects. Nonetheless, with respect to healthy heterozygous carriers of the 118G variant allele, our result supports the previously observed lack of a protective effect of the 118G allele against opioid-induced respiratory depression despite reduced analgesic response [46]. Thus, it appears that caution has to be exercised in subjects who heterozygously carry the *OPRM1* 118G allele when raising the opioid dose in order to produce adequate pain relief.

Dependently on the type of pain, opioid analgesia appears to be differently affected in heterozygous carriers of the 118G allele. To produce analgesia, they needed higher alfentanil concentrations than wild-type subjects only in the electrical pain test but not in the CO_2 pain model, emphasizing that the gene-dose effect of the 118G allele may differ among pain qualities. In contrast to homozygous carriers of the *OPRM1* 118G variant allele, a similar dosing advice for heterozygous carriers of the *OPRM1* 118G allele is therefore not possible. First, a decreased opioid potency to produce analgesia does not appear to apply to all kinds of pain. Therefore, a dose increase may not be generally required in pain therapy in heterozygous 118G carriers. Second, if inadequate relief of particular qualities of pain requires a dose increase, this may be associated with an increased risk for respiratory depression. Therefore, present evidence together with a similar previous finding [46] does not allow to emit an opioid dosing advice for heterozygous 118G carriers. In addition, the number of four heterozygous carriers of the variant 118G allele is lower than that of the six homozygous carriers, which further weakens dosing recommendations based on the present study results. Nonetheless, the central tendency of respiratory depression parameters found with heterozygous 118G carriers was similar to that found with wild-type controls and did not lay between genotypes 118AA and 118GG. Thus the present data contain no strong suggestion that with a greater number of 118AG carriers a sta-

tistical significance could have been easily reached for the difference between 118AA and 118AG carriers.

We observed a tendency toward less frequent vomiting in carriers of the 118G allele, but in contrast to a previous study [47] this did not reach statistical significance. A reason for this may be the comparatively lower opioid doses in the present study. While the administered alfentanil doses were high enough to trigger opioid side-effects including vomiting, judged by the overall side effects the opioid effects were much lower than the previous effects of morphine-6-glucuronide [47]. This interpretation concurs with other studies with comparatively lower opioid effects [49], where also the number of vomits did not significantly differ between carriers and non-carriers of SNP *OPRM1* 118A>G. This suggests that the 118A>G polymorphisms is not the only factor for opioid induced vomiting and other causes have to be addressed in separate studies focused on that particular side effect.

Although we interpret our results in a clinical context for a possible opioid dosing, great caution has to be exercised when applying the findings into clinical practice. On the one hand, our laboratory setting is quite distinct from the clinical setting of intra- and postoperative opioid analgesia. The subjects were healthy volunteers, who did not receive any co-medication to alfentanil, which differs from the perioperative medication where additive respiratory depressant drug interactions may occur. Also, we assessed experimental pain rather than clinical pain. Moreover, respiratory depression depends on the subjects arousal [119], a further difference between the present study and the clinical situation. Furthermore, the present estimates of therapeutic range are extrapolations from the obtained numerical results and the used pharmacodynamic model, which, as any extrapolation, demands great caution when applying it to another context. Despite these limitations, the present study provides a defined hypothesis of the consequences of the *OPRM1* 118A>G polymorphisms for wanted and unwanted effects of alfentanil for future clinical studies, which should evaluate the usefulness of the present findings for clinical therapy and may re-evaluate the question of heterozygous subjects in a greater number of participants.

5 Conclusion

In conclusion, the data demonstrate that the *OPRM1* 118A>G SNP primarily diminishes opioid effects on pain related brain activation in brain regions processing the sensory dimension of pain, which is in line with the repeatedly observed decrease of opioid analgesia in experimental pain and decrease of opioid-induced miosis in carriers of SNP *OPRM1* 118A>G. In contrast, regions processing the affective dimension of pain were unaffected by this receptor variant.

On the molecular level, this brain region-specific effect of SNP *OPRM1* 118A>G seems to result from a brain region-dependent modulation of μ-opioid receptor signalling by *OPRM1* 118A>G SNP. While the variant has no effects on μ-opioid receptor signalling in the lateral thalamus, it abolishes the increased μ-opioid receptor signalling efficacy in the S_{II}-region relative to that in the thalamus. Considering that S_{II} is a region that codes for pain intensity, these results provide a molecular correlate for the observed decrease of opioid effects in brain regions processing the sensory dimension of pain and the decreased potency of opioids to reduce the subjective pain intensity in carriers of the *OPRM1* variant 118G.

In addition, the data confirm the hypothesis that the SNP *OPRM1* 118A>G affects both the analgesic and respiratory depressive effects of alfentanil. However, while the analgesic effects are partly already decreased in heterozygous carriers, depending on the pain model, the respiratory depressive effects are decreased only in homozygous carriers of the variant 118G allele. Moreover, the therapeutic range of alfentanil was broadened in homozygous carriers, which is further evidence for the brain region-dependent effects of the *OPRM1* 118A>G SNP. Thus, the results demonstrate that the *OPRM1* polymorphism 118A>G protects against opioid-induced respiratory depression in homozygous carriers, whereas it does not seem to protect against opioid-induced respiratory depression in heterozygous carriers, despite reduced analgesic response in some kinds of pain.

As a consequence, these results introduce the brain-region specificity and interregional comparisons as important new components into analyses of the genetic modulation of the human opioid system, and they provide a solid basis for continuing investigations in larger study populations of patients to address the role of *OPRM1* 118A>G genotyping for pain therapy in the clinical context.

6 Abstract

The µ-opioid receptor is the primary target structure of most opioid analgesics and thus responsible for the predominant part of their wanted and unwanted effects. Carriers of the frequent genetic µ-opioid receptor variant N40D (allelic frequency 8.2 - 17 %), coded by the single nucleotide polymorphism A>G at position 118 of the µ-opioid receptor coding gene *OPRM1* (*OPRM1* 118A>G SNP), suffer from a decreased opioid potency and from a higher need of opioid analgesics to reach adequate analgesia. The aim of the present work was to identify the mechanism by which the *OPRM1* 118A>G SNP decreases the opioid potency and to quantify its effects on the analgesic potency and therapeutic range of opioid analgesics.

To elucidate the consequences of the *OPRM1* 118A>G SNP for the effects of opioid analgesics, brain regions of healthy homozygous carriers of the *OPRM1* 118A>G SNP were identified by means of functional magnetic resonace imaging (fMRI), where the variant alters the response to opioid analgesics after painful stimulation. Afterwards, the µ-opioid receptor function was analyzed on a molecular level in *post mortem* samples of these brain regions. Finally, the consequences of the *OPRM1* 118A>G SNP for the analgesic and respiratory depressive effects of opioids were quantified in healthy carriers and non-carriers of *OPRM1* 118A>G SNP by means of experimental pain- and respiratory depression-models.

To identify pain processing brain regions, where the variant alters the response to opioid analgesics after painful stimulation, we investigated the effects of different alfentanil concentration levels (0, 25, 50 and 75 ng/ml) on pain-related brain activation achieved by short pulses (300 msec) of gaseous CO_2 (66% v/v) delivered to the nasal mucosa using a 3.0 T magnetic head scanner in 16 non-carriers and nine homozygous carriers of the µ-opioid receptor gene variant *OPRM1* 118A>G. In brain regions associated with the processing of the sensory dimension of pain (pain intensity), such as the primary and secondary somatosensory cortices and the posterior insular cortex, the activation decreased linearly in relation to alfentanil concentrations, which was significantly less pronounced in *OPRM1* 118G carriers. In contrast, in brain regions known to process the affective dimension of pain (emotional dimension), such as the parahippocampal gyrus, amygdala and anterior insula, the pain-related activation disappeared already at the lowest alfentanil dose, without genotype differences.

Subsequently, we investigated the µ-opioid receptor-expression ([3H]-DAMGO saturation experiments, *OPRM1* mRNA analysis by means of RT-PCR), the µ-opioid receptor affinity ([3H]-DAMGO saturation and competition experiments) and µ-opioid receptor signaling ([35S]-

GTPγS binding experiments) in *post mortem* samples of the human S_{II}-region, as a cortical projection region coding for pain intensity, and lateral thalamus, as an important region for nociceptive transmission. Samples of 22 non-carriers, 21 heterozygous and three homozygous carriers of *OPRM1* 118A>G SNP were included into the analysis. The receptor expression and receptor affinity of both brain regions did not differ between non-carriers and carriers of the variant N40D. In non-carriers, the µ-opioid receptors of the S_{II}-region activated the receptor bound G-protein more efficiently than those of the thalamus (factor 1.55-2.27). This regional difference was missing in heterozygous (factor 0.78-1.66) and homozygous (factor 0.66-1.15) carriers of the N40D variant indicating a reduced receptor-G-protein-coupling in the S_{II}-region.

Finally, the consequences of the alteration of µ-opioid receptor function in carriers and non-carriers of the genetic variant was investigated using pain- and respiratory depression-models. Therefore, 10 healthy non-carriers, four heterozygous and six homozygous carriers of the µ-opioid receptor variant N40D received an infusion of four different concentrations of alfentanil (0, 33.33, 66.66 and 100 ng/ml). At each concentration level, analgesia was assessed by means of electrically (5 Hz sinus 0 to 20 mA) and chemically (200 ms gaseous CO_2 pulses applied to the nasal mucosa) induced pain, and respiratory depression was quantified by means of hypercapnic challenge according to Read and recording of the breathing frequency. The results showed that depending on the used pain model, both heterozygous and homozygous carriers of the variant N40D needed 2 – 4 times higher alfentanil concentrations to achieve the same analgesia as non-carriers. This increase seems to be at least for homozygous carriers unproblematic, because to reach a comparable respiratory depression as non-carriers, they needed 10-12 times higher alfentanil concentrations.

The results of this work demonstrate that the µ-opioid receptor variant N40D causes a regionally limited reduction of the signal transduction efficiency of µ-opioid receptors in brain regions involved in pain processing. Thus, the painful activation of sensory brain regions coding for pain intensity is not sufficiently suppressed by opioid analgesics in carriers of the variant N40D. Due to the insufficient suppression in hetero- and homozygous carriers of the variant N40D, the concentration of opioids has to be increased by a factor 2 - 4, in order to achieve the same analgesia as in non-carriers. At the same time, the respiratory depressive effects are decreased to a greater extent in homozygous carriers of the N40D variant as they need a 10 - 12 times higher opioid concentration to suffer from the same degree of respiratory depression as non-carriers. Due to the increased therapeutic range of opioid analgesics, an increase of the opioid dose seems to be harmless, at least for homozygous carriers of the N40D variant.

7 Deutsche Zusammenfassung

Opioidanalgetika sind bis heute das adäquate Mittel zur Behandlung schwerer Schmerzzustände. Dabei wird ihre breite Anwendbarkeit durch opioidtypische unerwünschte Nebenwirkungen wie Atemdepression, Benommenheit, Übelkeit bis zum Erbrechen, Obstipation, Miosis und juckende Hautreizung eingeschränkt. Das Ausmaß der auftretenden Opioidwirkungen variiert von Patient zu Patient. Fortschritte in der genetischen Forschung haben gezeigt, dass ein Teil der Variabilität von Opioidwirkungen in der genetischen Variabilität der Bevölkerung begründet liegt.

Opioide wirken über G-Protein-gekoppelte Rezeptoren, die Opioidrezeptoren, bestehend aus dem μ-, κ-, δ-Opioidrezeptor. Anhand von μ-Opioidrezeptor-Knockout-Mäusen konnte gezeigt werden, dass vor allem die μ-Opioidrezeptoren für den überwiegenden Teil der erwünschten und unerwünschten Wirkungen von Opioidanalgetika verantwortlich sind. Die μ-Opioidrezeptoren werden vom *OPRM1* Gen codiert. Bei einer häufigen genetischen Variante des μ-Opioidrezeptor-Gens *OPRM1* (Allelfrequenz ca. 8,2-17%) steht an Position 118 in Exon 1 das Nukleotid Adenin anstatt Guanin (*OPRM1*-118A>G-Polymorphismus). Als Folge wird anstelle von Asparagin die Aminosäure Aspartat an Position 40 (N40D) der N-terminalen extrazellulären Rezeptorbindungsdomäne eingebaut.

Bei Trägern der μ-Opioidrezeptor-Variante N40D wurde wiederholt eine Verminderung der Opioidpotenz und ein erhöhter Bedarf von Opioidanalgetika zur adäquaten Schmerzstillung im Vergleich zu Nichtträgern der Variante beobachtet. Desweiteren weisen einige Studien auf eine Erhöhung der therapeutischen Breite von Opioidanalgetika in Trägern dieser Variante hin. So benötigten Träger der N40D Variante im Vergleich zu Nichtträgern höhere Konzentrationen von Alfentanil (1,3-fach) bzw. Morphin (2-fach), um die gleiche Analgesie bei postoperativen Schmerzen zu erreichen, und dennoch waren sie weniger von opioidtypischen unerwünschten Wirkungen betroffen. Die miotischen Effekte von Morphin, seines aktiven Metaboliten Morphin-6-glucuronid (M6G) und Levomethadon waren in Trägern der N40D Variante verringert und Träger des varianten Allels mussten nach hohen Dosen M6G weniger erbrechen als Nichtträger. Es gibt aber auch eine Studie, deren Ergebnisse gegen eine erhöhte therapeutische Breite von Opioiden in Träger des varianten 118G-Allels sprechen. Diese zeigte, dass in heterozygoten Trägern des 118G Allels die Analgesie nach M6G Gabe zwar verringert war, die atemdepressiven Effekte von M6G aber unverändert waren. Dies deutet auf eine verminderte therapeutische Breite von Opioiden in heterozygoten Trägern hin.

Die der verminderten Opioidpotenz zu Grunde liegenden molekularen Mechanismen sind nicht eindeutig geklärt. So wurde in AV-12-Zellen, die mit der 118G Variante des µ-Opioidrezeptor-Gens transfiziert wurden, eine 3-fach höhere Affinität des N40D Rezeptors zu seinem endogenen Liganden β-Endorphin beobachtet, während die Affinität zu Opioiden wie Morphin oder dessen aktiven Metaboliten Morphin-6-glucuronid unverändert waren. Diese Ergebnisse erklären leider nicht die verminderte Opioidpotenz bei Trägern der 118G Variante. Eine mögliche Erklärung für die verminderte Opioidanalgesie wäre eine verminderte Rezeptorexpression in Trägern der 118G Variante. Die Möglichkeit einer verminderten Rezeptorexpression wird durch die Beobachtung gestützt, dass in Hirngewebsproben von Trägern der 118G Variante im Vergleich zu Nichtträgern tendenziell geringere Mengen an *OPRM1* mRNA gefunden wurden, was auf eine verminderte Expression des Rezeptorproteins hinweisen könnte. Diese Vermutung wird durch Ergebnisse aus Rezeptorexpressions-Experimenten in mit der 118G Variante des µ-Opioidrezeptor-Gens transfizierten HEK 293-Zellen und CHO-Zellen untermauert. Im Gegensatz dazu gibt es auch Veröffentlichungen, in denen die Rezeptorexpression in mit der 118G Variante transfizierten HEK 293-Zellen und COS-Zellen unverändert war. Daher ist der endgültige Beweis, dass die µ-Opioidrezeptorexpression in Trägern der 118G Variante verringert ist, noch nicht erbracht.

Die genau Bestimmung der Folgen der *OPRM1* 118A>G Mutation für die Potenz und therapeutische Breite von Opioidanalgetika ist für eine effektive und sichere Schmerztherapie bei Trägern des varianten 118G-Allels von größtem Interesse. Auch der molekulare Mechanismus, der der verminderten Opioidwirkung in Trägern des *OPRM1* 118A>G SNP zu Grunde liegt, kann nicht als endgültig geklärt betrachtet werden. Ziel dieser Arbeit war es daher, den Mechanismus zu identifizieren, der zu der Verminderung der Opioidpotenz und einem erhöhten Verbrauch von Opioidanalgetika in Trägern der µ-Opioidrezeptor-Variante N40D führt. Außerdem sollten die Auswirkungen auf die analgetische Wirkung und therapeutische Breite von Opioidanalgetika in Trägern der µ-Opioidrezeptor-Variante N40D untersucht werden.

Zur Aufklärung der Auswirkungen der N40D-Variante auf die Opioidwirkungen wurden mittels funktioneller Bildgebung diejenigen Hirnregionen identifiziert, in denen sich der *OPRM1*-118A>G-Genotyp auf die Schmerzverarbeitung auswirkt. Anschließend wurde die Opioidrezeptor-Signaltransduktion in *post-mortem* gewonnenen Proben aus diesen Hirnregionen mittels molekularbiologischer Methoden analysiert. Schließlich wurden die Auswirkungen dieser Veränderungen für Träger der Variante N40D anhand pharmakodynamischer Schmerz- und Atemdepressionsmodelle untersucht.

Im ersten Schritt wurde in einer klinischen Studie die Dosis-Wirkungsbeziehung von Alfentanil in schmerzverarbeitenden Hirnregionen von Nichtträgern und Trägern der N40D Variante untersucht. Hierdurch wurden Zielstrukturen im Gehirn identifiziert, die an der Schmerzverarbeitung beteiligt sind und in denen die schmerzbezogene Aktivierung nach Opioidapplikation bei Trägern der N40D Variante verändert ist. Dazu wurden 16 gesunden Nichtträgern und 9 homozygoten Trägern der *OPRM1* Variante 118G mittels computerisierter Infusion vier verschiedene Konzentrationen des schnell wirksamen Opioids Alfenanil infundiert, um Zielkonzentrationen am Wirkort (ZNS) von 0, 25, 50 und 75 ng/ml einzustellen. Mit Hilfe eines Magnetresonanztomographen (3.0T) und der dadurch möglichen funktionellen Bildgebung (fMRT) wurde bei jeder Zielkonzentration die schmerzkorrelierte Hirnaktivierung nach schmerzhafter chemischer Stimulation der Nasenschleimhaut durch kurze Reize gasförmigen CO_2 (66% v/v; Reizdauer 300ms) gemessen. Die an der Schmerzverarbeitung beteiligten Hirnregionen waren durch aufsteigende Alfentanilkonzentrationen unterschiedlich betroffen: An der Verarbeitung der sensorischen Schmerzkomponente beteiligte Hirnregionen, wie z.B. der primäre und sekundäre somatosensorische Cortex (S_I und S_{II}), zeigten eine von der Konzentration linear abhängige Abnahme der schmerzreiz-assoziierten Aktivierung, welche statistisch signifikant geringer in homozygoten Trägern der 118G Variante war. In die Verarbeitung der affektiven Schmerzkomponente involvierte Regionen, wie z.B. die Amygdala, zeigten dagegen bereits bei der niedrigsten Alfentanilkonzentration eine abrupte, nicht-lineare, stufenförmige Abnahme der schmerzreiz-assoziierten Aktivierung. Diese Hirnregionen waren nicht von der Mutation betroffen. Die Ergebnisse zeigen damit eine dosisabhängige Dissoziation von Opioidwirkungen auf die affektive und sensorische Dimension von Schmerzen. Dabei stellt die verringerte Wirkung von Alfentanil auf die schmerzbezogene Aktivierung sensorischer Hirnregionen in Trägern der 118G Variante ein neuroanatomisches Korrelat für die verminderte analgetische Wirkung von Opioiden in Trägern der Mutation dar.

Im zweiten Schritt wurde die S_{II}-Region, als eine Region, die die sensorische Komponente des Schmerzes kodiert, und der laterale Thalamus, als eine zentrale Schaltstelle für afferente nozizeptive Reize, mittels molekularbiologischer Methoden auf Veränderungen der Rezeptorexpression ([³H]-DAMGO-Saturierungsexperimente, *OPRM1* mRNA-Expressionsbestimmung mittels RT-PCR), der Rezeptor-Liganden-Affinität ([³H]-DAMGO-Saturierungs- und Verdrängungsexperimente) und der Rezeptor-Signaltransduktion ([³⁵S]-GTPγS-Bindungsexperimente) untersucht. Dazu wurde *post-mortem* Hirngewebe von 22 Nichtträgern, 21 heterozygoten und 3 homozygoten Trägern der µ-Opioidrezeptor Variante N40D entnommen. Die µ-Opioidrezepto-

ren beider Hirnregionen unterschieden sich signifikant hinsichtlich ihrer Expression, Affinität und Funktion. So war in der S_{II}-Region die *OPRM1*-mRNA-Expression um den Faktor 0,29-0,82 (p=0,025) und die μ-Opioidrezeptor-Expression um den Faktor 0,51-1,16 (p=0,005) niedriger als im lateralen Thalamus. Die *OPRM1*-mRNA-Expression und die Rezeptorproteinexpression unterschieden sich in beiden Hirnregionen jedoch nicht zwischen Trägern und Nichtträgern der Variante N40D. Desweiteren war in der S_{II}-Region die Rezeptoraffinität zu dem μ-Opioidrezeptor-spezifischen Agonisten [^{3}H]-DAMGO um den Faktor 1,07-2,14 (p=0,005) und die Potenz von DAMGO, die Rezeptor vermittelte Bindung des GTP Analogons [^{35}S]-GTPγS an das intrazellulär gebundene G-Protein zu erhöhen, um das 2,5-8,5 fache (p=0,004) niedriger als im lateralen Thalamus. Auch die Rezeptoraffinität zu [^{3}H]-DAMGO und die Potenz von DAMGO unterschied sich in beiden Hirnregionen nicht zwischen Trägern und Nichtträgern der Variante N40D. Obwohl die Rezeptorexpression in der S_{II}-Region signifikant niedriger war als im lateralen Thalamus, unterschieden sich beide Regionen nicht hinsichtlich der Nettozunahme der Rezeptor-gebundenen [^{35}S]-GTPγS Moleküle nach Stimulation durch DAMGO, was auf eine verringerte μ-Opioidrezeptor-G-Protein-Kopplungseffizienz im lateralen Thalamus im Vergleich zur S_{II}-Region schließen lässt. Die Unterschiede zwischen beiden Hirnregionen variierten dabei signifikant (p=0,008) zwischen Trägern und Nichtträgern der N40D Variante. Während die μ-Opioidrezeptor-G-Protein-Kopplungeffizienz in der S_{II}-Region von Nichtträgern der Variante um den Faktor 1,55-2,27 (p<0,001) höher war als im lateralen Thalamus, unterschied sie sich nicht in Trägern der 118G Variante (118AG: Faktor 0,78-1,66, p=0,36; 118GG: Faktor 0,66-1,15, p=0,72). Diese Beobachtung lässt auf eine verringerte G-Protein-Kopplung des Rezeptors in der S_{II}-Region von Trägern der 118G Variante schließen, welches die Unterschiede in der Dosisabhängigkeit der Opioideffekte in sensorischen Hirnregionen von homozygoten Trägern der *OPRM1* Variante 118G erklärt, die in den fMRI-Experimenten beobachtet wurden.

Im letzten Schritt wurden die klinischen Konsequenzen der μ-Opioidrezeptor-Variante N40D für die analgetische Potenz und die therapeutische Breite von Opioiden mittels experimenteller pharmakodynamischer Schmerz- und Atemdepressionsmodelle untersucht. Dazu wurden 10 gesunden Nichtträgern, 4 heterozygoten und 6 homozygoten Trägern der μ-Opioidrezeptor Variante N40D vier verschiedene aufsteigende Konzentrationen Alfentanil (0, 33.33, 66.66 und 100 ng/ml) infundiert. Bei jeder Alfentanilkonzentration wurde die Analgesie anhand elektrischer Schmerzstimulation am Mittelgelenk des linken Mittelfingers (5Hz Sinus mit Stromstärken 0-20mA) und anhand chemischer Schmerzstimulation der Nasenschleimhaut (gasförmiges CO_2; Reizdauer 200ms) gemessen. Die Atemdepression wurde mittels CO_2 Rückatmung nach

Read und durch Aufnahme der Atemfrequenz bestimmt. Mit zunehmender Alfentanilkonzent-ration am Wirkort (ZNS) nahm die Schmerztoleranz gegenüber den elektrischen Schmerzreizen bei hetero- und homozygoten Trägern der N40D Variante signifikant weniger stark zu als bei Nichtträgern (Faktor 0.454; $p<0.05$). Auch die Analgesie bei chemo-somatosensorischer Rei-zung der Nasenschleimhaut war bei homozygoten Träger der Variante weniger stark ausgep-rägt (Faktor 0.565; $p<0.05$). Alfentanil verursachte bei homozygoten Trägern des varianten 118G-Allels eine signifikant geringere Atemdepression als bei heterozygoten Trägern oder bei Nichtträgern der Variante (CO_2-Rückatmung: Faktor 0.416, Atemfrequenzmessung: Faktor 0.222; $p<0.01$). Homozygote Träger des *OPRM1* 118A>G Polymorphismus benötigten ca. 2- bis 4-fach höhere Alfentanilkonzentrationen, um dieselbe Analgesie, und ca. 10- bis 12-fach höhe-re Konzentrationen, um die gleiche Atemdepression wie Nichtträger zu erreichen. Die thera-peutische Breite von Alfentanil ist daher in homozygoten Trägern des *OPRM1* 118A>G-Polymorphismus gegenüber Nichtträgern vergrößert. In Übereinstimmung mit bereits veröf-fentlichten Ergebnissen anderer Arbeitsgruppen waren heterozygote Träger abhängig vom verwendeten Schmerzmodell wie die homozygoten Träger von einer verminderten Analgesie betroffen, litten aber im Gegensatz zu homozygoten Trägern unter der gleichen Atemdepres-sion wie Nichtträger der Mutation. Dies deutet auf eine Verminderung der therapeutischen Breite von Opioiden in heterozygoten Trägern im Gegensatz zu den homozygoten Trägern hin. Eine abschließende Bewertung bezüglich der therapeutischen Breite in heterozygoten Trägern kann aber aufgrund der zu geringen Teilnehmerzahl an dieser Stelle nicht getroffen werden.

Die Ergebnisse der Arbeit zeigen, dass die µ-Opioidrezeptor-Variante N40D eine regional be-grenzte Verminderung der Signaltransduktionseffizienz des µ-Opioidrezeptors in verschiede-nen Hirnregionen nach sich zieht. Dadurch wird bei Trägern der Variante N40D die schmerzhaf-te Aktivierung sensorischer, in die Verarbeitung der Schmerzintensität einbezogener Hirnre-gionen nicht ausreichend durch Opioidanalgetika unterdrückt. Bei unzureichender Schmerzstil-lung muss deshalb in hetero- und homozygoten Trägern der Variante N40D die Konzentration von Opioidanalgetika um einen Faktor 2 – 4 erhöht werden, um die gleiche Analgesie wie bei Nichtträgern zu erreichen. Gleichzeitig sind bei homozygoten Trägern der N40D-Variante die atemdepressiven Wirkungen in stärkerem Ausmaß vermindert und es wird eine 10 – 12 mal höhere Opioidkonzentration benötigt, um die gleiche Atemdepression wie bei Nichtträgern zu erreichen. Wegen der demzufolge erhöhten therapeutischen Breite von Opioiden scheint eine Erhöhung der Opioidkonzentration zur Gewährleistung ausreichender Analgesie zumindest bei homozygoten Trägern klinisch unbedenklich zu sein.

8 Literature

1. Melzack, R. and K.L. Casey, *Sensory, motivational and central control determinants of pain.* The Skin Senses, 1968.

2. Julius, D. and A.I. Basbaum, *Molecular mechanisms of nociception.* Nature, 2001. **413**(6852): p. 203-10.

3. Hermann, D.M., et al., *Afferent projections to the rat nuclei raphe magnus, raphe pallidus and reticularis gigantocellularis pars alpha demonstrated by iontophoretic application of choleratoxin (subunit b).* J Chem Neuroanat, 1997. **13**(1): p. 1-21.

4. Paredes, J., et al., *Afferents to the central nucleus of the amygdala and functional subdivisions of the periaqueductal gray: neuroanatomical substrates for affective behavior.* Brain Res, 2000. **887**(1): p. 157-73.

5. Price, D.D., *Psychological and neural mechanisms of the affective dimension of pain.* Science, 2000. **288**(5472): p. 1769-72.

6. Apkarian, A.V., et al., *Human brain mechanisms of pain perception and regulation in health and disease.* Eur J Pain, 2005. **9**(4): p. 463-84.

7. Coghill, R.C., et al., *Pain intensity processing within the human brain: a bilateral, distributed mechanism.* J Neurophysiol, 1999. **82**(4): p. 1934-43.

8. Becerra, L., et al., *Reward circuitry activation by noxious thermal stimuli.* Neuron, 2001. **32**(5): p. 927-46.

9. Peyron, R., B. Laurent, and L. Garcia-Larrea, *Functional imaging of brain responses to pain. A review and meta-analysis.* Neurophysiol. Clin., 2000. **30**: p. 263-288.

10. Tracey, I., *Nociceptive processing in the human brain.* Curr Opin Neurobiol, 2005. **15**(4): p. 478-87.

11. Friedman, D.P. and E.A. Murray, *Thalamic connectivity of the second somatosensory area and neighboring somatosensory fields of the lateral sulcus of the macaque.* J Comp Neurol, 1986. **252**(3): p. 348-73.

12. Greenspan, J.D., R.R. Lee, and F.A. Lenz, *Pain sensitivity alterations as a function of lesion location in the parasylvian cortex.* Pain, 1999. **81**(3): p. 273-82.

13. Willoch, F., et al., *Central poststroke pain and reduced opioid receptor binding within pain processing circuitries: a [11C]diprenorphine PET study.* Pain, 2004. **108**(3): p. 213-20.

14. Henderson, G. and A.T. McKnight, *The orphan opioid receptor and its endogenous ligand--nociceptin/orphanin FQ.* Trends Pharmacol Sci, 1997. **18**(8): p. 293-300.

15. Connor, M. and M.D. Christie, *Opioid receptor signalling mechanisms.* Clin Exp Pharmacol Physiol, 1999. **26**(7): p. 493-9.

16. Matthes, H.W., et al., *Loss of morphine-induced analgesia, reward effect and withdrawal symptoms in mice lacking the mu-opioid-receptor gene.* Nature, 1996. **383**(6603): p. 819-823.

17. Mignat, C., U. Wille, and A. Ziegler, *Affinity profiles of morphine, codeine, dihydrocodeine and their glucuronides at opioid receptor subtypes.* Life Sci, 1995. **56**(10): p. 793-9.

18. Law, P.Y., Y.H. Wong, and H.H. Loh, *Molecular mechanisms and regulation of opioid receptor signaling.* Annu Rev Pharmacol Toxicol, 2000. **40**: p. 389-430.

19. Trafton, J.A., et al., *Postsynaptic signaling via the [mu]-opioid receptor: responses of dorsal horn neurons to exogenous opioids and noxious stimulation.* J Neurosci, 2000. **20**(23): p. 8578-84.

20. Baumgartner, U., et al., *High opiate receptor binding potential in the human lateral pain system.* Neuroimage, 2006. **30**(3): p. 692-9.

21. Arvidsson, U., et al., *Distribution and targeting of a mu-opioid receptor (MOR1) in brain and spinal cord.* J Neurosci, 1995. **15**(5 Pt 1): p. 3328-41.

22. Hiller, J.M. and L.Q. Fan, *Laminar distribution of the multiple opioid receptors in the human cerebral cortex.* Neurochem Res, 1996. **21**(11): p. 1333-45.

23. Nestler, E.J., *Molecular neurobiology of addiction.* Am J Addict, 2001. **10**(3): p. 201-17.

24. Inturrisi, C.E., *Clinical pharmacology of opioids for pain.* Clin J Pain, 2002. **18**(4 Suppl): p. S3-13.

25. Greer, J.J., J.E. Carter, and Z. al-Zubaidy, *Opioid depression of respiration in neonatal rats.* J Physiol, 1995. **485 (Pt 3)**: p. 845-55.

26. Brown, D.L., *Postoperative analgesia following thoracotomy. Danger of delayed respiratory depression.* Chest, 1985. **88**(5): p. 779-80.

27. Byard, R.W. and J.D. Gilbert, *Narcotic administration and stenosing lesions of the upper airway--a potentially lethal combination.* J Clin Forensic Med, 2005. **12**(1): p. 29-31.

28. Garriott, J.C. and V.J. Di Maio, *Death in the dental chair: three drug fatalities in dental patients.* J Toxicol Clin Toxicol, 1982. **19**(9): p. 987-995.

29. Gerber, N. and G. Apseloff, *Death from a morphine infusion during a sickle cell crisis.* J Pediatr, 1993. **123**(2): p. 322-5.

30. Lotsch, J., et al., *Fatal respiratory depression after multiple intravenous morphine injections.* Clin Pharmacokinet, 2006. **45**(11): p. 1051-60.

31. Wang, J.B., et al., *mu opiate receptor: cDNA cloning and expression.* Proc Natl Acad Sci U S A, 1993. **90**(21): p. 10230-4.

32. Uhl, G.R., I. Sora, and Z. Wang, *The mu opiate receptor as a candidate gene for pain: polymorphisms, variations in expression, nociception, and opiate responses.* Proc.Natl.Acad.Sci.U.S.A, 1999. **96**(14): p. 7752-7755.

33. LaForge, K.S., V. Yuferov, and M.J. Kreek, *Opioid receptor and peptide gene polymorphisms: potential implications for addictions.* Eur J Pharmacol, 2000. **410**(2-3): p. 249-268.

34. Hoehe, M.R., et al., *Sequence variability and candidate gene analysis in complex disease: association of mu opioid receptor gene variation with substance dependence.* Hum.Mol.Genet., 2000. **9**(19): p. 2895-2908.

35. Lotsch, J. and G. Geisslinger, *Are mu-opioid receptor polymorphisms important for clinical opioid therapy?* Trends Mol Med, 2005. **11**(2): p. 82-9.

36. Lötsch, J. and G. Geisslinger, *Are mu-opioid receptor polymorphisms important for clinical opioid therapy?* Trends Mol Med, 2005. **11**(2): p. 82-9.

37. Bond, C., et al., *Single-nucleotide polymorphism in the human mu opioid receptor gene alters beta-endorphin binding and activity: possible implications for opiate addiction.* Proc Natl Acad Sci U S A, 1998. **95**(16): p. 9608-13.

38. Befort, K., et al., *A single nucleotide polymorphic mutation in the human mu-opioid receptor severely impairs receptor signaling.* J Biol Chem, 2001. **276**(5): p. 3130-7.

39. Beyer, A., et al., *Effect of the A118G polymorphism on binding affinity, potency and agonist-mediated endocytosis, desensitization, and resensitization of the human mu-opioid receptor.* J Neurochem, 2004. **89**(3): p. 553-60.

40. Margas, W., et al., *Modulation of Ca2+ channels by heterologously expressed wild-type and mutant human micro-opioid receptors (hMORs) containing the A118G single-nucleotide polymorphism.* J Neurophysiol, 2007. **97**(2): p. 1058-67.

41. Zhang, Y., et al., *Allelic expression imbalance of human mu opioid receptor (OPRM1) caused by variant A118G.* J Biol Chem, 2005.

42. Caraco, Y., Y. Maroz, and E. Davidson, *Variability in alfentanil analgesia may be attributed to polymorphism in the mu-opioid receptor [Abstract].* Clin Pharmacol Ther, 2001. **69**: p. 63.

43. Klepstad, P., et al., *The 118 A > G polymorphism in the human micro-opioid receptor gene may increase morphine requirements in patients with pain caused by malignant disease.* Acta Anaesthesiol Scand, 2004. **48**(10): p. 1232-9.

44. Chou, W.Y., et al., *Human opioid receptor A118G polymorphism affects intravenous patient-controlled analgesia morphine consumption after total abdominal hysterectomy.* Anesthesiology, 2006. **105**(2): p. 334-7.

45. Romberg, R., et al., *Pharmacokinetic-pharmacodynamic modeling of morphine-6-glucuronide-induced analgesia in healthy volunteers: absence of sex differences.* Anesthesiology, 2004. **100**(1): p. 120-33.

46. Romberg, R.R., et al., *Polymorphism of mu-opioid receptor gene (OPRM1:c.118A>G) does not protect against opioid-induced respiratory depression despite reduced analgesic response.* Anesthesiology, 2005. **102**(3): p. 522-30.

47. Skarke, C., et al., *Analgesic effects of morphine and morphine-6-glucuronide in a transcutaneous electrical pain model in healthy volunteers.* Clin Pharmacol Ther, 2003. **73**(1): p. 107-21.

48. Lotsch, J., et al., *The polymorphism A118G of the human mu-opioid receptor gene decreases the pupil constrictory effect of morphine-6-glucuronide but not that of morphine.* Pharmacogenetics, 2002. **12**(1): p. 3-9.

49. Lötsch, J., et al., *Modulation of the central nervous effects of levomethadone by genetic polymorphisms potentially affecting its metabolism, distribution, and drug action.* Clin Pharmacol Ther, 2006. **79**(1): p. 72-89.

50. Lötsch, J., et al., *Does the A118G polymorphism at the mu-opioid receptor gene protect against morphine-6-glucuronide toxicity?* Anesthesiology, 2002. **97**(4): p. 814-9.

51. Franke, P., et al., *Nonreplication of association between mu-opioid-receptor gene (OPRM1) A118G polymorphism and substance dependence.* Am J Med Genet, 2001. **105**(1): p. 114-9.

52. Compton, P., D.H. Geschwind, and M. Alarcon, *Association between human mu-opioid receptor gene polymorphism, pain tolerance, and opioid addiction.* Am J Med Genet, 2003. **121B**(1): p. 76-82.

53. Drakenberg, K., et al., *Mu opioid receptor A118G polymorphism in association with striatal opioid neuropeptide gene expression in heroin abusers.* Proc Natl Acad Sci U S A, 2006. **103**(20): p. 7883-8.

54. Wand, G.S., et al., *The mu-opioid receptor gene polymorphism (A118G) alters HPA axis activation induced by opioid receptor blockade.* Neuropsychopharmacology, 2002. **26**(1): p. 106-14.

55. Hernandez-Avila, C.A., et al., *Association between the cortisol response to opioid blockade and the Asn40Asp polymorphism at the mu-opioid receptor locus (OPRM1).* Am J Med Genet, 2003. **118B**(1): p. 60-65.

56. Ronaghi, M., et al., *Real-time DNA sequencing using detection of pyrophosphate release.* Anal Biochem, 1996. **242**(1): p. 84-9.

57. Hardy, G.H., *Mendelian proportions in a mixed population.* Science, 1908. **28**: p. 49-50.

58. Hummel, T., et al., *Chemo-somatosensory event-related potentials in response to repetitive painful chemical stimulation of the nasal mucosa.* Electroencephalogr.Clin.Neurophysiol., 1994. **92**: p. 426-432.

59. Bingel, U., et al., *Subcortical structures involved in pain processing: evidence from single-trial fMRI.* Pain, 2002. **99**(1-2): p. 313-21.

60. Oertel, B.G., et al., *The Partial 5-Hydroxytryptamine(1A) Receptor Agonist Buspirone does not Antagonize Morphine-induced Respiratory Depression in Humans.* Clin Pharmacol Ther, 2007. **81**(1): p. 59-68.

61. Scott, J.C., K.V. Ponganis, and D.R. Stanski, *EEG quantitation of narcotic effect: the comparative pharmacodynamics of fentanyl and alfentanil.* Anesthesiology, 1985. **62**(3): p. 234-41.

62. Shafer, S.L., et al., *Pharmacokinetics of fentanyl administered by computer-controlled infusion pump.* Anesthesiology, 1990. **73**: p. 1091-1102.

63. Angst, M.S., et al., *Pharmacodynamics of orally administered sustained- release hydromorphone in humans.* Anesthesiology, 2001. **94**(1): p. 63-73.

64. Skarke, C., et al., *Analgesic effects of morphine and morphine-6-glucuronide in a transcutaneous electrical pain model in healthy volunteers.* Clin Pharmacol Ther, 2003. **73**(1): p. 107-21.

65. Oertel, B.G., et al., *The mu-opioid receptor gene polymorphism 118A>G depletes alfentanil-induced analgesia and protects against respiratory depression in homozygous carriers.* Pharmacogenet Genomics, 2006. **16**(9): p. 625-36.

66. Kobal, G., *Pain-related electrical potentials of the human nasal mucosa elicited by chemical stimulation.* Pain, 1985. **22**(2): p. 151-163.

67. Steen, K.H., et al., *Protons selectively induce lasting excitation and sensitization of nociceptors in rat skin.* J. Neurosci., 1992. **12**: p. 86-95.

68. Reeh, P.W. and M. Kress, *Molecular physiology of proton transduction in nociceptors.* Curr. Opin. Pharmacol., 2001. **1**: p. 45-51.

69. Huttunen, J., et al., *Cortical responses to painful CO2 stimulation of nasal mucosa; a magnetoencephalographic study in man.* Electroencephalogr.Clin.Neurophysiol., 1986. **64**: p. 347-349.

70. Kobal, G., T. Hummel, and M. Hoesl, *Pain-related electrical evoked potentials by chemical stimuli: Effects of fentanyl*, in *Advances in pain research and therapy*, S. Lipton, Editor. 1989, Raven Press: New York. p. 95-98.

71. Roy, C.S. and C.S. Sherrington, *On the regulation of the blood supply of the brain.* J Physiol Lond, 1890. **11**: p. 85-108.

72. Fox, P.T. and M.E. Raichle, *Focal physiological uncoupling of cerebral blood flow and oxidative metabolism during somatosensory stimulation in human subjects.* Proc. Natl. Acad. Sci. U. S. A., 1986. **83**: p. 1140-1144.

73. Becerra, L., et al., *Functional magnetic resonance imaging measures of the effects of morphine on central nervous system circuitry in opioid-naive healthy volunteers.* Anesth Analg, 2006. **103**(1): p. 208-16, table of contents.

74. Wise, R.G., P. Williams, and I. Tracey, *Using fMRI to Quantify the Time Dependence of Remifentanil Analgesia in the Human Brain.* Neuropsychopharmacology, 2004. **29**(3): p. 626-635.

75. Cusack, R., M. Brett, and K. Osswald, *An evaluation of the use of magnetic field maps to undistort echo-planar images.* Neuroimage, 2003. **18**(1): p. 127-42.

76. Jezzard, P. and R.S. Balaban, *Correction for geometric distortion in echo planar images from B0 field variations.* Magn Reson Med, 1995. **34**(1): p. 65-73.

77. Read, D.J., et al., *Regulation of ventilation during rebreathing at imposed respiratory frequencies.* Respir Physiol, 1966. **2**(1): p. 88-98.

78. Behne, M., et al., *Respiratory effects and tolerability of Mr 2264 Cl. A new opiate partial agonist in comparison with morphine and placebo.* Eur J Clin Pharmacol, 1994. **46**(4): p. 301-4.

79. Lötsch, J., et al., *The 5-hydroxytryptamine 4 receptor agonist mosapride does not antagonize morphine-induced respiratory depression.* Clin Pharmacol Ther, 2005. **78**(3): p. 278-87.

80. Bradford, M.M., *A rapid and sensitive method for the quantitation of microgram quantities of protein utilizing the principle of protein-dye binding.* Anal Biochem, 1976. **72**: p. 248-54.

81. Cheng, Y. and W.H. Prusoff, *Relationship between the inhibition constant (K1) and the concentration of inhibitor which causes 50 per cent inhibition (I50) of an enzymatic reaction.* Biochem Pharmacol, 1973. **22**(23): p. 3099-108.

82. Ko, M.C., et al., *Studies of micro-, kappa-, and delta-opioid receptor density and G protein activation in the cortex and thalamus of monkeys.* J Pharmacol Exp Ther, 2003. **306**(1): p. 179-86.

83. Maher, C.E., D.E. Selley, and S.R. Childers, *Relationship of mu opioid receptor binding to activation of G-proteins in specific rat brain regions.* Biochem Pharmacol, 2000. **59**(11): p. 1395-401.

84. Sim, L.J., et al., *Differences in G-protein activation by mu- and delta-opioid, and cannabinoid, receptors in rat striatum.* Eur J Pharmacol, 1996. **307**(1): p. 97-105.

85. Worsley, K.J. and K.J. Friston, *Analysis of fMRI time-series revisited--again.* Neuroimage, 1995. **2**(3): p. 173-81.

86. Friston, K.J., et al., *Analysis of fMRI time-series revisited.* Neuroimage, 1995. **2**: p. 45-53.

87. Friston, K.J., et al., *Statistical parametric maps in functional imaging: a general linear approach.* Hum Brain Mapp, 1995(2): p. 189-210.

88. Friston, K.J., et al., *Spatial registration and normalization of images.* Hum Brain Mapp, 1995(3): p. 165-89.

89. Evans, A.C., et al., *3D statistical neuroanatomical models from 305 MRI volumes.* Proc IEEE Nucl Sci Symp Med Imaging, 1993(1-3): p. 1813-17.

90. Worsley, K.J., *Local maxima and the expected euler characteristic of excursion sets of χ^2, F and t fields.* Adv Appl Prob, 1994(26): p. 13-42.

91. Boeckmann, A.J., L.B. Sheiner, and S.L. Beal, *NONMEM user's guide*. 1994, San Francisco: University of California San Francisco.

92. Yafune, A. and M. Ishiguro, *Bootstrap approach for constructing confidence intervals for population pharmacokinetic parameters. I: A use of bootstrap standard error.* Stat Med, 1999. **18**(5): p. 581-99.

93. Parke, J., N.H. Holford, and B.G. Charles, *A procedure for generating bootstrap samples for the validation of nonlinear mixed-effects population models.* Comput Methods Programs Biomed, 1999. **59**(1): p. 19-29.

94. Bushnell, M.C., et al., *Pain perception: is there a role for primary somatosensory cortex?* Proc Natl Acad Sci U S A, 1999. **96**(14): p. 7705-9.

95. Ferretti, A., et al., *Functional topography of the secondary somatosensory cortex for nonpainful and painful stimulation of median and tibial nerve: an fMRI study.* Neuroimage, 2004. **23**(3): p. 1217-25.

96. Craig, A.D., et al., *Thermosensory activation of insular cortex.* Nat Neurosci, 2000. **3**(2): p. 184-90.

97. Bornhovd, K., et al., *Painful stimuli evoke different stimulus-response functions in the amygdala, prefrontal, insula and somatosensory cortex: a single-trial fMRI study.* Brain, 2002. **125**(Pt 6): p. 1326-36.

98.   Gosselin, N., et al., *Emotional responses to unpleasant music correlates with damage to the parahippocampal cortex.* Brain, 2006. **129**(Pt 10): p. 2585-92.

99.   Fulbright, R.K., et al., *Functional MR imaging of regional brain responses to pleasant and unpleasant odors.* AJNR Am. J. Neuroradiol., 1998. **19**: p. 1721-1726.

100.   Derbyshire, S.W., *A systematic review of neuroimaging data during visceral stimulation.* Am J Gastroenterol, 2003. **98**(1): p. 12-20.

101.   Saper, C.B., *Convergence of autonomic and limbic connections in the insular cortex of the rat.* J Comp Neurol, 1982. **210**(2): p. 163-73.

102.   Price, D.D., et al., *A psychophysical analysis of morphine analgesia.* Pain, 1985. **22**: p. 261-269.

103.   Vogt, B.A., *Pain and emotion interactions in subregions of the cingulate gyrus.* Nat Rev Neurosci, 2005. **6**(7): p. 533-44.

104.   Jones, A.K., et al., *In vivo distribution of opioid receptors in man in relation to the cortical projections of the medial and lateral pain systems measured with positron emission tomography.* Neurosci Lett, 1991. **126**(1): p. 25-8.

105.   Wise, R.G., et al., *Combining fMRI with a pharmacokinetic model to determine which brain areas activated by painful stimulation are specifically modulated by remifentanil.* Neuroimage, 2002. **16**(4): p. 999-1014.

106.   Romberg, R., et al., *Pharmacodynamic effect of morphine-6-glucuronide versus morphine on hypoxic and hypercapnic breathing in healthy volunteers.* Anesthesiology, 2003. **99**(4): p. 788-98.

107.   Lötsch, J., et al., *The polymorphism A118G of the human mu-opioid receptor gene decreases the pupil constrictory effect of morphine-6-glucuronide but not that of morphine.* Pharmacogenetics, 2002. **12**(1): p. 3-9.

108.   Oertel, B.G., et al., *Differential opioid action on sensory and affective cerebral pain processing.* Clin Pharmacol Ther, 2007. **(accepted)**.

109.   Zhang, Y., et al., *Allelic expression imbalance of human mu opioid receptor (OPRM1) caused by variant A118G.* J Biol Chem, 2005. **280**(38): p. 32618-24.

110.   Kroslak, T., et al., *The single nucleotide polymorphism A118G alters functional properties of the human mu opioid receptor.* J Neurochem, 2007. **103**(1): p. 77-87.

111.   Wagner, K.J., et al., *Imaging human cerebral pain modulation by dose-dependent opioid analgesia: a positron emission tomography activation study using remifentanil.* Anesthesiology, 2007. **106**(3): p. 548-56.

112. Zubieta, J.K., et al., *COMT val158met genotype affects mu-opioid neurotransmitter responses to a pain stressor.* Science, 2003. **299**(5610): p. 1240-3.

113. Berthele, A., et al., *COMT Val108/158Met genotype affects the mu-opioid receptor system in the human brain: evidence from ligand-binding, G-protein activation and preproenkephalin mRNA expression.* Neuroimage, 2005. **28**(1): p. 185-93.

114. Gonzalez-Maeso, J., R. Rodriguez-Puertas, and J.J. Meana, *Quantitative stoichiometry of G-proteins activated by mu-opioid receptors in postmortem human brain.* Eur J Pharmacol, 2002. **452**(1): p. 21-33.

115. Pan, Y.X., et al., *Identification and characterization of two new human mu opioid receptor splice variants, hMOR-1O and hMOR-1X.* Biochem Biophys Res Commun, 2003. **301**(4): p. 1057-61.

116. Pan, L., et al., *Identification and characterization of six new alternatively spliced variants of the human mu opioid receptor gene, Oprm.* Neuroscience, 2005. **133**(1): p. 209-20.

117. Chakrabarti, S., et al., *Expression of the mu-opioid receptor in CHO cells: ability of mu-opioid ligands to promote alpha-azidoanilido[32P]GTP labeling of multiple G protein alpha subunits.* J Neurochem, 1995. **64**(6): p. 2534-43.

118. Kleuss, C., et al., *Different beta-subunits determine G-protein interaction with transmembrane receptors.* Nature, 1992. **358**(6385): p. 424-6.

119. Latasch, L., et al., *Antagonisation of fentanyl-induced respiratory depression by nalbuphine.* Acta Anaesthesiol Belg, 1989. **40**(1): p. 35-40.

9 Appendix

9.1 Abbreviations

$[^{35}S]$-GTPγS	Guanosine-5'-(γ-$[^{35}S]$)-thiotriphosphate
$[^3H]$-DAMGO	^3H-[D-Ala^2,N-MePhe^4,Gly-ol^5]-enkephalin
°C	Temperature in degree Celsius
ACTB	Gene coding for β-Actin
ANOVA	Analysis of variance
Asn	Asparagine
Asp	Aspartic Acid
bp	Base pair
B_0	Baseline response (e.g. basal binding)
B_{Max}	Maximum response (e.g. maximum binding)
BSA	Bovine serum albumin
cDNA	Copy DNA
COMT	Gene coding for the Catechol-O-methyltransferase
Conc.	Concentration
D	Aspartic Acid
DNA	Deoxyribonucleic acid
dpm	Decays per minute
DTT	Dithiothreit
EC_{50}	Effective concentration 50% (Conc. of agonist that provokes a response half way between the baseline (e.g. B_0) and maximum response (e.g. B_{Max}))
e.g.	For example
EEG	Electroencelography
EGTA	Ethylene glycol tetraacetic acid (chelating agent)
fM	Femtomolar (fmol/l)
fMRI	Functional magnetic resonance imaging
g	Gramm
GDP	Guanosine-5'-diphosphate
GIRK	G-protein activated inwardly rectifying potassium (K$^+$) channel
GTP	Guanosine-5'-triphosphate
h	Hours
H_2O	Aqua purificata
HCl	Hydrochloric acid
IC_{50}	Inhibitory concentration 50% (Basically the same as the EC_{50} but mainly used in competition binding experiments)
i.e.	That is
K_D	Equilibrium dissociation constant
LC-MS/MS	Liquid chromatographic tandem mass spectrometric
M	Molar
mg	Milligram
$MgCl_2$	Magnesium chloride
min	Minutes
msec	Milliseconds
mM	Millimolar (mmol/l)

N	Asparagine
ng	Nanogramm
nM	Nanomolar (nmol/l)
OPRM1	Gene coding for the μ-Opioid receptor
PCR	Polymerase chain reaction
RNA	Ribonucleic acid
RT-PCR	Real time polymerase chain reaction
S_I	Primary somatosensory cortex
S_{II}	Secondary somatosensory cortex
sec	Seconds
SEM	Standard error of the mean
SNP	Single nucleotide polymorphism
t	Tesla
Tris	Tris(hydroxymethyl)aminomethan
μg	Microgram
μl	Microliter
μM	Micromolar (μmol/l)

9.2 Danksagung

9.3 Curriculum vitae

Persönliche Daten
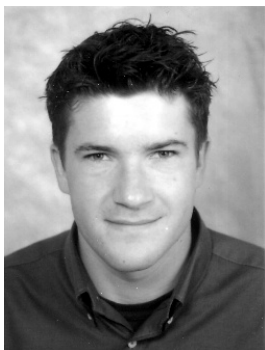
Bruno Georg Oertel

Grüne Straße 26 a

60316 Frankfurt am Main

Geboren am 24. März 1976 in Neuburg an der Donau

Deutschland

verheiratet

Hochschulausbildung

2003-heute	Wissenschaftlicher Mitarbeiter am Institut für Klinische Pharmakologie der Johann Wolfgang Goethe-Universität in Frankfurt am Main; seit 2005 Stipendiat des Europäischen Graduiertenkollegs GRK 757
2003	Approbation als Apotheker
2002-2003	Pharmaziepraktikum in der Abteilung Arzneimittelzulassung und –labelling der Sanofi-Aventis Deutschland GmbH in Bad Soden am Taunus
	Pharmaziepraktikum in der Falken-Apotheke in Frankfurt am Main
1998-2002	Studium der Pharmazie
	an der Johann Wolfgang Goethe-Universität in Frankfurt am Main

Schreinerlehre

1995-1998	Firma Eckert in Neuburg a. d. Donau

Schulausbildung

1990-1995	Descartes-Gymnasium in Neuburg an der Donau
1986-1990	Gymnasium bei St. Stephan in Augsburg

Publikationen des Autors

Oertel BG, Scholich K, Kettner M, Renne C, Schmidt P, Geisslinger G and Lötsch J. *The genetic µ-opioid receptor variant N40D extinguishes differences in receptor signaling between brain regions.* (under review; J Biol Chem 2007).

Oertel BG, Lötsch J. *Genetic mutations which prevent pain: implications for future pain medication.* Pharmacogenomics 2007 (accepted).

Oertel BG, Preibisch C, Wallenhorst T, Hummel T, Geisslinger G, Lanfermann H and Lötsch J. *Differential opioid action on sensory and affective cerebral pain processing.* Clin Pharmacol Ther 2007 (accepted).

Oertel BG, Schneider A, Rohrbacher M, Schmidt H, Tegeder I, Geisslinger G, et al. *The partial 5-hydroxytryptamine1A receptor agonist buspirone does not antagonize morphine-induced respiratory depression in humans.* Clin Pharmacol Ther 2007;81(1):59-68.

von Hentig N, Muller A, Rottmann C, Wolf T, Lutz T, Klauke S, Kurowski M, **Oertel BG**, Dauer B, Harder S, Staszewski S. *Pharmacokinetics of saquinavir, atazanavir and ritonavir in a boosted double-protease inhibitor twice-daily regimen.* Antimicrob Agents Chemother 2007 Apr;51(4):1431-9.

Oertel BG, Schmidt R, Schneider A, Geisslinger G, Lötsch J. *The mu-opioid receptor gene polymorphism 118A>G depletes alfentanil-induced analgesia and protects against respiratory depression in homozygous carriers.* Pharmacogenet Genomics 2006;16(9):625-36.

Lötsch J, Skarke C, Wieting J, **Oertel BG**, Schmidt H, Brockmoller J, et al. *Modulation of the central nervous effects of levomethadone by genetic polymorphisms potentially affecting its metabolism, distribution, and drug action.* Clin Pharmacol Ther 2006;79(1):72-89.

Oertel BG, Lötsch J. *NSAIDs, Pharmacokinetics.* Encyclopedia of Pain (Springer Verlag) 2006.